ISBN 978-82-326-6613-3 (printed ver.)
ISBN 978-82-326-6451-1 (electronic ver.)
ISSN 1503-8181 (printed ver.)
ISSN 2703-8084 (electronic ver.)

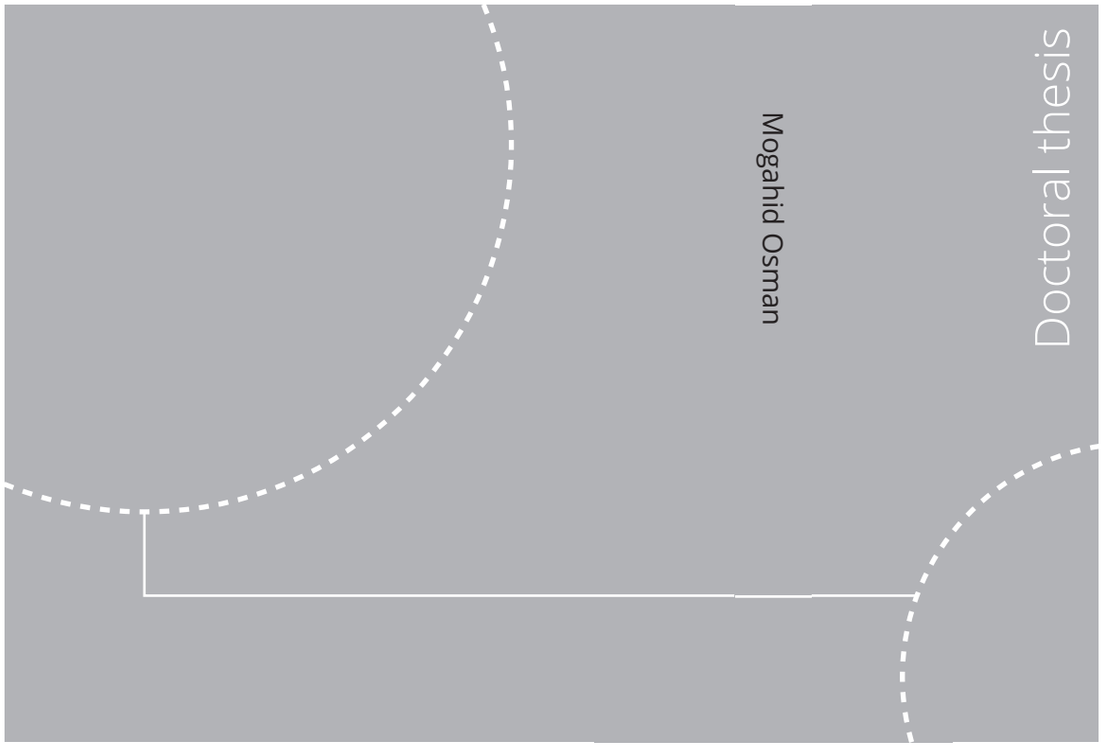

Doctoral theses at NTNU, 2021:223

Mogahid Osman

A pressurized Internally Circulating Reactor (ICR) for streamlining development of chemical looping technology

NTNU
Norwegian University of
Science and Technology
Thesis for the degree of
Philosophiae Doctor
Faculty of Engineering
Department of Energy and Process Engineering

NTNU
Norwegian University of
Science and Technology

Doctoral theses at NTNU, 2021:223

NTNU

NTNU
Norwegian University of
Science and Technology

Mogahid Osman

A pressurized Internally Circulating Reactor (ICR) for streamlining development of chemical looping technology

Thesis for the degree of Philosophiae Doctor

Trondheim, June 2021

Norwegian University of Science and Technology
Faculty of Engineering
Department of Energy and Process Engineering

NTNU
Norwegian University of
Science and Technology

NTNU
Norwegian University of Science and Technology

Thesis for the degree of Philosophiae Doctor

Faculty of Engineering
Department of Energy and Process Engineering

ISBN 978-82-326-6613-3 (printed ver.)
ISBN 978-82-326-6451-1 (electronic ver.)
ISSN 1503-8181 (printed ver.)
ISSN 2703-8084 (electronic ver.)

Doctoral theses at NTNU, 2021:223

PRINTED IN NORWAY
NO - 1598

NORDIC SWAN ECOLABEL
Printed matter
2041 0731

Printed by Skipnes Kommunikasjon AS

Preface

This thesis is submitted in partial fulfilment of the requirements for the degree of Philosophiae Doctor (Ph.D.) at the Norwegian University of Science and Technology (NTNU). The thesis work is a result of a doctoral study carried out at the Department of Energy and Process Engineering (EPT), NTNU with close collaboration with SINTEF Industry. Dr. Shahriar Amini has been the main Supervisor and Dr. Abdelghafour Zaabout has been the co-supervisor. This work was financed by the Research Council of Norway.

March 2021

Mogahid Osman

Summary

Increased level of carbon dioxide in the atmosphere as a result of fossil-fuel utilization is considered to be the dominant factor for global warming and climate change. All major energy roadmaps project continued increases in fossil fuel consumption up to 2040 and beyond driven primarily by continued increases in both population and economic growth. As a result, urgent technology innovations are needed to mitigate CO_2 emissions in order to meet the international commitment to limit the increase in average Earth temperature well below 2°C. According to the International Energy Agency (IEA), Energy efficiency and Carbon Capture, Utilization and Storage (CCUS) can both achieve half of the total emission reduction target for the pathways scenario of the global energy system. Chemical looping process has great potential for reducing the energy penalty and associated costs of CO_2 capture from fossil fuel-based power and chemical production while maintaining high energy efficiency. Pressurized operation of the chemical looping process is a prerequisite for maximizing energy efficiency in most proposed chemical looping configurations. In power generation, pressurized chemical looping has the potential for maximizing the power plant efficiency by using a combined cycle instead of the Rankine cycle used with atmospheric pressure boilers. For hydrogen production, high-pressure operation improves the overall efficiency and lowers the cost associated with hydrogen separation and compression. For syngas production, high-pressure operation is required for improving the efficiency of syngas to liquids processes. Moreover, high-pressure operation significantly reduces the process footprint, thus resulting in a more compact system.

Considering the immense advantages of pressurized chemical looping process, this PhD thesis focused on the development of a novel reactor configuration, the internally circulating reactor (ICR). The ICR is based on the circulating fluidized-bed (CFB) configuration, but with a simplified solids circulation mechanism that enables pressurized chemical looping operation. In the ICR, the functionality of two reactors, two cyclones and two loop seals of the CFB are packaged into a single vessel, which can be designed and operated in a single pressure shell. The main objective of the thesis was to assess the technical viability of ICR concept applied to pressurized chemical looping processes for power generation and syngas/hydrogen production with high efficiency and low energy penalty of CO_2 capture. Extensive efforts of this PhD thesis have been devoted toward commissioning of the ICR unit for high-pressure application of different chemical looping processes. Upon successful commissioning of the unit, a series of experimental campaigns have been conducted to gain a deep understanding of the effect of

various operating parameters on the ICR performance as well as to evaluate its potential for autothermal pressurized chemical looping combustion and reforming processes. A detailed mapping of the operating conditions for the ICR system was developed with over 100+ hours of stable operation for up to 4 kW_{th} of thermal gaseous fuel input and operating pressure up to 6 bar. The results of these campaigns illustrated the ability of ICR concept to achieve stable pressurized operation over a wide range of operating conditions, which also provided valuable insights for future scale-up of the ICR configuration. Furthermore, a process simulation study has been carried out to evaluate the potential of applying the ICR concept for industrial applications (integration in methanol production plant) by means of technical evaluation and subsequent comparison with the conventional autothermal reforming technology (ATR). Simulation results revealed that the chemical looping reforming (CLR) based plant can achieve higher methanol production efficiency compared to the ATR-based plant. A detailed parametric study was also conducted to study the sensitivity of the overall methanol plant performance to the operating pressure of the CLR and the gas leakage between the two reactors section when using the ICR system. In the light of the reliable pressurized ICR operation and excellent technical performance demonstrated in this study, further scale-up of the ICR concept to 0.1-1 MW_{th} pilot plant size for application to pressurized chemical looping is highly recommended.

To those who fill my moment with love and pleasure, my wife Sittana, my family, my friends..

For everyone who taught me that nothing is out of reach..

Acknowledgements

I would like to acknowledge my indebtedness and gratitude to my supervisor Dr. Shahriar Amini for his guidance, unlimited support and encouragement throughout this study. Thank you Shahriar for your kindness and for being always available for support for my PhD related matters as well as for my personal life. Additionally, I am truly thankful to my Co-supervisor, Dr. Abdelghafour Zaabout for your immense guidance throughout the experimental part of this thesis. Thank you Abdelghafour for following every step of this work, making useful suggestions, corrections and directing the whole course of the work. I have learned so much from you that I am sure will have profound impacts on my future. My deep appreciation also goes to Dr. Schalk Cloete, your deep knowledge and expertise on the research field transferred to me in the form of guidance, critic, suggestions and help. Thanks Schalk to those many discussions, help in analyzing results, guidance in the process simulation, correcting and commenting on the papers.

I am also grateful to all the technical support by Paul Svendsen and Martin Bustadmo in the VATL Lab at EPT. Your help in building the ICR unit and finding solutions to all kind of problems was priceless. Thank you Paul and Martin for your support. Special thanks goes out to Wenche, Ingrid, Anita, and all EPT administration team for your support and always being willing and available for help.

My new life at NTNU and Trondheim would not be easy without being surrounded by nice friends. Thank you Arpit, Shareq, Henri, Joana, Ambrose, Chaitanya, and Mohammed Khan. I thank you all, you all made my life great at NTNU. Thanks for those great moments during experiments, lunch, dinner, and in the office.

Last but never the least but the closest, my family, my sincere gratitude goes to my lovely wife Sittana, your endless support and patience during all my busy period of my PhD work at the office and the lab are really appreciable. Special thanks to my family, my parents, brothers and sister who dedicates a lot of their precious time, assistance, and for their understanding and endless love, through the duration of my study.

Contents

Chapter 1 Introduction

1.1 The Grand Challenge

Fossil fuels (oil, coal and natural gas) utilization for power generation and chemical production have led to a profound global economic growth since the turn of the 20th century. However, the massive use of fossil fuels resulted in an increase in the concentration of carbon dioxide in the atmosphere. The Intergovernmental Panel on Climate Change (IPCC) recognized that this exponential CO_2 concentration in the atmosphere is the dominant factor for global warming and climate change. Figure 1 shows the continuous increments of CO_2 level since the industrial revolution until today (blue line), which was found to relate to the global mean surface temperature increase (red line). It can be seen that the current CO_2 level is exceeded 400 ppm, which is an alarming level that was only reached around four million years ago, when the global temperatures were 2 - 4°C warmer and sea levels were 10 - 25 meters higher than they are today. Continuous emission of greenhouse gases will therefore put the Earth's ecosystems on a trajectory towards rapid climate change that is catastrophic and irreversible.

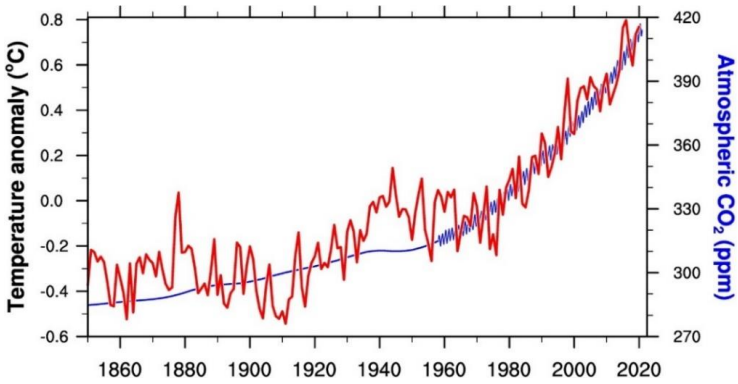

Figure 1. CO_2 level since the industrial revolution until today (blue line), the global mean surface temperature (red line) [1].

As a response to this alarming crisis, international efforts such as the United Nations Framework Convention on Climate Change (UN, 1992) and the Paris Agreement (UN, 2015) have set clear goals to limit greenhouse gases emissions to a certain level. For instance, the Paris Agreement, which was signed by 197 countries, has stated the aims of "Holding the increase in the global average temperature to well below 2°C above pre-industrial levels and pursuing efforts to limit the temperature increase to 1.5°C above pre-industrial levels". A recent study [2] reveals that to achieve this goals, the CO_2 level in the atmosphere would need to be

reduced from the current level of ~410 to 353 ppm. The CO_2 level in the atmosphere was last 350 ppm in the year 1988, and the global Earth surface temperature was then +0.5°C relative to the preindustrial period. This implies that there are urgent needs for innovative technologies that enable removing CO_2 from the atmosphere as well as providing alternative ways for supplying human needs from energy and products in a more sustainable manner.

According to the 2018 Energy Outlook issued by the international energy agency IEA [3], the global energy demand projected to rise by 25% by 2040, and hence fossil fuels will most likely remain the backbone of the global energy system for the coming decades. Therefore, urgent decarbonization solutions are needed to mitigate CO_2 emissions from fossil fuel utilization. Several options can be used to mitigate CO_2 emissions from fossil fuel utilization that include 1) improving the process efficiency, 2) switch to renewable energy sources, 3) replacement of fossil fuel with a low carbon intensity sources (e.g. coal by natural gas or hydrogen) and 4) applying Carbon Capture, Utilization and Storage (CCUS).

The International Energy Agency (IEA) has developed pathways scenarios for the global energy system consistent with the Paris Agreement in limiting the temperature increase to 2.0°C, while securing sufficient energy supply to the society. Figure 2 presents the different pathways and their overall forecasted contributions in CO_2 emission reduction. As it can be seen, the energy efficiency and CCS together represent more than a half of the total emission reduction. Energy efficiency is the most important factor in this pathway options as it reduces the overall demand, however, it cannot lead to deep decarbonization without support from other pathways.

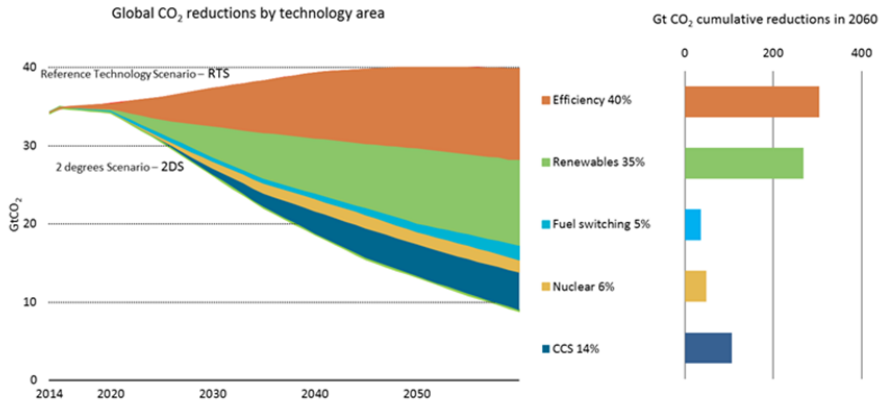

Figure 2. The different pathways for the global energy system consistent with the Paris Agreement and its overall contribution in CO_2 emission reduction [3].

CCUS is a crucial element in most mitigation scenarios to meet the global warming targets [4]. CCUS technologies can be applied to large stationary point sources where a capture system can extract CO_2 directly from a gas stream, such as power generation plants as well as most industrial sectors (as shown in Figure 3). In fact, CCUS is the prime option for the hard-to-abate energy intensive industries (such as cement and steel), in achieving deep emissions reductions.

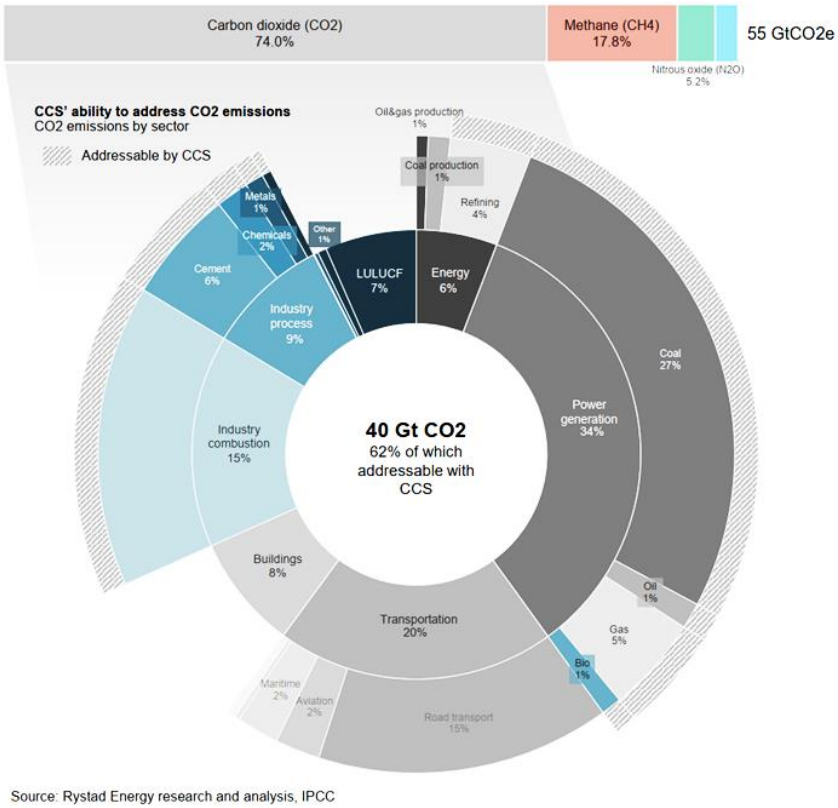

Figure 3. Global CO_2 emissions by different sector, 2018 and the potential of CCUS in the different sectors [5].

Four main categories have been explored for CCUS technologies: 1) post-combustion, 2) pre-combustion, 3) oxy-combustion, and 4) chemical looping process [6]. Figure 4 illustrates the different CO_2 capture technologies applied to power plant. The post-combustion option achieved by CO_2 separation from the flue-gaseous after the combustion process, and it can be applied to currently installed fossil fuel-based power plants. Pre-combustion capture involves the separation of CO_2 and H_2, resulting in a hydrogen-rich fuel that can be used in many different applications. The oxy-fuel process uses pure oxygen from an air separation unit (ASU) for combusting the fuel instead of using air, therefore, it resulted in a pure CO_2 stream

after combustion that is ready from compression, transportation, storage or utilization. As it can be seen all these three options require gas separation units that is very costly and will decrease the global efficiency of the plant that has a large effect on the economics [7]. Chemical looping process avoids the need for gas separation unit and therefore the energy penalty for CO_2 capture is very low as compared to other techniques. The focus of this PhD thesis is on the chemical looping processes.

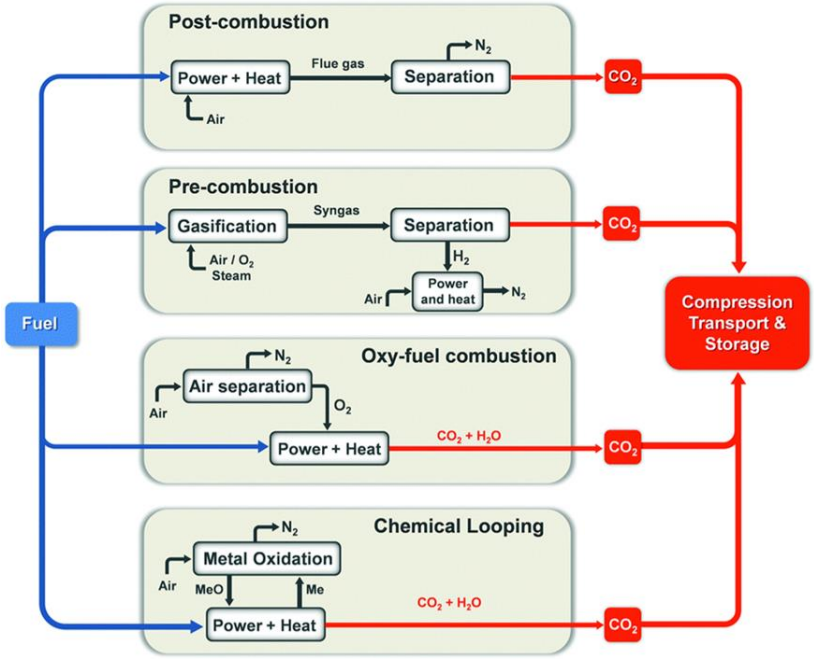

Figure 4. Various CO_2 capture technologies applied to a power plant [8].

1.2 Chemical Looping Process: a Promise Meets Practical Challenges

Chemical looping technology is a promising technology that is increasingly viewed as a competitive technology for carbon capture and storage (CCS). Hence, it provides the means to converting fossil fuel to electricity with inherent separation of CO_2 and without significant energy penalties. The concept also advanced into other platform technologies for the production of various chemicals beyond the utility industry (e.g. syngas and hydrogen). In the chemical looping system, chemical reactions take place following a reacting scheme consisting of multiple sub-reactions using chemical intermediates (a metal oxides) that react and regenerate in a cyclic manner which allows designing the chemical looping process sub-reactions to reduce the exergy losses [9]. The term "Chemical-Looping" was first coined by Ishida et al. in 1987 for a process where metal oxides used as an oxygen-carrier intermediate for a redox reaction in power production, which led to substantial increase in the exergy efficiency compared to conventional combustion [9].

The principle of chemical looping combustion (CLC) is to carry out the process in two steps (Figure 5); in the fuel reactor (FR) the fuel reacts with the oxygen carrier to fully oxidize to CO_2 and H_2O producing heat for power generation in a steam cycle or a combined cycle (depending on the CLC operating pressure). The reduced metal oxide is re-oxidized in a flow of air in the air reactor (AR) ready to start a new cycle. The main characteristics of CLC can be summarized as follows:

- The two steps are conventionally carried out in a two fluidized-bed-reactors unit, and the solid oxygen carrier is pneumatically circulated between them.
- The process avoids direct contact between fuel and air, hence CO_2 and water are the only major products in the fuel reactor with absence of nitrogen, where water can be condensed subsequently to generate a sequestration-ready CO_2 stream.
- The total heat evolved from the reduction/oxidation cycle remains the same compared to conventional combustion; therefore, energy penalty for CO_2 capture is minimized.
- The oxidation reaction at the air reactor is exothermic, where the energy released can be extracted from the solids particle or the spent air utilized for power generation, either through steam or combined cycle.

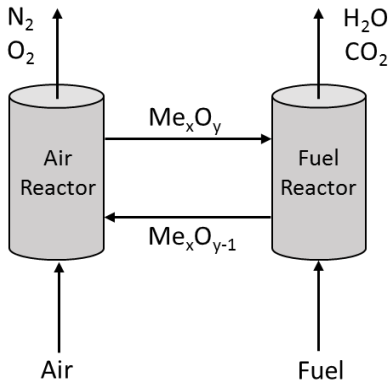

Figure 5. Chemical Looping Combustion CLC.

The CLC system performance is highly depends on the reactor design and the intimate contact between the oxygen carrier and the fuel. There are many aspects that must be consider for the CLC reactors design including:

1. The oxygen carrier is the most important element of the CLC system; it should have a combination of favorable chemical and physical properties.
2. There should be good contact between oxygen carriers and fuel to achieve complete fuel conversion to CO_2 and H_2O.
3. Suitable residence time for the oxygen carrier and the fuel/air to achieve maximum conversion.
4. The gas-solid contacting pattern, gas velocity and bed height are the main parameters affecting the fuel conversion.
5. The reaction of air with the metal oxide is exothermic, hence heat should be well circulated throughout the reactor to prevent particle melting or sintering, which can deactivate the oxygen carrier and cause operability issues.
6. High temperature as well as high pressure operation leads to a higher overall efficiency of the CLC system and the latter being also favorable to CO_2 sequestration.
7. CO_2 leakage should be minimized or prevented between the fuel reactor and the air reactor to maximize the separation efficiency.

Based on the above enlisted requirements, there are numerous configurations proposed for CLC system, where the most common is the interconnected dual fluidized bed reactors. Other reactor configurations have also been considered such as alternated packed or fluidized-bed reactor, rotating reactor and moving bed. Several works have been carried out to study the more appropriated design of the CLC system. The conventional dual circulating fluidized bed

configuration has been demonstrated experimentally at lab and small pilot scales in several studies [10–12] but is facing numerous technical and operational challenges which arise mainly from the interconnected reactor configuration. Solids circulation between the two reactors requires costly particle separation systems together with loop seals to prevent gas leakage. Particle separation can be particularly expensive due to the capital costs and pressure losses associated with high-volume high-temperature cyclones and particle degradation leading to losses of the oxygen carrier material. The interconnected nature of the standard CLC setup also introduces significant uncertainties regarding process scale-up, thereby requiring many years of incremental scale-up, testing and demonstration.

These complexities are magnified by the necessity to operate under pressurized conditions in order to achieve high efficiency and cost-competitive power generation using gaseous fuels. Pressurized operation allows for the use of a combined cycle for power generation leading to higher efficiencies and is mandatory for CLC with gaseous fuels in order to compete with standard combined cycle plants with post combustion CO_2 capture. In addition, high pressure operation also allows for the use of much smaller reactors and reduces the energy penalty involved in CO_2 compression. Operating the chemical looping systems at high pressures can result in difficulties with the solids circulation between the air and fuel reactors and represents an important additional challenge to be overcome. Very large solids circulation rates are required and unwanted pressure fluctuations in the reactors can originate due to imperfect back-pressure controllers. Increased solids entrainment also causes problems related to the clogging of cyclones and damages to gas turbines.

The circulating fluidized-bed configuration remains an attractive option for chemical looping applications considering its steady-state nature and high achievable fluidization velocities. The needs for pressurized operation of chemical looping system inspired the development of a novel reactor configuration; the internally circulating reactor (ICR), which is the prime focus of the current PhD thesis. The ICR concept is based on the circulating fluidized-bed configuration but with simplified solids circulation mechanism to simplify pressurized operation. In the ICR, the cyclones and loop seals involved in solids circulation in conventional CLC are replaced by simple ports between two sections in a single reactor.

1.3 The Internally Circulating Reactor (ICR): a Game Changer?

The Internally circulating reactor (ICR) is a novel system for circulating fluidized particles within a single vessel, which has the same advantages as the dual-circulation systems that are widely used for the FCC process and coal/biomass combustion and gasification systems. The ICR is a promising reactor configuration that has the potential to simplify the design, accelerate the commercialization, reduce the process cost, and enable pressurized operation of the circulating fluidized-bed processes. The system combines two sections in a single vessel that maintains the feature of continuous solid circulation while preventing the gas mixing between the two sections. The solids can act as a catalyst, oxygen carrier or a heat carrier. The solid circulate between the two sections with separate gas feed aimed at delivering a different process or different step of the process in each section. The different gas velocities considered in each section introduce different voidage fraction. The section that fluidize vigorously creates a higher voidage fraction, which originates a different pressure, this pressure difference drive the circulation of solids. In the port-opening connecting the two sections, the bulk density of solids is high since the particle are in the form of a packed rather than a fluidized-bed, provides a driving force for the solid circulation from one section to another. As a result of the vigorous fluidization in the fast section; the port is continuously recharged keeping the smooth solid circulation. The compactness of the ICR system countering its advantage for pressurized operation, which is challenging to achieve in the conventional systems.

An early study on the ICR concept was developed by Chong et al. [13] for oil shale retorting, in which the shale and ash continually circulate between the two sections, while keeping the combustion gas and the retort product gases separate. The ICR concept has been further investigated by He et al. [14] and Fang et al. [15] for coal combustion and gasification. For chemical looping process applications, ICR configuration has been applied on a small scale to evaluate the performance of different oxygen carrier materials [11,16–18]. The simplicity of the unit helped in providing a profound knowledge about CLC and CLR performance for different oxygen carrier materials. Herguido et al. [19] also applied ICR concept for hydrogen separation using the steam-iron process at atmospheric pressure. However, these studies have not considered the scale-up and pressurization issues.

This PhD thesis aims to demonstrate a pressurized lab-scale ICR reactor for chemical looping process applications. The design of this reactor was based on the hydrodynamic study and the CFD reactive simulations (Figure 6) conducted by SINTEF Industry. The hydrodynamic

investigation on the pseudo-2D cold-flow unit has revealed that a stable solids circulation and minimum gas leakage could be achieved with the ICR over a wide range of operating conditions [20]. This conclusion was confirmed by reactive multiphase flow modelling of a large-scale ICR unit (100 MW_{th}) reactor [21].

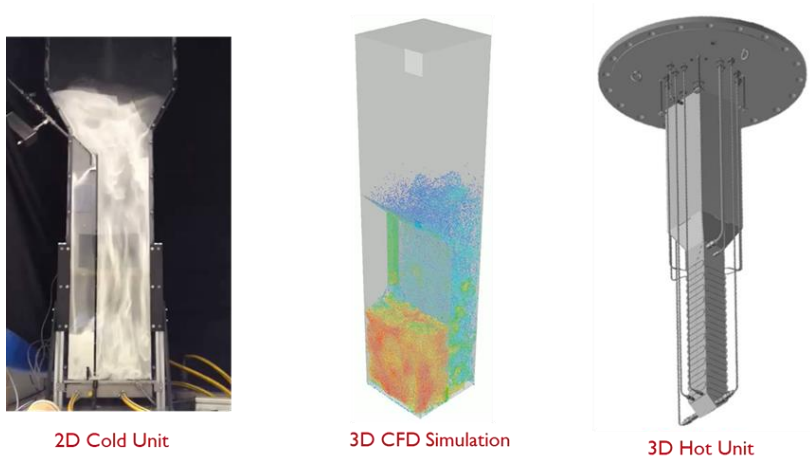

Figure 6. pseudo-2D ICR cold-flow unit (left), the 3D CFD reactive simulations (middle), CAD drawing of the 3D ICR unit (right).

In light of the promising results from the hydrodynamic study and the reactive simulations, the ICR unit shown in Figure 7 has been constructed and commissioned during the course of this PhD research. The design of this ICR unit offers a significant simplification in comparison to conventional chemical looping systems. Replacement of the cyclones and loop seals typically used in the solids transport lines connecting the air and fuel reactors by two simple ports will reduce capital costs, reduce heat and pressure losses, simplify process control and accelerate process scale-up, especially for pressurized systems. The integrated design is based on bubbling/turbulent beds that will reduce undesired particle attrition and elutriation while keeping a relatively small overall system footprint (the fast section freeboard is expanded over the slow section).

The ICR reactor was designed for gaseous fuel processes with an upper capacity of 5 kW_{th} fuel thermal input. The mass loading of the oxygen carrier material is in the range of 1 to 4 kg depending on the particle properties and the fuel thermal input. The reactor was made of Inconel material (Inconel Alloy 625) to withstand high temperature conditions. The reactor was placed in a cylindrical shell designed to withstand pressures up to 12 bar at 1000°C. The reactor heated up to the target operating temperature using external electrical heaters surrounding the

bottom part of the reactor body. Insulating material (glass wool) was placed around the reactor to minimize heat losses.

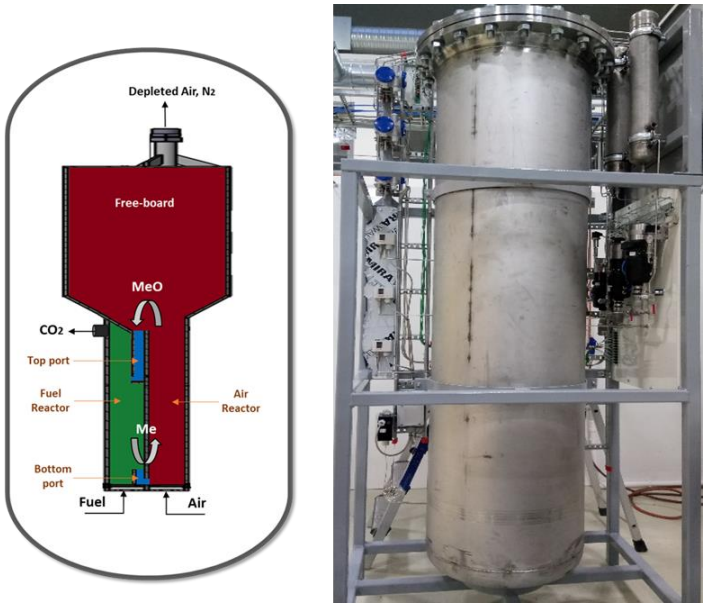

Figure 7. a simplified scheme of the ICR design, and the ICR unit under operation inside the shell.

Figure 8 illustrates the P&ID of the unit showing its different auxiliary components. The reactor exhaust stream is cooled with a water cooler installed at the outlet of each reactor section. A low temperature particle filter (5 μm size) is installed after the cooler to prevent fine particles elutriation to the environment. The outlet gas flowrates from each section were adjusted to be equal to the respective inlet gas flowrates by means of a controlling valve placed on the outlet of the FR, while a flowmeter was placed on the outlet of each sections. The pressure inside the reactor and the shell is controlled using back-pressure regulators installed at the outlet of each reactor section and the shell. The dry gas compositions (sampled after the flowmeter) are measured using a syngas analyzer. Other devices are also used to control and monitor the reactor operation, including mass flow controllers for gas feed, flowmeter for gas outlet measurement, thermocouples, pressure sensors and valves.

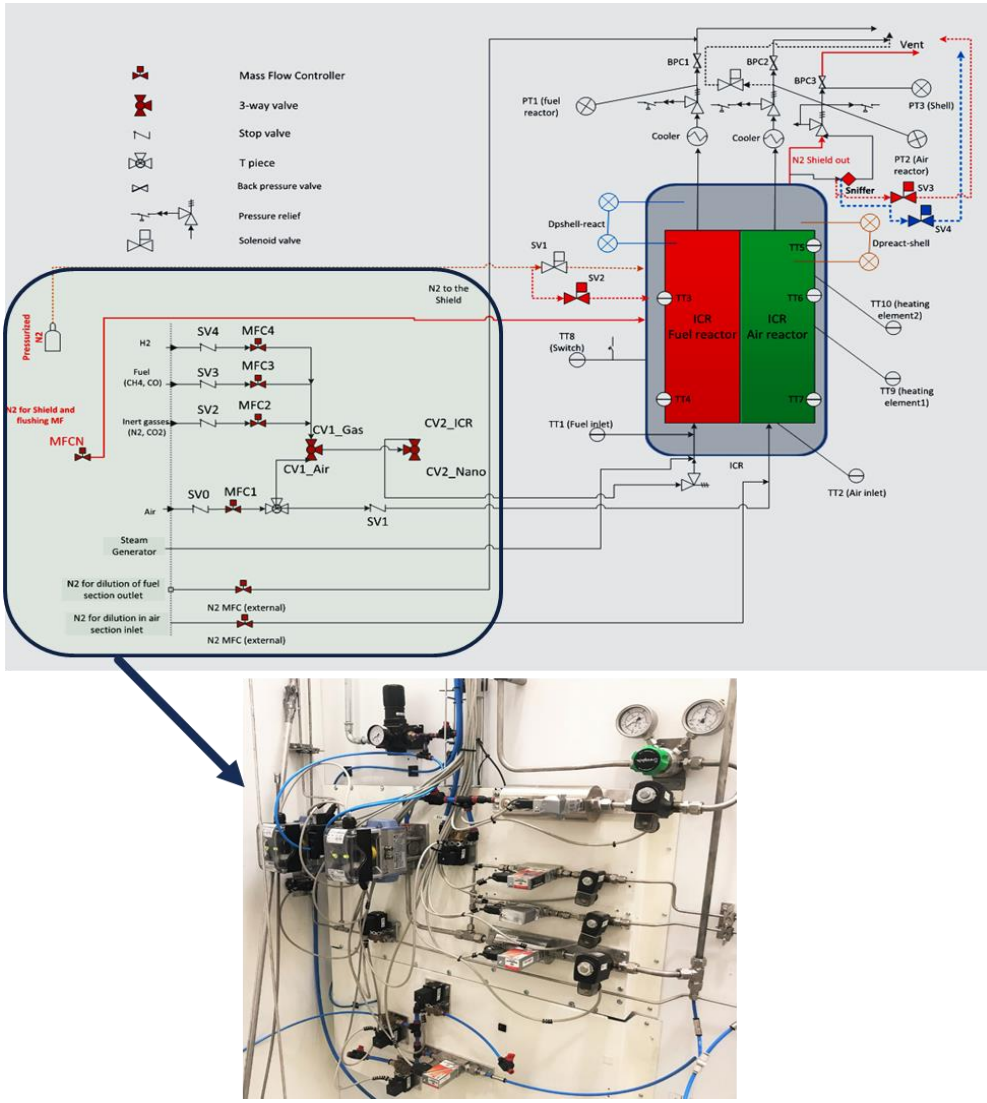

Figure 8. P&ID diagram of the ICR unit.

1.4 Objectives

The primary hypothesis to be investigated in this PhD work is that the Internally Circulating Reactor (ICR) can greatly simplify the design and scale-up of pressurized chemical looping technology for enhanced process efficiency and lower energy penalty for CO_2 capture. The main goal is to experimentally demonstrate that the ICR concept can achieve standalone pressurized autothermal operation for a number of different chemical looping technologies without encountering any major technical obstacles. The specific objectives are as follows:

- Develop and commission the Internally Circulating Reactor (ICR) for chemical looping applications at high pressure and temperature.
- Develop a comprehensive understanding for the effect of various operating parameters on the overall ICR performance measures; specifically, map out the operating conditions that enable achieving high fuel conversion and low gas leakage between the two reactor sections.
- Experimental demonstration of the ICR for chemical looping combustion, and chemical looping reforming process at realistic operating conditions in term of pressure, temperature, and fuel feed.
- Develop a process model using Aspen Plus to study the potential of applying the ICR concept for industrial applications and evaluate its performance against a conventional technology.

1.5 Contribution

The main contributions of this PhD thesis can be summarized as follow:

- Developed a first-of-its-kind experimental unit, the internally circulating reactor (ICR), for streamlining development of pressurized chemical looping technology.
- Delivered a first experimental demonstration of the ICR for chemical looping combustion and reforming processes at pressurized conditions up to 6 bar.
- Developed a comprehensive understanding for the effects of the various operating conditions on the ICR performances during chemical looping operation.
- Expanded the knowledge within the field of pressurized circulating fluidized-bed reactor.
- Provided a strong base for future scale-up efforts of the ICR concept.
- The results from this thesis were published through articles in scientific journals and presented in international conferences.

1.6 Thesis structure

The thesis is a collection of five papers, four of which are the thesis main focus on the experimental demonstration of the ICR concept, and one paper is a review paper on pressurized chemical looping processes. Chapter 2 presents a comprehensive literature review of pressurized chemical looping processes. Chapter 3 to Chapter 6 present the four papers that provide the main results of the thesis. Chapter 7 concludes the thesis with a summary of the main achievements obtained in the different papers and provides recommendations for future work.

1.7 List of Publications

The following list contains the publications developed during the work in this PhD thesis, and the presentation given in international conferences.

Papers in international journals:

[1] **Mogahid Osman**, Abdelghafour Zaabout, Schalk Cloete, Shahriar Amini, Internally circulating fluidized-bed reactor for syngas production using chemical looping reforming, Chem. Eng. J. 377 (2019) 120076.

[2] **Mogahid Osman**, Abdelghafour Zaabout, Schalk Cloete, Shahriar Amini, Mapping the operating performance of a novel internally circulating fluidized bed reactor applied to chemical looping combustion, Fuel Process. Technol. 197 (2020) 106183.

[3] **Mogahid Osman**, Abdelghafour Zaabout, Schalk Cloete, Shahriar Amini, Experimental demonstration of pressurized chemical looping combustion in an internally circulating reactor for power production with integrated CO2 capture, Chem. Eng. J. 401 (2020) 125974.

[4] **Mogahid Osman**, Abdelghafour Zaabout, Schalk Cloete, Shahriar Amini, Pressurized chemical looping methane reforming to syngas for efficient methanol production: experimental and process simulation study, (Under review, submitted to Advances in Applied Energy, 2021).

[5] **Mogahid Osman**, Mohammed.N. Khan, Abdelghafour Zaabout, Schalk Cloete, Shahriar Amini, Review of pressurized chemical looping processes for power generation and chemical production with integrated CO2 capture, Fuel Process. Technol. 214 (2021) 106684.

Presentations in international conferences:

[1] Fluidization XVI Conference, May (2019), Guilin, China.

[2] The 5th International Conference on Chemical Looping, September (2018), Utah, USA.

[3] The Greenhouse Gas Control Technologies Conference (GHGT-14), October (2018), Melbourne, Australia.

[4] International Conference on Chemical Reaction Engineering (ISCRE-25), May (2018), Florence, Italy.

[5] The 10th World Congress of Chemical Engineering, October (2017), Barcelona, Spain.

Chapter 2 Review of pressurized chemical looping process

This chapter is based on the following paper:

Review of pressurized chemical looping processes for power generation and chemical production with integrated CO_2 capture

Mogahid Osman, Mohammed.N. Khan, Abdelghafour Zaabout, Schalk Cloete, Shahriar Amini

Fuel Process. Technol. 214 (2021) 106684

Abstract

Chemical looping has great potential for reducing the energy penalty and associated costs of CO_2 capture from fossil fuel-based power and chemical production while maintaining high efficiency. However, pressurized operation is a prerequisite for maximizing energy efficiency in most proposed chemical looping configurations, introducing significant complexities related to system design, operation and scale-up. Understanding the effects of pressurization on chemical looping systems is therefore important for realizing the expected cost reduction of CO_2 capture and speed up the industrial deployment of this promising class of technologies.

This chapter reviews studies that investigated three key aspects associated with pressurized operation of chemical looping processes. First, the effect of pressure on the kinetics of the various reactions involved in these processes was discussed. Second, the different reactor configurations proposed for chemical looping were discussed in detail, focusing on their suitability for pressurized operation and highlighting potential technical challenges that may hinder successful operation and scale-up. Third, techno-economic assessment studies for these systems were reviewed, identifying the process configuration and integration options that maximize the energy efficiency and minimize the costs of CO_2 avoidance.

Prominent conclusions from the review include the following. First, the frequently reported negative effect of pressure on reaction kinetics appears to be overstated, implying that pressurization is an effective way to intensify chemical looping processes. Second, no clear winner could be identified from the six pressurized chemical looping reactor configurations reviewed. Further information on elements such as oxygen carrier durability, technical feasibility of downstream high-temperature valves and filters, and scale-up challenges will be required to select the best configuration. Third, the maximum reactor temperature imposes a major constraint for combined cycle power production applications, requiring an extra combustor after the reactor. Hydrogen production applications do not face such constraints and can approach the techno-economic performance of unabated benchmarks. Flexible power and hydrogen chemical looping plants appear promising for integrating renewable energy. Based on these findings, pressurized chemical looping remains a promising decarbonization pathway and further development is recommended.

Mogahid Osman wrote the first draft of the paper (except of the techno-economic analysis chapter, which was written by Mohammed N. Khan). All co-authors contributed on writing, reviewing and editing the paper.

2.1 Introduction

Greenhouse gas emissions from fossil fuel utilization can be reduced by several options that include i) improving the process efficiency, ii) switch to renewable energy sources, iii) replacement of coal by natural gas (containing less carbon content) and iv) applying Carbon Capture, Utilization and Storage (CCUS). According to the Intergovernmental Panel on Climate Change (IPCC), CCUS would play a major role in most mitigation scenarios to meet the global warming targets [4]. Four main categories have been explored for CO_2 capture technologies: 1) post-combustion, 2) pre-combustion, 3) oxy-combustion, and 4) chemical looping process [6]. For power production, the first three concepts incur a significant loss of efficiency and power output that has a large effect on the economics [7]. The chemical looping process is an alternative option that has the potential to intrinsically reduce the energy losses associated with CO_2 capture [9]. The chemical looping system carried is out in two steps; in the fuel reactor (FR) the fuel reacts with an oxygen carrier (metal oxide) to form CO_2 and H_2O; the reduced metal oxide is then circulated for re-oxidization in a flow of air in the air reactor (AR). The exothermic oxidation reaction in the AR produces heat that is utilized for power production [11,22,23]. Beyond power production, the chemical looping concept has been applied in the production of hydrogen [24–26], syngas [11,12,22] and oxygen [27,28]. Recent reviews on chemical looping process can be found in Adánez et al. [29], Mattisson et al. [30], Lyngfelt et al. [31], and Zhu et al. [32]. Figure 9. shows an overview of the various technologies that utilize oxygen carriers in a chemical looping system.

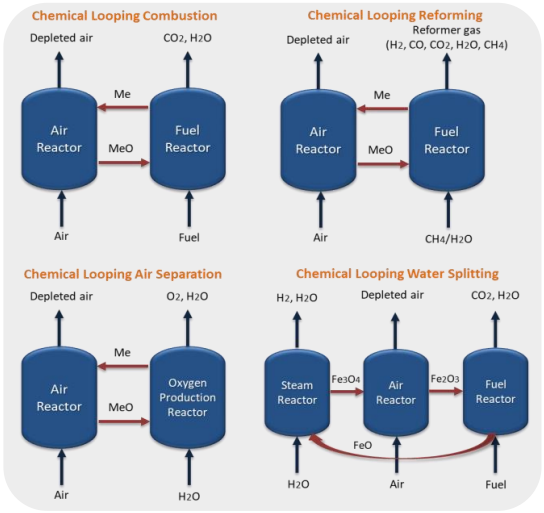

Figure 9. Chemical looping process for different applications.

In power generation, pressurized chemical looping has the potential for maximizing the power plant efficiency by using a combined cycle instead of the Rankine cycle used with atmospheric pressure boilers. The pressurized hot depleted air from the AR is used to drive a gas turbine (Brayton Cycle) followed by a heat-recovery steam generator (HRSG) for additional power generation (Rankine Cycle). The CO_2 rich stream from the FR could also be expanded and used for heat recovery for additional power generation, followed by water condensation then CO_2 compression and sequestration. Moreover, high-pressure combustion increases the temperature at which the steam in the FR outlet stream condenses; hence, some of the heat of condensation can be utilized within the process, which increases the thermal energy recovery from the fuel (the higher heating value instead of the lower heating value). This is especially interesting for CLC with natural gas given the high moisture content in the FR flue gas (2 parts H_2O and 1 part CO_2). The high temperature condensate can be utilized for preheating the water feed of the Rankine cycle, which reduces or eliminates the need of extracting part of the steam from the cycle and hence increasing the efficiency of the system (steam extraction is inevitable in atmospheric combustion process to achieve target feed water temperature).

Other benefits for high-pressure CLC (PCLC) operation include reduced power consumption for CO_2 compression or refrigeration steps, and increased heat transfer rates. Thermodynamic investigations have revealed that the integration of PCLC with a natural gas fired combined cycle (NGCC) can achieve a power efficiency of 52 to 55% (LHV), which is higher than NGCC with post-combustion CO_2 capture by 3-5% points [33,34]. For hydrogen production, high-pressure operation improves the overall efficiency and lowers the cost associated with hydrogen separation and compression [35]. For syngas production, high-pressure operation is required for improving the efficiency of syngas to liquids processes [35]. Moreover, high-pressure operation significantly reduces the process footprint (increasing pressure reduces the gas volume), thus resulting in more compact reactors.

Considering these advantages, several experimental and modelling studies, reported in the literature, investigated pressurized chemical looping systems. While elevated pressures fundamentally have a positive influence on the overall plant efficiency, there are many contradictions in the literature on the effect of pressurized conditions on the overall performance of chemical looping systems. Pressurized operation influences the process performance in terms of reaction kinetics, heat and mass transfer rate, CO_2 capture efficiency, product selectivity and fuel conversion. Considering these parameters, experimental campaigns in the literature were carried out in various systems and configurations such as pressurized

thermo-gravimetric analyzer (PTGA), fluidized-bed, fixed-bed and moving-bed systems. Likewise, modelling and simulation studies were carried out to gain insights into the effect of pressure on the behavior of several oxygen-carriers for chemical looping systems.

This chapter aims to establish a comprehensive review of the research outcomes of pressurized chemical looping processes with emphasis on kinetics, reactor configurations, and techno-economic studies. The different factors affecting the reaction kinetics in pressurized chemical looping are highlighted and the suitability of the various reactor configurations reported in the literature for pressurized operation is discussed based on their working principle and their level of advancement achieved to date.

2.2 Kinetic analysis

This section reviews studies conducted to reveal the effect of pressure on the kinetics of the reactions involved in the chemical looping systems. The section is divided into two sub-sections: oxygen carrier reactivity studies and kinetic models.

2.2.1 Oxygen carrier reactivity studies

In principle, there are three types of pressure effects on the reduction kinetics: 1) effect of total pressure at a constant fuel partial pressure, 2) effect of total pressure at a constant fuel molar fraction, and 3) effect of fuel partial pressure at a constant total pressure. The following three sub-sections classify and discuss the reported results based on the above-mentioned effects. The last section presents the results reported for the oxidation kinetics at pressurized conditions. Table 1 summarizes the various operating conditions used for studying oxygen carrier reactivity and kinetics under high pressure.

Table 1. Summary of the experimental techniques and operating conditions used for oxygen carrier reactivity and kinetics studies under high pressure.

Reference	Oxygen-carrier/Fuel	Experimental conditions
García et al. (2006) [36]	**OC:** CuO/Al_2O_3 Fe_2O_3/Al_2O_3 NiO/Al_2O_3 **Fuel**: CO and H_2	• 800°C • P: 1 - 30 bar **Type of Experiments:** • Constant gas partial pressure of 1 bar and different total pressures
Abad et al. (2007) [37]	**OC:** CuO/Al_2O_3 Fe_2O_3/Al_2O_3 NiO/Al_2O_3 **Fuel:** Syngas	• T: 550 - 950°C • P: 1 and 20 bar **Type of Experiments:** • Two kinds of experiments: constant partial pressure and constant volume fraction of the fuel gas

Siriwardane et al. (2007) [38]	**OC:** NiO/bentonite **Fuel:** Syngas	• T: 800°C • P: 1, 3.5, 7 bar **Type of Experiments:** • Constant fraction of the fuel gas
Gu et al. (2013) [39]	**OC:** Iron Ore (Hematite, Fe_2O_3) **Fuel:** CO	• T: 800°C • P: 1 and 6 bar **Type of Experiments:** • Constant volume fraction of the fuel gas
Zhang et al. (2014) [40]	**OC:** Iron ore (Hematite, Fe_2O_3) **Fuel:** Bituminous coal	• T: 950°C • P: 1, 5 and 10 bar • 18.9 % steam in N_2 used as gasifying agent **Type of Experiments:** • Constant fraction of the fuel gas
Luo et al. (2014) [41]	**OC:** Fe_2TiO_5 Iron-titanium composite metal oxide (ITCMO) **Fuel:** CH_4	• T: 950°C • P: 1-10 bar **Type of Experiments:** • Constant mole fraction of the fuel gas
Hamers et al. (2015) [42]	**OC:** CuO/Al_2O_3 $NiO/CaAl_2O_4$ **Fuel:** CO H_2	• T: 550 - 950°C • P: 1-20 bar **Type of Experiments:** • Two kinds of experiments: constant partial pressure of the fuel at 1 bar, constant gas mole fraction of the fuel at 20%
Deshpande et al. (2015) [43]	**OC:** Fe_2TiO_5 Iron-titanium composite metal oxide (ITCMO) **Fuel:** H_2	• T: 900°C • P: 1-10 bar **Type of Experiments:** • Three kinds of experiments: 1) constant partial pressure, 2) constant mole fraction of the fuel gas, 3) constant total pressure with various partial pressure of the fuel
Lu et al. (2016) [44]	**OC:** ilmenite ore (titanium-iron oxide, $FeTiO_3$) **Fuel:** CO	• T: 950°C • P: 16 and 24 bar **Type of Experiments:** • Two kinds of experiments: 1) constant partial pressure, 2) constant total pressure with various fuel partial pressure
San Pio et al. (2017) [45]	**OC:** CuO/Al_2O_3 **Fuel:** H_2	• T: 800°C • P: 1-10 bar **Type of Experiments:** • Two kinds of experiments: 1) constant partial pressure of H_2 and constant gas flowrate, 2) constant partial pressure of H_2 and increasing the gas flowrate with pressure
Tan et al. (2017) [46]	**OC:** ilmenite ore (titanium-iron oxide, $FeTiO_3$) **Fuel:** Natural gas	• T: 750 - 950°C • P: 6, 9, 16 bar **Type of Experiments:** • Two kinds of experiments: 1) constant partial pressure, 2) constant total pressure with various fuel partial pressure
Tan et al. (2017) [47]	**OC:** ilmenite ore (titanium-iron oxide, $FeTiO_3$) **Fuel:** CH_4	• T: 850 - 950°C • P: 6-16 bar **Type of Experiments:**

		• Two kinds of experiments: 1) constant partial pressure, 2) constant total pressure with various fuel partial pressure
Chen et al. (2017) [48]	**OC:** ilmenite ore (titanium-iron oxide, $FeTiO_3$) Red mod (bauxite residue contains ~50% Fe_2O_3) **Fuel:** Coal char	• T: 950°C • P: 1, 2, 4, 6 bar **Type of Experiments:** • Constant amount of solid-fuel and with increasing the gas flowrate linearly with pressure (constant superficial gas velocity). • • Steam used as gasification agent.
Rana et al. (2019) [49]	**OC:** ilmenite ore (titanium-iron oxide, $FeTiO_3$) **Oxidation agent:** Air	• T: 800 - 1050°C • P: 1-16 bar **Type of Experiments:** • Two kinds of experiments: 1) constant O_2 partial pressure, 2) constant total pressure with various O_2 partial pressure
Díez-Martín et al. (2018) [50]	**OC:** CuO **Oxidation agent:** Air	• T: 850°C • P: 1-10 bar **Type of Experiments:** • Constant O_2 concentration

2.2.2 Constant fuel partial pressure

Experimental studies conducted at constant fuel partial pressure while increasing the total pressure by dilution with inert gas revealed a contradicting effect of the pressure on the reduction rates for all oxygen carriers and fuels studied. For instance, García et al. [36] conducted a kinetics investigation using a pressurized thermogravimetric analysis (PTGA) for different oxygen carriers based on Cu, Fe and Ni in a pressure range of 1 to 30 bar. The reduction rates were found to decrease with increasing the total pressure. It was reported that the reaction rate was highly affected by the gas dispersion of the system, especially during the initial stage of introducing the reacting gas to the sample cell. It should be noted that, the term “gas dispersion” used by the authors of this study and on the following studies is most properly referred to as "the external mass transfer resistance", i.e. the finite rate of reacting species transport to the outer surface of the particles. The work of Lu et al. [44] showed that the reduction of ilmenite ore (a titanium-iron oxide, $FeTiO_3$) with CO at constant partial pressure and increasing the total pressure (by increasing CO_2 partial pressure) revealed a negative effect of pressure. They attributed this result to the increase of CO_2 partial pressure along with the total pressure, which from a thermodynamic point of view has a negative effect on the reduction rate. Tan et al. [46,47] extended the kinetic study of ilmenite ore with CH_4 and simulated natural gas as fuel (simulated natural gas is a gas mixture similar to the natural gas composition). The results showed that increasing the total pressure at constant fuel feed and CO_2 partial pressure reduced the reduction rate of the ilmenite ore. Increasing the temperature reduced the negative impact of

the total pressure during the reduction phase. Tan et al. [46,47] explanation to the adverse effect of the total pressure was that increasing total pressure slowed down the product gas diffusion away from the gas-solid interface, and hence reduced the reactant gas ability to reach the active sites.

Hamers et al. [42] revealed the same phenomenon in the reduction kinetics of Cu and Ni based oxygen carriers at operating pressures up to 20 bar, which was attributed to the competitive adsorption of the inert gas with the reactive gases on the oxygen carrier surface. With higher inert dilution, larger space of the cavities was being blocked reducing the reaction rate. This effect becomes more pronounced at higher total pressure which is translated by the observed higher fluctuations in the experimental transient solids conversion at higher pressures (Figure 10a). This is in line with the observations in the works of García et al. [36] and Lu et al. [44].

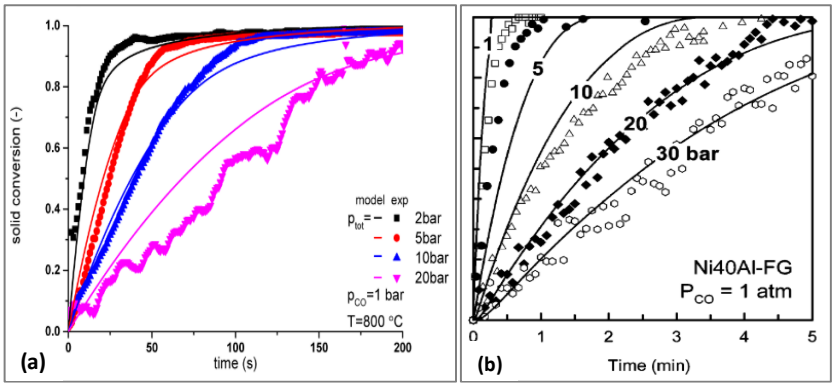

Figure 10. Effect of the total pressure on the reduction kinetics of Ni-based oxygen carriers at a constant fuel partial pressure (1 bar) at 800°C. The markers show the experimental data, and the lines show the model predictions. a) [42] "Adapted with permission, Copyright (2015) ACS ", b) [36] "Adapted with permission, Copyright (2006) ACS ".

To minimize the effect of the gas dispersion (external mass transfer resistance) with elevated pressures; Deshpande et al. [43] used a constant gas space velocity in a reduction study of an ilmenite-based oxygen carrier. They showed an increase in the reduction rate with increasing the total pressure, thus counteracting the negative impact of gas dispersion in the unit cell that occurs when the flowrate was maintained constant. The work of San Pio et al. [45] supported this finding as shown in Figure 11, showing that increasing the molar flowrate with the total pressure counteracted the negative effect of pressure on the reduction kinetics. This study was conducted using a Cu-based oxygen carrier and H_2 as fuel in a pressure range of 1 to 10 bar.

Looking through these results (Figure 11), it can clearly be seen that the external mass transfer resistance negatively affects the reduction kinetics and should partially be avoided by increasing the total molar flowrate with increasing the total pressure.

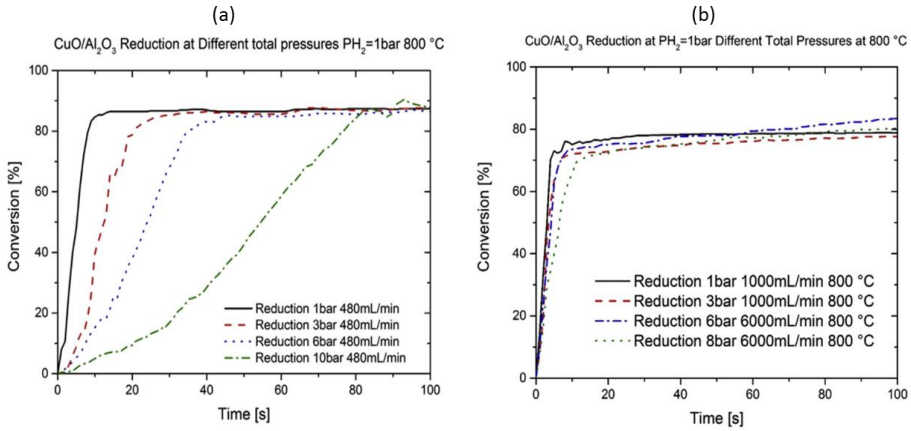

Figure 11. Reduction conversions with different total pressure and constant fuel partial pressure at 800°C, a) at constant molar flowrate, b) at different molar flowrate [45], "Adapted with permission, Copyright (2017) Elsevier BV".

Similar results of the negative effects of total pressure on the reduction kinetic have been also reported in other non-catalytic gas-solid reactions; for example, for the capture of H_2S and CO_2 by calcium-based sorbents [51–57], and the coal gasification process [58,59]. Although no consistent explanations were proposed for the negative effects of pressure, there was a common explanation that the intra-particle diffusion was hindered with increasing total pressure. The gas diffusivity coefficient combines both the molecular and Knudsen diffusivities. The molecular diffusivity is inversely proportional to the system pressure; however, the Knudsen diffusivity is independent of pressure as it depends only on the structure of the pore network. Therefore, increasing total pressure decreases the molecular diffusivity, which leads to a decrease in the effective gas diffusivity that could lead to the decrease in the overall conversion rate [60].

The external mass-transfer resistance could also be the main reason for the negative effect of the total pressure in all these studies; given that the authors used a constant gas flowrate among all pressurized kinetic tests. Increasing the total pressure of the system lowers the volumetric and superficial velocities of the gas; this will increase the time required for the gas to diffuse through the boundary layer to the particle surface, which would result in increased external

mass-transfer resistance. By using higher superficial velocity, the boundary layer thickness decreases and therefore the film diffusion will no longer be a limiting step, and the observed reaction rate approaches the intrinsic reaction rate. Hecker et al. [59] studied the kinetic of char oxidation at high total pressure and constant O_2 partial pressure while increasing the total flowrate with pressure. They reported that the intrinsic char oxidation rate, activation energy, and oxygen reaction order were found to be independent of the total pressure implying that maintaining the superficial gas velocity constant had successfully reduced the negative effect of the external mass transfer on the observed reaction rates. A positive effect of pressure was reported by Butler et al. [61] for the kinetic of CO_2 carbonation using un-diluted CO_2 in a pressure range of 5 to 20 bar. Increasing the carbonation pressure was found to increase the carbonation rate and the calcium utilization over 100 cycles.

The reactant gas flowrate is not the only parameter that affects the intrinsic reaction rate but also other factors such as the solid weight, the solid holder geometry and the solid-particle dispersion [62]. In order to obtain a reliable kinetic parameters, all these factors should be optimized during the kinetics experiment to isolate any physical effect on the reaction kinetic. Kibria et al, [63] proposed a systematic experimental procedure to minimize the effects of the rate-influencing factors during CO_2 gasification of biomass char. Their strategy involves testing the effects of all the rate-limiting factors during TGA experiments and optimize the experimental conditions accordingly. Figure 12 shows the results of the gasification rate for the changes in the various factors and the optimized condition, which revealed the highest reaction rate as it was free from all heat and mass transfer limitations. Pressurized gas-solids reaction kinetics exhibits more intrusion of the transport effects in the reaction rate measurement; therefore, a careful consideration of all physical factors is highly recommended for future kinetics studies to ensure accurate design and operation of the large-scale reactor.

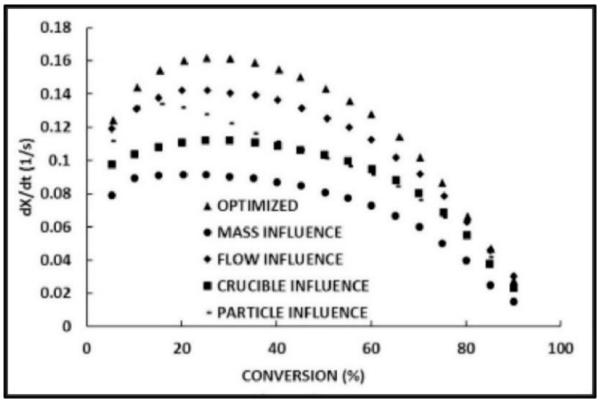

Figure 12. The reaction rate during CO_2 gasification of biomass char for various rate-influencing factors and the optimized condition (triangle) [63], "Adapted with permission, Copyright (2019) Elsevier BV".

Fewer studies were reported for the kinetic of solid-fuel chemical looping combustion/gasification at elevated pressure [40,48,64]. In a typical coal-based CLC system, the reactions between coal, oxygen carrier and the gasification agent (H_2O or CO_2) occurs as a results of various reactions as following:

$$\text{Coal} \rightarrow \text{Char} + \text{Volatiles} \quad (2\text{-}1)$$

$$\text{Char} + H_2O \rightarrow CO + H_2 \quad (2\text{-}2)$$

$$\text{Char} + CO_2 \rightarrow 2CO \quad (2\text{-}3)$$

$$CO + H_2O \rightarrow CO_2 + H_2 \quad (2\text{-}4)$$

$$H_2 + \text{Metal Oxide} \rightarrow \text{Reduced Metal Oxide} + H_2O \quad (2\text{-}5)$$

$$CO + \text{Metal Oxide} \rightarrow \text{Reduced Metal Oxide} + CO_2 \quad (2\text{-}6)$$

Coal pyrolysis (Equ.(2-1)) is the first stage of the CLC process, followed by char gasification (Equ.(2-2),(2-3)). The rate of char gasification is much slower than that of coal pyrolysis. The WGSR (Equ.(2-4)) catalyzed by the OC, also affects the composition of the final gaseous products. The presence of the OC primarily improves the gas phase conversion for complete oxidation of the combustible gases (Equ.(2-5),(2-6)); thus reducing hydrogen inhibition effect on char gasification and ultimately promoting char conversion further. Effects of pressure on the rate of coal CLC reactions is affected by the two stages (coal pyrolysis and char gasification) and the interaction of mass transfer and reaction of gas-solid and solid-solid phases.

Zhang et al, [40] carried out kinetic investigation of coal chemical looping combustion using a pressurized TGA. Iron ore was used as oxygen carrier at a reaction pressure of 1, 5 and 10 bar. Their results showed that the reaction rate decreased with increasing pressure in the initial coal pyrolysis stage, however, in the subsequent char gasification stage, the reaction rate was found to improve at higher pressure. The overall reaction rate was found to be increasing with increasing the pressure up to 5 bar then decreased at 10 bar, which was attributed to the negative effect of pressure on the coal pyrolysis stage [40]. Chen et al, [48] studied the effects of pressure

on the reactivity of ilmenite and red mud OCs (red mud is a bauxite residue contains ~50% Fe_2O_3) on char gasification reactions using a fluidized-bed system. Figure 13 showed the effect of pressure on the gasification rate for the various OCs and without the OCs. For all cases, increasing pressure in the range of 1 to 6 bar led to increasing the char gasification rate. The red mud OC (line-2 in Figure 13) improves the gasification rate by about 140-190% compared to conventional steam gasification without OC (line-1 in Figure 13). The promotion effect of the red mud OC is due to its catalytic functionality and to the rapid consumption of syngas, hence decreasing the inhibition effects of syngas on char gasification. Similar results were reported by Guo et al. [64] for char gasification using Fe_2O_3/Al_2O_3 as OC in a pressure range of 1 to 12 bar.

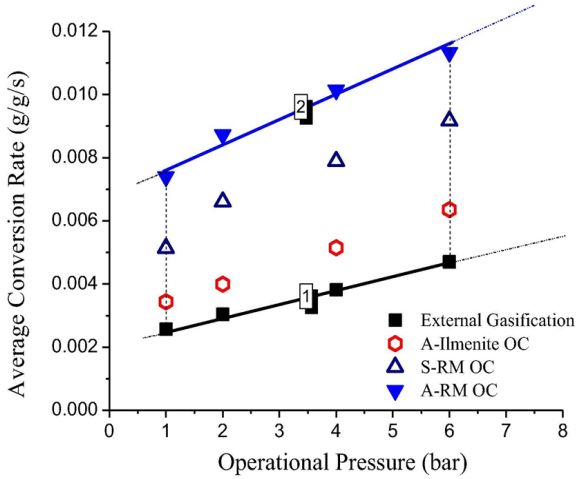

Figure 13. The average gasification rate of PCLC and external gasification at various pressures [48], "Adapted with permission, Copyright (2017) Elsevier BV".

2.2.3 Constant fuel molar fraction

Increasing the total pressure while keeping the fuel molar fraction constant, would improve the reduction rate (due to increased fuel partial pressure). However, reduction kinetic studies revealed contradicting effects on the reaction rates among different studies. García et al. [36] showed a slight decrease in the reduction rate with increasing the total pressure up to 30 bar while keeping the molar fraction of the fuel constant at 10%. They stated that various parameters affected the experimental results simultaneously including, gas dispersion, total pressure and partial pressure. Similar result was obtained by Hamers et al. [42] which was attributed to the decrease of the oxygen vacancies at higher pressures.

Positive effects of the pressure on the reduction kinetic were shown by Siriwardane et al. [38] using NiO based oxygen carrier supported on bentonite (bentonite is an aluminum phyllosilicate clay) for CLC with simulated syngas (12% CO_2, 36% CO, 25% He, and 27% H_2). Increasing the total pressure while keeping the reacting gas molar fraction constant showed an increase in the reduction rate, which was more significant at higher solid conversion. The positive effect of pressure at constant fuel molar fraction on the reduction rate is consistent with the work of Luo et al. [41] and Deshpande et al. [43] on the reduction kinetics of iron-titanium composite oxygen carrier (Fe_2TiO_5) with H_2 and CH_4. At a constant fuel molar fraction of 50%, the reduction rate with H_2 was doubled when increasing the pressure from 1 to 10 bar, while CH_4 reduction rate increased by 5 time the atmospheric reduction rate. The increase of the reduction rate with pressure was due to the use of constant space velocity for all pressures, which decreased the extent of the negative effect of gas dispersion with increasing the pressure [41,43]. Another conclusion shown in the works of Luo et al. [41] and Deshpande et al. [43] was that the reduction of Fe_2TiO_5 with CH_4 followed three distinct stages with respect to the reduction rate, resulting in a sinusoidal reaction conversion curve as a function of time [41,43]. Higher operating pressure resulted in early occurrence of carbon deposition (at lower solid conversion), which was consistent with the thermodynamic analysis. Figure 14Figure 14. shows the reduction conversion curve obtained using CH_4 between 1 and 10 bar, where the three distinct reduction stages can clearly be identified. After analyzing this result with calculating the reduction rate for each stage, Deshpande et al. [43] have shown that a plateau in the reduction rate of stage I and III was found (Figure 14), while an exponential increase of the reduction rate was found for stage II [43]. The overall reduction rate was mostly affected by stage II reduction rate which is the slowest stage (the rate determining step) [43].

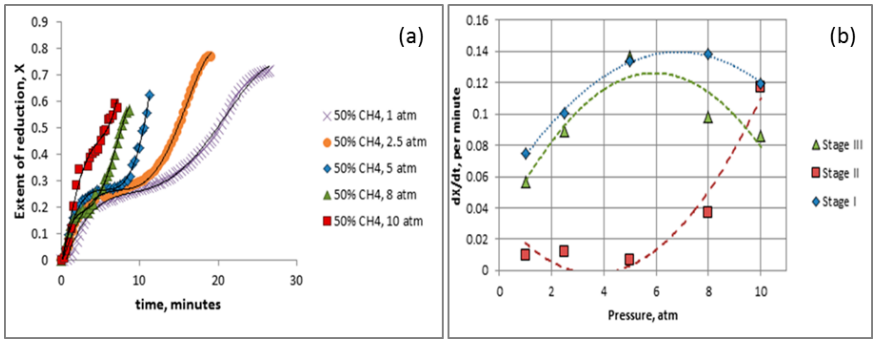

Figure 14. Effect of the total pressure on the reduction kinetics of iron-based oxygen carriers with a constant fuel mole fraction (CH_4=50%) at 950°C, a) the reduction conversions, b) the reaction rate for the three-step reduction [43], "Adapted with permission, Copyright (2015) ACS".

2.2.4 Constant total pressure

Conducting oxygen carrier reduction at constant total pressure while increasing the fuel partial pressure increases the fuel concentration and hence increases the contribution of the gas phase to the overall reaction rate, and thus higher solid reduction rates are expected. Deshpande et al. [43] demonstrated this positive effect using H_2 as fuel and iron-titanium composite as oxygen carrier. The work of Luo et al. [41] and Tan et al. [46,47] also revealed the same conclusion using ilmenite ore and CO, CH_4 and simulated natural gas as fuel (simulated natural gas is a gas mixture similar to the natural gas composition). They found that increasing the fuel partial pressure while keeping the same fuel/CO_2 ratio and total pressure boosted the ilmenite reduction rate. However, the oxygen carrying capacity decreased with increasing the fuel partial pressure, especially at higher temperature. The authors attributed this negative effect to the fast reaction rate at high partial pressure that may have caused coverage of the oxygen carrier surface that hindered further reaction to happen. The faster the reaction rate, more of the OC active sites will be covered quickly and hence the product gas diffusion become slower, controlling the reaction process, which hinders further reactions. With higher temperature, the involved reactions proceed even faster so this effect became more pronounced.

2.2.5 High pressure oxidation kinetics

Fewer studies were conducted for the oxidation kinetics at high pressure. Rana et al. [49] reported oxidation kinetics of a natural ilmenite ore at a temperature of 900°C and a pressure range of 1 to 16 bar. The results showed a negative effect of pressure on the oxidation rate when keeping the O_2 partial pressure constant. The authors did not provide an explanation for this effect; however, a possible explanation could be that the gas flowrate was not high enough to overcome the increased mass transfer resistance with pressure. When keeping the O_2 molar fraction constant, Rana et al. [49] revealed a positive effect on increasing the total pressure up to 8 bar, above which increasing the pressure had a negligible effect on the oxidation rate. Díez-Martín et al. [50] revealed a similar result for the oxidation kinetics of a CuO-based OC, in which increasing the total pressure (1 to 10 bar) while fixing the O_2 molar fraction resulted in a slight increase in the oxidation rate.

2.2.6 Kinetic Models

In this section, the kinetic models reported for high-pressure redox reactions are presented and discussed. The fuel reaction with the oxygen carrier is considered as a non-catalytic gas-solid reaction and the design and performance of the chemical looping reactors are strongly

dependent on the kinetics of these reactions. Therefore, a kinetic model able to accurately predict the overall reaction rate is essential for successful chemical looping process design. To estimate the kinetic parameters, two approaches were followed in the literature for the inclusion of the pressure effects on the kinetic model of the redox reactions. One approach is by incorporating an empirical fitting parameter for the pressure to a kinetic model developed based on data conducted at atmospheric conditions [36,42,65]. The second is by developing the kinetic model based on pressurized experiments [44,46,47]. The second one is the most accurate approach to capture the effects of pressure in a kinetic model that can be utilized for design and optimization of the larger scale process. Table 2. summarizes the different kinetic models and kinetic parameters reported by different studies on pressurized chemical looping process.

García et al. [36] applied the changing grain size model (CGSM) to the reduction reactions of Cu-, Ni- and Fe- based oxygen carriers. They considered two different grain geometries based on the structural differences and the preparation methods of the oxygen carriers. CuO-based OC prepared by impregnation method while Fe- and Ni-based OC prepared by freeze-granulation method. A SEM-EDX analysis of the three OC showed that Fe- and Ni-based OC had a granular structure while the Cu-based OC appears to be well-dispersed in the porous surface of the support structure. Accordingly, a spherical grain was considered for Fe- and Ni-based oxygen carriers, while a plate-like geometry was considered for the CuO-based oxygen carrier. The CGSM assumes that a number of uniform grains form the solids particles and it individually reacts based on a shrinking core model. The grain size changes as the reaction progresses, while the unreacted core shrinks. In their study, the kinetic parameters were obtained based on atmospheric pressure experiments, while an empirical parameter was used to fit the experiments conducted at higher pressure. The equations that describe the CGSM are shown in Table 2. , where the kinetic constant follows the temperature-dependence Arrhenius equation as follow:

$$k = k_0\, e^{-E/RT} \tag{2-7}$$

The apparent pre-exponential factor was estimated based on the total pressure and the pre-exponential factor obtained at atmospheric pressure as in Equ. (2-8) below:

$$k_{0,p} = \frac{k_0}{P^d} \tag{2-8}$$

Various kinetic parameters were obtained depending on the reaction and oxygen carrier considered, the resulted activation energy and reaction order are listed in Table 2.

The changing grain size model (CGSM) was also used by Lu et al. [44] for the reduction of the ilmenite ore with CO. In this study, they applied the model to data obtained at high pressure (16 bar). The reduction rate was accurately captured by the model for conversions below 70%. The activation energy and the reaction order values are listed in Table 2. Hamers et al. [42] developed a particle model with considering reaction kinetics, molecular diffusion, and Knudsen diffusion to capture the reduction rate inside the OC particles (NiO-based OC). They followed the same approach of García et al. [36] by extracting the kinetics parameters using experiments conducted at atmospheric pressure and by applying fitted parameters for the pressurized experiments. The OC particles used have a particle size of 1.1 mm, which is suitable for packed-bed chemical looping reactor configuration (to maintain a low pressure drop over the reactor). Using a large OC particle could impose a significant influence on the internal diffusion limitations that could lead to decreasing the effective reaction rates. However, the results of Hamers et al. [42] showed that increasing the pressure led to decreasing the effects of the diffusion limitations, which was attributed to the decrease in the reaction rates and the increase in the diffusion fluxes caused by Knudsen diffusion.

Tan et al. [46,47] adopted a kinetic model based on a phase-boundary-controlled mechanism with a contracting sphere for the reduction of ilmenite ore with methane and simulated natural gas. Tan et al. [46,47] used TGA experiments conducted at 9 and 16 bar to estimate the kinetic parameters. Table 2. listed the resulted activation energies at 9 and 16 bar. The model was able to capture the experimental results for a conversion ratio up to 70%.

Zhang et al. [65] described the reduction rate of iron-based oxygen carrier with CO as fuel considering an adapted random pore model (as shown in Table 2.). The random pore model avoids the assumption of the grain model of constant grain and shape factors that in reality change in size during the reaction. The model incorporates the pore size distribution, pore growth and coalescence, which affects the diffusion inside the pores and surface area for reaction, all of which can be related to the initial properties of the oxygen carrier particles undergoing the reaction. These properties determine whether the overall reaction is reaction controlled or reaction-diffusion controlled or a combination of these as described by Everson et al. [66]. The model also incorporates several resistances that might be the reduction rate limiting steps, including external mass transfer, intra-particle diffusion, product layer diffusion,

and chemical reaction. The model was developed using experiments carried out at atmospheric pressure and applied to the pressurized reaction kinetics up to 5 bar. The model indicated that the reduction of Fe_2O_3/Al_2O_3 exhibits a surface reaction controlled mechanism. The reaction order for surface reaction was close to 1 at 3 bar. The activation energy for the Fe_2O_3/Al_2O_3 were found to be (102 $kJ.mol^{-1}$) higher than those for the pure Fe_2O_3 oxygen carrier particles (61 $kJ.mol^{-1}$) and was attributed to the effect of Al_2O_3 support material on the reaction mechanism [65]. The presence of Al_2O_3 support improves the product layer diffusivity and hence enhances solid state diffusion facilitating the interaction of the active solid surface to the reducing gas [65].

Table 2. Summary of the different kinetic models and kinetic parameters reported by different studies on pressurized chemical looping

References	Experimental conditions	Kinetics Model	Kinetic Parameters
García et al. (2006) [36]	▪ OC: Cu, Fe and Ni based ▪ Fuel: CO and H_2 ▪ Pressure: 1 - 30 bar ▪ Kinetic parameters obtained at atmospheric pressure ▪ Fitted parameter (d) used for pressurized experiments	The changing grain size model (CGSM) under chemical reaction rate control. Spherical grains: $\frac{t}{\tau} = 1 - (1 - X)^{1/3} \qquad \tau = \frac{\rho_m r}{bk(C^n - C_{eq}{}^n)}$ Plate-like geometry: $\frac{t}{\tau} = X \qquad \tau = \frac{\rho_m L}{bkC^n} \quad k_{0,p} = \frac{k_0}{P^d}$	Reduction: $k_0 = 5.9 \times 10^{-6}$ - 2.3×10^{-3} E = 14 – 33 kJ.mol^{-1} n = 0.5 – 1.0 d = 0.47 – 1.03 Oxidation: $k_0 = 4.7 \times 10^{-6}$ – 1.8×10^{-3} E = 7 – 15 kJ.mol^{-1} n = 0.2 – 1.0 d = 0.46 – 0.84
Lu et al. (2016) [44]	▪ OC: ilmenite ore ▪ Fuel: CO. ▪ Total Pressure: 16 bar ▪ P_{CO}: 3.2 - 8.0 bar ▪ Temperature: 850 - 1050°C	The changing grain size model $\frac{t}{\tau} = 1 - (1 - X)^{1/3}$ $\tau = \frac{\rho_m r_g}{b k_s P_G^n}$	Reduction: $k_0 = 2.46 \times 10^{-2}$ (mol m^{-2} Pa^{-n} s^{-1}) E = 115 kJ.mol^{-1} n = 0.67
Hamers et al. (2015) [42]	▪ OC: NiO and CuO. ▪ Fuel: CO. ▪ Pressure: 1 - 20 bar ▪ Kinetic parameters obtained at atmospheric pressure ▪ Fitted parameter (d) used for pressurized experiments	copper: $r_i = \varepsilon_{g,p} k_0 \exp\left[\frac{-E_{act}}{R \cdot T}\right] C_g^n \left(\frac{p_{tot}}{10^5}\right)^{-q}$ nickel: $r_i = \frac{\varepsilon_{s,p} \rho_s \omega_{act}^0}{b \cdot M_j} \frac{dX}{dt} \qquad \frac{dX}{dt} = \frac{\frac{3C_g^n}{b \cdot r_0 \cdot C_s}}{\left(\frac{1}{k}(1-X)^{-\frac{2}{3}} + \frac{r_0}{D}(1-X)^{-\frac{1}{3}} - \frac{r_0}{D}\right)}$	Reduction: n = 0.6 – 0.8 d = 0.47 – 1.03 Oxidation: n = 0.2 – 1.0 d = 0.46 – 0.84

Tan et al. (2017) [47]	▪ OC: ilmenite ore ▪ Fuel: Methane ▪ Total Pressure: 9 and 16 bar ▪ Temperature: 850 - 930°C	Phase-boundary controlled model with contracting sphere: $kt = 1 - (1 - X_r)^{1/3}$	P = 9 bar: A = 0.17 s^{-1} E = 28.2 $kJ.mol^{-1}$ P = 16 bar A = 21.82 s^{-1} E = 76.4 $kJ.mol^{-1}$
Tan et al. (2017) [46]	▪ OC: ilmenite ore ▪ Fuel: Methane, Natural gas mixture ▪ Total Pressure: 9 bar ▪ Temperature: 750 - 900°C	Phase-boundary controlled model with contracting sphere: $kt = 1 - (1 - X_r)^{1/3}$	E = 69 $kJ.mol^{-1}$ (pure CH_4) E = 56 $kJ.mol^{-1}$ (Natural gas mixture)
Zhang et al. (2018) [65]	▪ OC: Fe_2O_3/Al_2O_3 ▪ Fuel: CO ▪ Total Pressure: 1 - 5 bar ▪ Temperature: 450 – 700°C ▪ Kinetic parameters obtained at atmospheric pressure	Adapted random pore model: $k' = \frac{k'_{s,0} c_{CO,s} S_0 (1 - X)\sqrt{1 - \psi \ln(1 - X)}}{(1 - \varepsilon_0)(M_{Fe_2O_3} c_{CO,b})}$	E = 102 $kJ.mol^{-1}$ k_0 = 1.8 x 10^{-3} (mol m^{-2} Pa^{-n} s^{-1})

2.3 Reactor analysis

In this section, the different reactor configurations proposed and investigated for pressurized chemical looping system are presented and discussed. The section is divided into four sub-sections: 1) Fluidized-bed, 2) Fixed-bed, 3) Moving-bed and 4) Rotating-bed reactors.

2.3.1 Fluidized-bed Reactor

The fluidized-bed reactor is the most widely used configuration for chemical looping systems [31]. For atmospheric operation, extensive investigations had been conducted using the dual circulating fluidized-bed reactor at a lab and pilot scales [31,67], however, fewer studies were reported for pressurized operation. In principle, the main effects of pressure on the fluidization characteristics are related to the increase of the gas density. Solid-solid interactions are not directly changed with elevated pressure due to the rigidity of the solids [68], but a denser gas increases the gas-particle drag, which also leads to less solid-solid collisions. As a result, it produces a more homogeneous gas-solid flow structure and decreases the incipient fluidization velocity.

Using electrical capacitance tomography (ECT), Rhodes et al. [69] revealed that for Geldart B particles, U_{mf} slightly decreases with pressure whilst bed-voidage at U_{mf} (ε_{mf}) was unaffected. Recently, the use of a borescopic technique was adopted to study the hydrodynamics of a fluidized-bed at elevated pressure [70]. The technique allows image visualization of the interior of the fluidized bed during the pressurized fluidization. The results revealed that, with increasing the pressure, the solids radial distribution becomes more or less uniform depending on the superficial gas velocity. Moreover, it was shown that the bubble size decreased in the central regions and increased near the wall regions with increasing the pressure [70]. Table 3 summarizes the effects of pressure on the main hydrodynamic parameters of fluidized-bed [71]. More extensive review on the effects of pressure on the hydrodynamic of fluidized-bed can be found in Grace et al. [72] and Chaouki et al. [73]. The following sections presents the current research advancements on the use of fluidize-bed reactor for pressurized chemical looping applications.

Table 3. Pressure effects on the hydrodynamics of fluidized-bed reactor.

Hydrodynamic parameter	Effect of pressure
Minimum fluidization velocity u_{mf}	• Increasing pressure decreases u_{mf}. This effect becomes more pronounced as the particle size increases.

Bed voidage	• There is no clear correlation between pressure increase and bed expansion. • ε_{mf} is independent of pressure. • ε_{mb} increases with pressure for particles close to the group A-B boundary.
Bubbling characteristics	• High pressure results in smaller, more frequent bubbles. These effects are more pronounced for group A particles than for group B ones.
Entrainment and elutriation	• The bubble flow u-u_{mf} increases with pressure, leading to higher entrainment rate. • The terminal velocity decreases with increasing pressure (due to the increase in gas density), hence enhancing the entrainment/elutriation rate.
Hydrodynamic scaling	• Unlike atmospheric fluidized-bed reactors, cold flow laboratory model (operating with air at ambient temperature and atmospheric pressure) of a pressurized fluidized-bed at 12 bar and 860°C is approximately the same size as the commercial unit [74].

2.3.1.1 Dual circulating fluidized-bed reactor

Wang et al. [75] from Xi'an Jiaotong University conducted chemical looping combustion of coke-oven gas (COG) using a high-pressure circulating fluidized-bed system. Four types of oxygen carriers, composed of Fe_2O_3/CuO and $MgAl_2O_4$, have been investigated. The laboratory unit was designed for gaseous fuel for a fuel power range of 3-10 kW_{th}. The experiments were completed at a reactor pressure of 3 bar and temperatures up to 950°C. The experimental results showed that the COG conversion increases from 69.8% at 750°C to 92.33% at 900°C. After successful continuous operation of the unit for 15 hours, it revealed high fuel reactivity, and all the OC maintained its stability. However, the 3 bar operation pressure could be too low to show the main challenges that may arise from a pressurized CLC system.

Xiao et al. [76] from Southeast University, China, carried out an experimental study on a 50 kW_{th} pressurized dual circulating fluidized-bed reactor (Figure 15) to investigate CLC of bituminous coal using an iron-based oxygen carrier. The FR and AR were designed to operate at fast fluidization and turbulent fluidization regimes, respectively. Three operating pressures have been studied (1, 3 and 5 bar) while maintaining temperature constant; 950°C in FR and 970°C in AR. High pressure operation was found to improve carbon conversion, CO_2 capture purity and combustion efficiency. This improvement was attributed to the combined positive effect that elevated pressure has on the iron oxygen carrier reduction and coal gasification. Controlling the experiments at elevated pressure encountered some difficulties compared to the

atmospheric pressure operation. Solids elutriation rate increased with pressure due to a decrease in the FR cyclone capture efficiency at elevated pressure [76]. This challenge can be circumvented by dedicated cyclone design for a given elevated operating pressure.

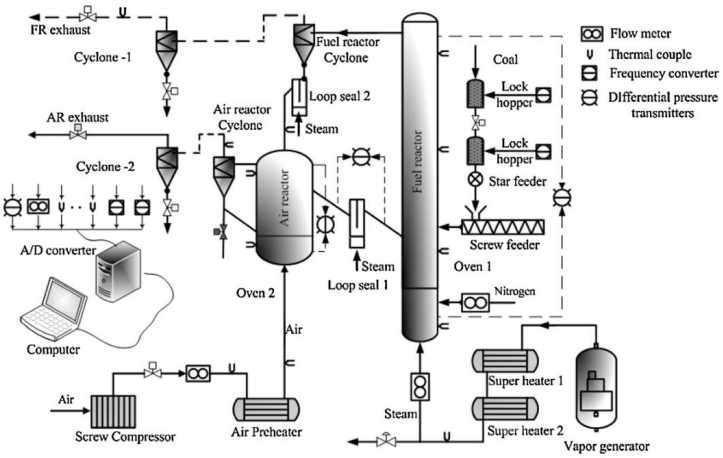

Figure 15. A schematic diagram of the 50 kW_{th} pressurized dual circulating fluidized-bed reactor [76], "Adapted with permission, Copyright (2012) Elsevier BV".

Another 50 kW_{th} direct coal-fueled pressurized CLC unit is under development at University of Kentucky, USA [77]. They plan to use an iron-based OC developed from solid waste to provide catalytic gasification and improve coal combustion rate. More recently, a 0.5 MW_{th} pressurized chemical looping system (Figure 16) is under development at Korea Institute of Energy Research [78]. Conceptual design of the proposed unit by means of mass and energy balance calculations confirmed its feasibility. After successful installation of the unit, a hydrodynamic investigation was carried out that revealed a stable solid circulation at ambient temperature and atmospheric pressure for up to 7.5 hr. They plan demonstrating the unit with syngas delivered from a stand-alone coal gasifier unit operating at pressures up to 5.0 bar [78]. Another 0.6 MW_{th} pressurized chemical looping combustion pilot-plant also under development at CanmetENERGY research center [79].

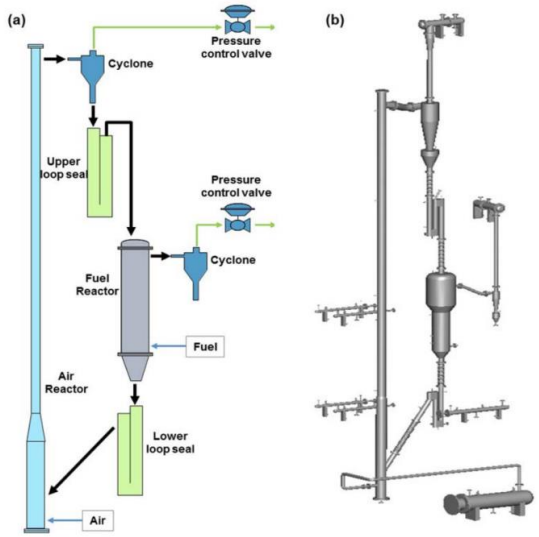

Figure 16. A pressurized 0.5 MWth chemical looping combustion system, (a) schematic diagram, (b) 3D view [78].

2.3.1.2 Single fluidized-bed reactor

Several studies investigated the pressurized chemical looping process in a single fluidized-bed reactor to gain understanding of the pressure effect on hydrodynamics, fuel reactivity, product selectivity and oxygen carrier integrity. Other researchers aimed to examine the potential of using a single fluidized-bed reactor as an alternative technology to the conventional dual-circulating fluidized-bed system; proposing the so-called gas-switching concept in which gases are alternated into a single fluidized-bed reactor. More details about the studies on this reactor configuration are given in the following section.

Ortiz et al. [23] from Instituto de Carboquı´mica (CSIC) utilized a semi-continuous fluidized-bed reactor to investigate the effect of the total pressure on chemical looping methane reforming to syngas. The effect of pressure was studied in the range of 1-10 bar using a Ni-based oxygen carrier and methane as fuel. The results of Ortiz et al. [23] showed that pressurized operation had no negative effect on the product distribution of the process. Methane conversion was above 98% at all operating pressures studied and no carbon formation was detected. Oxygen carrier characterization analyses before and after the pressurized experiments revealed no negative effect of the pressure [23].

Zhang et al. [40] from Southeast University studied a coal-fueled CLC in a single fluidized-bed reactor. The experiments were performed using iron ore as oxygen carrier while the operating pressures ranged between 1.0 and 6.0 bar at a constant operating temperature of 970°C. Carbon conversion increased with the pressure up to 5 bar, while further increase to 6 bar led to lower carbon and OC conversion (Figure 17Figure 17.). Zhang et al. [34] proposed three phenomena that might explain the decrease of coal-fueled CLC performance at pressures higher than 5.0 bar:

1. Experimental results revealed higher CH_4 concentration at 6.0 bar, suggesting a shift in the thermodynamic equilibrium favoring methanation reaction of the mixture H_2, CO and steam (from the feed), thus decreasing the extent of oxygen carrier reduction.
2. Higher pressure suppresses the initial pyrolysis of coal gasification, decreasing the total volatile which leads to the decrease of char reactivity.
3. The inhibition effect of CO and H_2 on the coal gasification products could be more pronounced at high pressure.

The same unit of Zhang et al. [40] had been used in a fixed-bed mode running the pressurized coal-fueled CLC process at similar operating pressure and temperature conditions for comparison with the fluidized-bed mode. Similar trend of performance was observed in both modes, although the fixed-bed mode enhanced the carbon conversion compared to the fluidized-bed mode (Figure 17Figure 17.). The lower carbon conversion in the fluidized-bed mode could be due to significant gas channeling led to poor mass transfer between the bubble and the emulsion phases, thus lowering the conversion of the gasification and volatiles products. On the contrary, the fixed-bed mode enhanced the gas-solid contact resulting in higher carbon conversion. However, sintering and agglomeration could happen due to excessive reduction of the iron-based oxygen carrier to iron or hot spot formation due to the highly exothermic oxidation reaction. When considering long-term stable coal-fueled CLC operation, the fluidized-bed mode is more favorable.

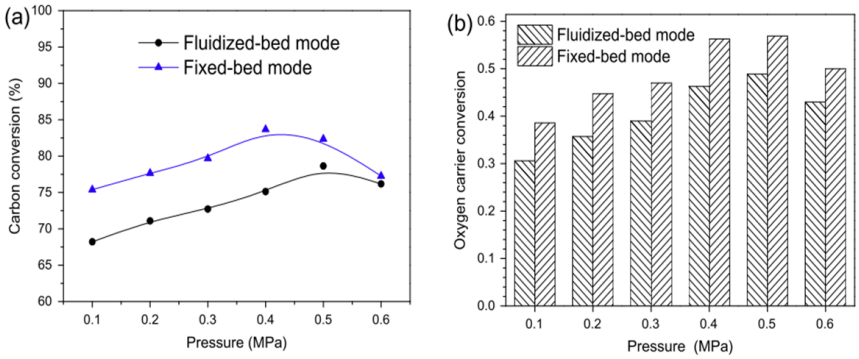

Figure 17. Effect of pressure on carbon conversion and oxygen carrier conversion under fluidized-bed and fixed-bed conditions [40], "Adapted with permission, Copyright (2014) Elsevier BV".

Recently the gas switching concept has been proposed by SINTEF, Norwegian University of Science and Technology, and Eindhoven University of Technology [80–82]. In this configuration (Figure 18), a cluster of reactors was employed to establish a continuous supply of gases to downstream process components. Following are the main advantages of this concept compared to the dual circulating fluidized-bed reactor for chemical looping applications: 1) Solid circulation is intrinsically avoided, hence no need for complicated cyclone and loop seal for gas-solids separation. 2) Compact reactor design. 3) Better oxygen carrier utilization. 4) Reduced attrition rate of the OC particles due to gentler fluidization. 5) Simpler scale-up of chemical looping process due to the simple standalone nature of bubbling fluidized bed gas switching reactors.

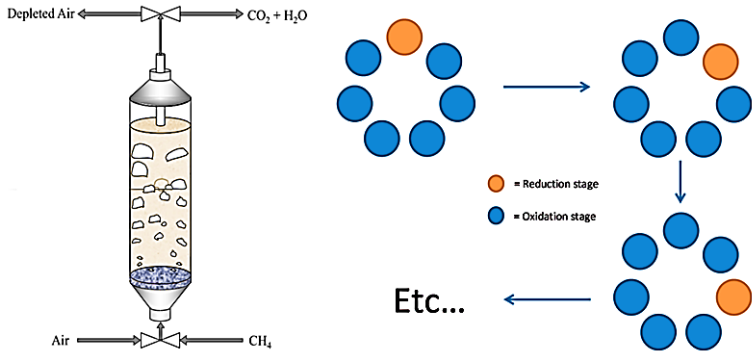

Figure 18. A simplistic illustration of the gas switching reactor and the reactors cluster operating under the combustion mode; each disc represents one reactor [82,83], "Adapted with permission, Copyright (2013) ACS". This is an illustration reflecting that the oxidation step is six times longer than the reduction step requiring six reactors in the oxidation (large part of the feed air is used for

removing the generated heat in the cycle with only a small part is used for reoxidizing the oxygen carrier) and only one in the reduction.

The dynamic operation of this concept can be challenging in a full-scale plant, because it would need a system of high temperature valves to be placed on the outlet of each reactor to switch between the stages (for most of the targeted processes where the downstream systems to integrated with the gas switching require high temperature gases). An additional challenge that arises from the transient nature of this process is the change in the temperature across the stage which may decrease the power plant electric efficiency. Nonetheless, with proper heat management strategies in the cycle [84], a coordinated cluster of gas-switching reactors can produce a continuous exhaust of pressurized hot stream suitable for a full-scale plant.

Experimental demonstration of the gas switching concept was achieved using a lab-scale reactor for CLC and CLR up to 5 bar pressure, using iron-based [85,86], ilmenite [80], Ni-based [82] and $CaMnO_{3-\delta}$ based oxygen carriers [81]. Gas switching combustion (GSC) using ilmenite showed that the pressure slightly improves the overall CO conversion confirming the results reported from TGA experiments with ilmenite when the superficial gas velocity was maintained constant [43]. This was attributed to the enhancement of diffusion resistance due to the change in the particle morphology. Using $CaMnO_{3-\delta}$ based oxygen carriers, negative effects of the pressure was found for CO conversion as in Zaabout et al. [81]. In this oxygen carrier, gaseous oxygen is released (through the well-known CLOU effect) and reacted with the fuel. This oxygen release is negatively affected by the pressure, thus leading to an overall decrease of fuel conversion rate as the pressure is increased. Note that, in these experiments, the molar gas flow rate was increased proportionally to the pressure in all the process stages to maintain a constant superficial velocity in the reactor thus cancelling out the negative effect of increased external mass transfer caused by the pressure as reported in TGA studies in Section 2.2. Using H_2 as fuel, revealed no effect of pressure on the reactor performance. Zaabout et al. [81] also conducted a parametric study to evaluate the effects of various parameters on the GSC reactor performance. Future development of the gas-switching concept will involve the use of a larger scale cluster of reactors to achieve continuous pressurized operation for various chemical looping technologies: combustion, reforming and water splitting [87].

Another concept employing the gas switching concept was proposed using a H_2-selective membrane for the production of pure hydrogen employing the concept of Chemical Looping Reforming [88]. In this concept, a single fluidized-bed reactor is used alternating oxidation,

reduction and reforming reaction stages (Figure 19). A H_2-selective membrane was inserted inside the fluidized-bed reactor for hydrogen recovery in the reforming stage. The main advantage of hydrogen recovery is the shift of the reaction equilibrium towards larger methane conversion rates at lower operating temperature compared to SMR.

Experimental demonstration of the Membrane-Assisted Gas Switching Reforming concept (MA-GSR) was demonstrated at Eindhoven University of Technology (jointly with SINTEF and Norwegian University of Science and Technology) using a fluidized-bed reactor containing a Palladium-based membrane and a Ni-based oxygen carrier at operating pressures up to 5 bar as in Wassie et al. [88]. The reactor performance was studied at low temperatures (<550°C). The results illustrated pure hydrogen production with higher methane conversion (>50%) than the equilibrium level of the conventional fluidized-bed due to the use of membrane. The main limitation of the MA-GSR concept is the membrane stability, where defects were found on the membrane surface due to the harsh conditions of cyclic oxidation and reduction [88].

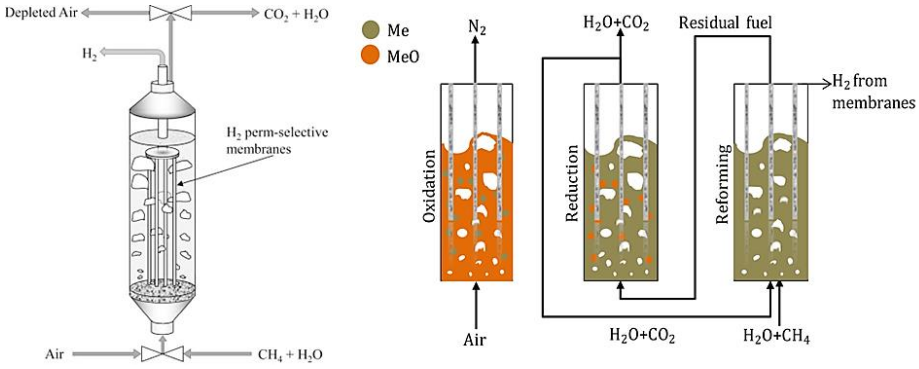

Figure 19. Illustration of the membrane-assisted gas switching reforming reactor concept [89], "Adapted with permission, Copyright (2018) Elsevier BV".

2.3.1.3 Internally circulating fluidized-bed reactor (ICR)

The circulating fluidized-bed configuration remains an attractive option for chemical looping applications considering its steady-state nature and high achievable fluidization velocities. The needs for pressurized operation of chemical looping system inspired the development of a novel reactor configuration; the internally circulating reactor (ICR), which is based on the circulating fluidized-bed configuration but with simplified solids circulation mechanism to simplify pressurized operation [20]. The ICR uses a single unit composed of two chambers connected with two simple ports (replacing the complex sealing system of the conventional CFB) and a

freeboard (replacing the cyclone of the conventional CFB) (Figure 20) [20,90]. In this way, the ICR simplifies the design, eases the solids circulation, and enables operating at high pressure easily in a single pressurized vessel. The oxygen carrier circulation in the ICR is attained through a higher gas velocity in the air reactor (AR) than in the fuel reactor (FR). This simple solids-circulation-mechanism combined with the compact design make the ICR concept very suitable for pressurized operation. The major trade-off of the simplicity obtained by the ICR concept is the gas leakage between the two reactor sections through the connecting ports, decreasing CO_2 capture efficiency and purity. However, the demonstration of the ICR concept by Osman et al. [91] (Figure 20) for atmospheric CLC operation showed that the gas leakage can be minimized by controlling the fluidization velocity ratio of the two chambers and the solids inventory, achieving CO_2 capture efficiency and purity greater than 95%.

The ICR unit of Osman et al. [91] has also been used for chemical looping reforming of methane at atmospheric operation as in Osman et al. [90]. The reactor showed promising performance in term of gas leakage (up to 95% syngas purity), solids circulation rate, fuel conversion (up to 98% methane conversion) and revealed a simple approach to control its performance over a wide range of operating conditions.

An early study on ICR concept was developed by Chong et al. [13] for oil shale retorting, in which the shale and ash continually circulate between the two sections, while keeping the combustion gas and the retort product gases separate. The ICR concept has been further investigated by He et al. [14] and Fang et al. [15] for coal combustion and gasification processes. Further studies of ICR on chemical looping process were conducted at Chalmers University of Technology, where extensive experimental campaigns were carried out at atmospheric pressure [11,16–18]. The simplicity of the unit helped in providing a profound knowledge about CLC and CLR performance for different oxygen carrier materials. Herguido et al. [19] also applied ICR concept for hydrogen separation using the steam-iron process at atmospheric pressure.

Recently, Osman et al. [92] successfully demonstrated the ICR unit for high-pressure chemical looping combustion using NiO-based oxygen carrier. The results showed a stable operation with high fuel conversion for about 40 hours of CLC operation at pressures up to 6 bar, achieving high CO_2 purity and capture efficiency up to 97%. The results of Osman et al. [92] also revealed that the solids circulation rate increases with increasing the operating pressure at constant superficial gas velocity.

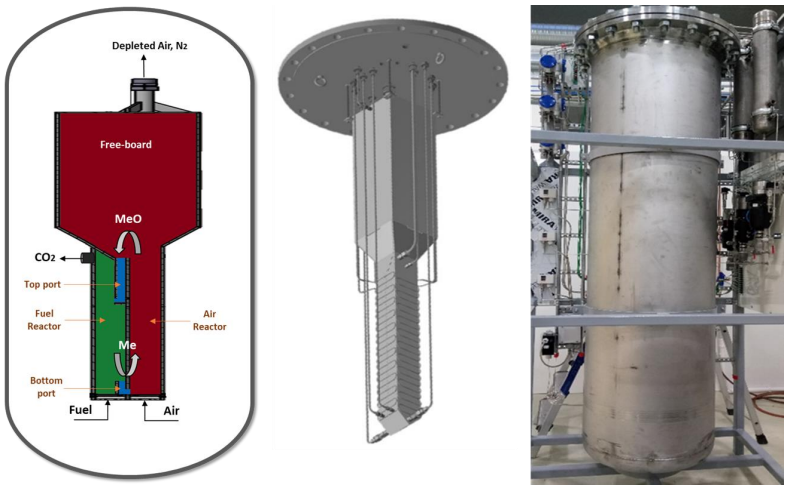

Figure 20. A simplified scheme of the ICR design, CAD drawing of the ICR unit, and the ICR unit under operation inside the shell [90].

2.3.2 Fixed-bed Reactor

In the fixed-bed reactor system, the gas feeds are alternated to a fixed-bed of oxygen carrier to establish cyclic reduction and oxidation stages (Figure 21), similar to the gas switching concept using fluidized-bed reactors discussed in section (2.3.1.2). The main benefits of this reactor concept are that solids circulation and solids attrition are intrinsically avoided, more compact reactor design with ease of pressurization in a single vessel [93]. The disadvantages of the fixed-bed reactors are the requirement of a high temperature switching valve system (in most targeted processes), and highly exothermic oxidation reaction creates large transient thermal gradients that can damage the oxygen carrier by sintering or other defect on the morphological properties of the OC [94]. Additionally, larger particles should be used to minimize the pressure drop, which may lead to intra-particle diffusion limitation lowering the utilization of the oxygen carriers [95]. A direct comparison of packed and fluidized gas switching configurations concluded that the plug flow nature of packed beds makes this configuration most suitable for achieving high efficiencies and high CO_2 capture rates, but the material development is a large challenge due to the extreme thermochemical stresses imposed by the sharp heat and reaction fronts [96].

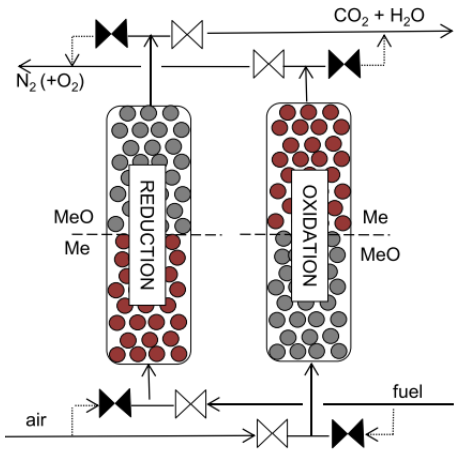

Figure 21. A schematic diagram of a fixed-bed CLC reactor [97], "Adapted with permission, Copyright (2016) Elsevier BV".

Ishida et al. [98] used a fixed-bed reactor to study the effect of pressure on the reaction kinetics of chemical looping methane reforming to syngas with a Ni-based material as oxygen carrier. It was found that the reduction rate at moderately pressurized conditions (3 bar) was lower than atmospheric pressure reduction rate, attributing this to the endothermic reaction of methane with NiO. Ishida et al. [101] suggested that increasing the H_2O/CH_4 ratio offer the capacity to improve the reactivity at high pressure.

Gallucci et al. [99,100] from Eindhoven University of Technology (TU/e) successfully demonstrated a cyclic steady state operation of chemical looping combustion of syngas in a 10 kW_{th} pressurized fixed-bed reactor using NiO-based and ilmenite-based oxygen carriers. The reactor system has been demonstrated up to 7.5 bar. The mass flow rates were fixed during all experiments implying an increase in the residence time with the pressure. Using NiO-based oxygen carrier, the reactor performance at various pressure showed negligible effects of the pressure on the reduction and the oxidation cycle indicating that the increased gas residence time with the pressure had compensated the expected negative effects of gas dispersion and diffusion resistance to the particles. Carbon deposition enhanced at higher pressures, which could be the result of the higher level of oxygen carrier reduction achieved due to the higher fuel concentration as the pressure was increased. Addition of steam effectively suppressed carbon deposition, but also promoted CO conversion into CO_2 and H_2 through the WGS reaction. The maximum temperature rise achieved in the cyclic reduction/oxidation was 340°C with possibility of autothermal operation (no external heat supply) after about three full cycles.

Using a fixed-bed reactor, pressurized hydrogen production with chemical looping water splitting system was investigated by a research group at Graz University of Technology [101–105]. The authors proposed a new concept that combines conventional steam reforming and the steam-iron process in a single fixed-bed reactor containing both the oxygen carrier and the reforming catalyst (Figure 22). The process involved the following steps: 1) catalytic hydrocarbon reforming to syngas, 2) reduction of the iron-based OC using syngas, and 3) oxidation of the reduced OC using steam to produce pure hydrogen. Based on thermodynamic analysis they revealed that the oxidation could be achieved at pressurized conditions, however, the reforming and the reduction step should be carried out at atmospheric pressure to maximize the conversion efficiency [101]. The experiments of Zacharias et al. [105] were carried out at atmospheric pressure for the reforming/reduction step and at high pressure up to 95 bar for the steam oxidation step. The results revealed no negative effect of the elevated pressure on the reactor performance in the oxidation stage. High purity hydrogen was attained in the range of 99.95-99.999% with CO and CO_2 only as impurities given that no air feed is needed in the process. The practicality of operating the oxidation and reduction stages at very different pressures and the feasibility of autothermal operation of the process are potential challenges of this configuration.

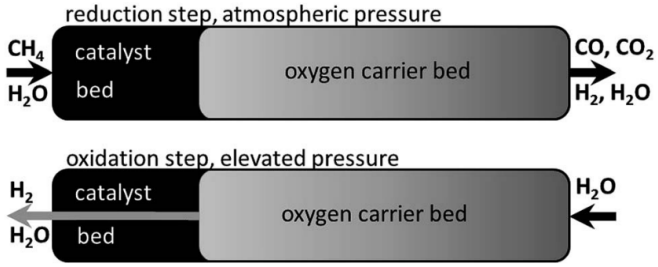

Figure 22. The reformer steam-iron process schematic in a fixed bed reactor [103], "Adapted with permission, Copyright (2016) RSC".

In-situ solid-fuel gasification under CLC mode has been investigated in a high-pressure fixed-bed system at Southeast University [106–108]. The study focused on the pressure effects on the cyclic performance rather than the reactor design, operation and scale-up. Chinese bituminous coal was used as fuel together with different types of iron ore-based oxygen carriers, while steam was used as a gasification agent. Initial investigation by Xiao et al. [106] for up to 5 reduction/oxidation cycles showed that the reduction rate increased with pressure up to 5 bar

then slightly decreased at 6 bar. Subsequent study of 20 reduction/oxidation cycles showed an improvement of the reaction rate with increasing the pressure, which was attributed to the increase of the steam partial pressure and the gas residence time, thus simultaneously enhancing the coal char gasification and reduction of the iron ore [107,108].

The utilization of bulk monolithic OC for CLC in a fixed-bed reactor has been proposed by Gu et al. [109] to limit the temperature fluctuations, minimize the pressure drop and to decrease the intra-particle diffusion limitation associated with the use of large pellets in fixed-beds system. The results of Gu et al. [109] showed high activity of Ce-Zr-F-O/Al_2O_3 oxygen carrier for methane combustion as a result of the strong active component to support interaction, that was similar to that of the powder oxygen carrier. Zhang et al. [110,111] extended this concept to a 10 kW_{th} prototype using a honeycomb CLC reactor (Figure 23) with NiO-based and iron-based oxygen carriers. The results of Zhang et al. [110,111] showed superior performance in term of methane conversion, reduction kinetic, overall reactor stability and limited cyclic temperature fluctuation (50 K) benefiting from the homogeneous distribution of the reaction heat inside the surface of the honeycomb reactor. These preliminary studies proved the feasibility of the concept, but pressurized CLC operation using the monolithic structure yet to be completed to demonstrate the full potential of this configuration in solving the technical challenges facing pressurized chemical looping systems.

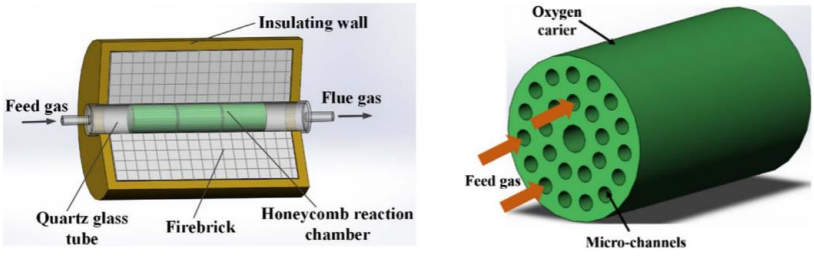

(a) Configuration of the central section (b) Honeycomb chamber

Figure 23. Illustration of the honeycomb CLC reactor [111], "Adapted with permission, Copyright (2018) Elsevier BV".

2.3.3 Moving-bed Reactor

The moving-bed reactor designed with gas-solid countercurrent contact pattern can achieve higher fuel conversion and higher oxygen carrier utilization compared to the conventional CFB, thus presenting new prospects in chemical looping applications. In addition, moving-bed

reactors offer minimal particles attrition, and encounters low pressure imbalances across dual reactors as the operating gas velocity is below the minimum fluidization velocity of the OC particles and hence would be easier to operate under high pressure compared to fluidized-bed reactors. However, the low gas velocity to keep the particles falling against the gas flow requires large reactor vessels that would result in a larger footprint compared to the conventional circulating fluidized bed configuration. This drawback could however be minimized by using large oxygen carrier particles, but this brings challenges associated with mass and heat transfer limitations within the oxygen carriers imposing the use of engineered oxygen carrier with high production costs.

A research group at Ohio State University carried out extensive studies on the potentiality of applying the moving-bed reactor concept in chemical looping for hydrogen production with inherent CO_2 separation, using the steam iron-process [112–115]. The research group developed a process named syngas chemical looping (SCL), utilizing an iron-based OC and consists of three reactors namely the reducer, the oxidizer, and the combustor (Figure 24). In the reducer, a coal-derived syngas was used to reduce Fe_2O_3-based OC to a mixture of Fe and FeO, while producing a mixture of CO_2 and steam. In the oxidizer, pure hydrogen produced by using the steam-iron process in which steam is used to partially oxidize the reduced OC into Fe_3O_4. In the combustor, the oxidized Fe_3O_4 particles are further oxidized to Fe_2O_3 to allow a complete cycle while providing the necessary heat to the process through the exothermic oxidation reaction. The reducer and the oxidizer are operated in a moving-bed mode to counteract the equilibrium limitation of the involved reactions thus maximizing fuel, oxygen carrier and steam conversion. The combustor operates as a fluidized-bed mode to fully oxidize the OC and to transfer the solids back to the reducer. Thermodynamic analysis carried out by Li et al. [114] showed that higher fuel and oxygen carrier conversions can be obtained in moving-beds than in fluidized-beds. This will decrease the required solid circulation rate, minimizing the reactor volume, and maximizing the overall efficiency of the process.

The demonstration of the SCL process has successfully been validated using a 2.5 kW_{th} bench scale unit and a 25 kW_{th} sub-pilot scale unit [112–115]. The concept of the counter-current moving-bed reactor confirmed that nearly pure H_2 could be produced with full syngas conversion to CO_2 and H_2O. Following these outcomes, a 250 kW_{th} pressurized syngas chemical looping pilot plant has been commissioned and successfully demonstrated the concept as in Hsieh et al. [116]. The first operation of the SCL pilot plant was completed at 10 bar and resulted in syngas and OC conversion close to the thermodynamic limits validating the benefit

of using the moving-bed configuration in the reducer and the oxidizer [116]. Yet, a techno-economic assessment taking in consideration the results from the pilot demonstration campaign is needed to confirm the potential of the moving bed in bringing down the cost of hydrogen production through this process.

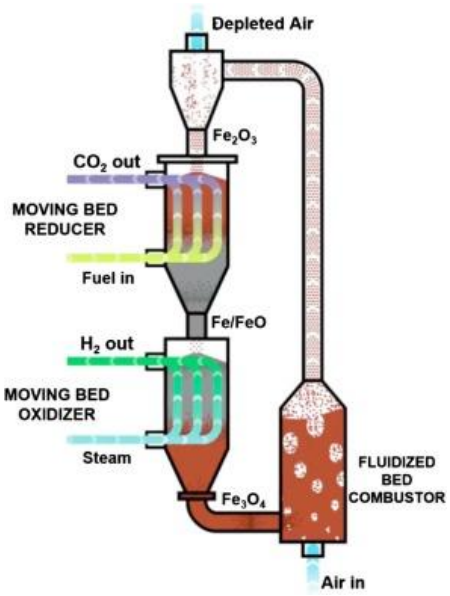

Figure 24. A conceptual design of syngas chemical looping pilot unit with a counter-current moving bed reducer and oxidizer reactors [116], "Adapted with permission, Copyright (2018) Elsevier BV".

2.3.4 Rotary-bed Reactor

The rotary-bed reactor is an extended version of the fixed-bed reactor, in which the oxygen carrier particles are placed in a rotating fixed-bed while a static fuel and air flow radially outward through the rotating-bed [117,118]. Figure 25 shows an illustration of a rotary-bed reactor divided to four sections for air, fuel and two inert gas sectors in-between to avoid gas leakage between the air and fuel zones. The main advantages of this concept are the separation of gas and solids is intrinsically avoided, the compactness of the reactor, continuous operation without the need of solids circulating and scale-up potential [118]. These advantages facilitate the operation at high pressure offering prospects for higher process efficiency, but challenges with gas leakage between air and fuel sections, temperature fluctuation and oxygen carrier thermal expansion should be expected [118]. A limited number of studies have investigated the feasibility of rotary-bed reactors applied to chemical looping restricted to atmospheric conditions. Blom

et al. [117,119,120] conducted a series of experimental studies on a lab-scale rotary-bed reactor using CuO-based oxygen carrier and methane, achieving 90% fuel conversion, 90% CO_2 capture efficiency and up to 65% CO_2 purity. Ghoniem et al. [118,121–126] focused on modelling and techno-economic assessment of chemical looping in this configuration. More research is still needed, especially experimental studies under high pressure, in order to comprehend the feasibility of the concept.

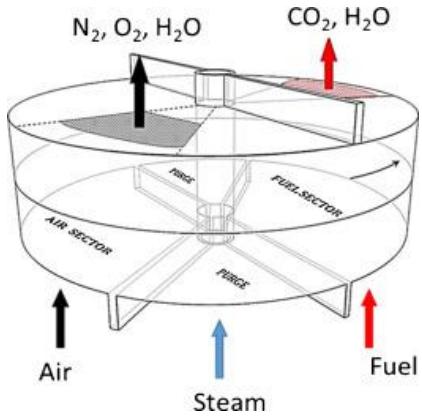

Figure 25. Simple illustration of the rotary-bed reactor [124], "Adapted with permission, Copyright (2015) Elsevier BV"..

2.3.5 Summary of different pressurized reactor configurations

Table 4 provides a qualitative comparison of different pressurized chemical looping configurations over a range of important performance measures. A simple scoring system was used to highlighting the pros and cons of each configuration. The comparison shows that each configuration has strengths and weaknesses. Thus, the choice between these configurations will depend on the relative importance of the different performance criteria for a given application.

The dual CFB has received the highest research focus for chemical looping and reached the highest TRL level, but with very limited studies under pressurized conditions. This gives limited grounds for judging its suitability to pressurized operation. Nevertheless, the key uncertainty arises from the stability of solids circulation in a closed loop involving many components; two reactors operating at different fluidization regimes, cyclones and loop seals. The internally circulating reactor (ICR) configuration has the potential to retain most of the advantages of dual CFB configuration, but with scarifying a small losses in separation efficiency. Values above 90% CO_2 purity and capture efficiencies were achieved at operating

pressures up to 6 bar, which is promising against the large design simplification brought by this configuration. Improved port design could further improve CO_2 separation performance [91]. Packed and fluidized bed switching based concepts has received the second largest focus with dozens of studies completed for different chemical looping processes. Pressurized operation proved to be simple for these configurations, but the high temperature valve to be placed on the outlet of each reactor in the cluster, remains the highest uncertainty. Solving this challenge could be compromised by operating the process at lower temperature or applying an additional firing step to boost the temperature of the gas stream before being sent to the downstream power train. However, this would result in reduced CO_2 capture efficiency if natural gas is used for added firing and higher costs if hydrogen is used. The relative pros and cons of the fluidized and fixed bed configurations are related to their fundamental behavior as well mixed and plug flow reactors, respectively.

The moving-bed reactor is the most suitable for chemical looping processes involving thermodynamically limited reactions such as the steam-iron process. The large reactor footprint imposed by the need to operate at gas superficial velocities below minimum fluidization could be reduced by using large particles, but this measure will be compromised by the increased mass and heat transfer resistance in the particle. The rotating bed is the least developed, and high-pressure operation is yet to be demonstrated.

Table 4: Comparison of different reactor configurations for pressurized chemical looping: Advantage (+), Neutral (o), Disadvantage (-).

Reactor configuration	Experience with pressurized operation	Ease of scale-up	Ease and flexibility of operation	Small plant footprint	Mechanical stresses on the OC	Thermo-chemical stresses on the OC	CO_2 separation efficiency	Others
Dual CFB	Limited	-	-	+	-	+	+	+ (highest TRL, but under atmospheric conditions)
Gas switching	Fair	+	+	-	o	+	o	- (need for high temperature valves)
ICR	Limited	o	o	o	o	+	o	o (Connecting ports design requires further optimization)
Packed bed	Fair	+	o	-	+	-	+	- (need for high temperature valves)
Moving bed	Limited (restricted to the	o	-	-	o	o	+	+ (high conversion for

	steam-iron process)							equilibrium reactions)
Rotating bed	None	+	o	o	+	-	-	Not enough experimental demonstration to judge it

Table 5 gives an overview of the current development of the different reactor configurations. Clearly, most configurations are demonstrated at pressures well below the targeted operating pressure for the respective industrial applications (20-40 bar). In addition, no configuration has thus far reached the MW-scale required for proper identification of scale-up challenges. Further R&D investments are needed to demonstrate successful operation under industrially relevant pressures at pilot scale. Such demonstration studies will facilitate a better understanding of the relative importance of the qualitative performance criteria discussed in Table 4, allowing further scale-up efforts to focus on the most promising configurations.

Table 5: Current level of development of different reactor configurations for pressurized chemical looping.

	First proposed (year)	**Largest scale (kW)**	**Highest pressure (bar)**	**Pressurized CL technologies demonstrated**
Dual CFB	2001	50	5 (50 kW)	Solid fuel CLC
Gas switching	2013	60	5 (2 kW)	Combustion and reforming
ICR	2016	4	6 (3 kW)	Combustion
Packed bed	2007	100	100 (10 kW)	Combustion, reforming, steam-iron process
Moving bed	2010	250	10 (250 kW)	Steam-iron process
Rotating bed	2011	0.5	1 (0.5 kW)	Combustion

2.4 Techno-economic Analysis

Pressurization of the chemical looping systems is of interest for increasing the overall process efficiency. In power production, for example, a pressurized combustion process can utilize a combined power cycle instead of only a Rankine cycle. The former can achieve efficiencies of 64% (modern natural gas combined cycle plants), whereas the latter achieves about 45% efficiency (modern supercritical pulverized coal power plants). In hydrogen production, high pressure reforming is essential to facilitate hydrogen production in a pressure swing adsorption (PSA) unit without having to invest a large amount of compression work. Many other chemical processes consuming syngas also operate at high pressures, implying that large compression work savings are possible if the reforming process also takes place at high pressures.

Even though pressurized equipment is more expensive for a given size, equipment size reduces under pressurized conditions to limit any increases in CAPEX. Furthermore, due to higher pressure the energy required for CO_2 compression will be reduced significantly. Due to these advantages of pressurized operations, the production cost will be cheaper than that of non-pressurized systems for most gas-fueled processes. Consequently, several technical and economic studies of chemical looping concepts either for power production or hydrogen generation or with diverse plant integrations have been conducted for pressurized conditions. These studies show the promise of this concept at large scale. The results from several recent studies are summarized in Table 6 and Table 7. Even though levelized costs of electricity (LCOE) and hydrogen (LCOH) from the various studies varied widely due to different economic assumption employed, most studies reported that pressurized chemical looping configurations significantly outperformed reference plants based on conventional CO_2 capture technologies. These studies are reviewed in more detail below.

Table 6: Summary of the techno-economic studies on power generation using pressurized chemical looping concepts (in 2019 $) (*without CO_2 capture)

Reference	Technology	Pressure (bar)	Electrical efficiency (LHV)	LCOE ($/MWh)	CO_2 avoidance cost ($/ton)	Reference plant efficiency (LHV)	Reference plant LCOE ($/MWh)
Ogidiama et al. (2018) [127]	Chemical looping combustion with combined cycle plant	15	55.6%	55.4	26.3	50.6%	58.3
Zhu et al. (2018) [128]	Chemical looping combustion with combined cycle plant	6-18	50.1%	74.5	-	49.4%	88.2
Porrazzo et al. (2016) [129]	Chemical looping combustion with combined cycle plant	10	52.0%	85.1	-	51.0%	120.0
Ogidiama et al. (2018) [130]	Solar assisted chemical looping combustion with absorption chiller	15	63.4% (thermal)	46.8	-	-	-
Diglio et al. (2018) [131]	Fixed bed chemical looping combustion with gas turbine cycle	20	51.0%	56.7	33.7	55.0%*	46.0*
Iloeje et al. (2018) [132]	Rotary Chemical looping combustion with Brayton cycle plant	5	56.0%	52.5	-	-	-
Khan et al. (2020) [133]	Chemical looping combustion with combined cycle plant	22	50.7%	97.0	117.3	54.0%	91.2
Khan et al. (2020) [133]	Chemical looping combustion with additional combustor fired by NG	22	60.7%	73.0	60.3	54.0%	91.2
Khan et al. (2020) [133]	Chemical looping combustion with additional combustor fired by H_2	22	60.7%	91.0	96.3	54.0%	91.2
Mancuso et al. (2017) [134]	Chemical looping combustion with coal-fired and IGCC	17	40.8%	116.4	37.0	35.3%	128.1
Cloete et al. (2018) [135]	Chemical looping combustion and oxygen production IGCC	17	45.4%	85.6	50.1	37%	104
Farooqui et al. (2018) [136]	Chemical looping syngas production with oxy-fuel combined cycle plant	2	50.7%	122.3	96.3	54.9%*	-
Nazir et al. (2018) [137]	Chemical looping reforming with combined cycle power plant	18	43.4%	132.7	183.1	49.5%	-

Nazir et al. (2018) [138]	Gas switching reforming	18	47.4%	115.3	123	58.4%*	84.1*

Table 7: Summary of the techno-economic studies on hydrogen generation using pressurized chemical looping concepts (in 2019 $) (*without CO_2 capture)

Reference	Technology	Pressure (bar)	Efficiency (LHV)	LCOH ($/kg)	CO_2 avoidance cost ($/ton)	Reference plant efficiency (LHV)	Reference plant LCOH ($/kg)
Nazir et al. (2020) [139]	Gas switching reforming	33	80%	1.8	18.0	79.3%*	1.9*
Wassie et al. (2018) [140]	Membrane-assisted gas switching reforming	50	81%	3.5	89.5	67.0%	3.6
Spallina et al. (2016) [141]	Membrane-assisted chemical looping reforming	50	82%	2.3	-40.7	67.0%	3.6
Spallina et al. (2017) [142]	Chemical looping reforming	20	75%	3.6	99.6	67.0%	3.7
Cloete et al. (2019) [143]	Membrane assisted autothermal reforming	50	81%	1.72	-	80.0%	1.7
Khan and Shamim (2016) [144]	Three reactor chemical looping reforming with combined cycle plant	20	71.8%	1.9	-	-	2.7
Khan and Shamim (2019) [145]	Three reactor chemical looping reforming with combined cycle plant	20	74.5%	1.7	-	-	2.7
Chisalita and Cormos (2019)	Chemical looping hydrogen production	30	75.8%	1.5	21.2	74.1%	1.6
Chisalita and Cormos (2019) [146]	Sorption enhanced chemical looping reforming	30	70.4%	1.8	65.6	74.1%	1.6
Xiang and Zhou (2018) [147]	Chemical looping hydrogen generation using coke oven gas	10	68.5% (exergetic)	2.9	-	-	-

2.4.1 Chemical looping combustion

A lot of attention has been given to the primary concept of chemical looping for power generation. Below are the summaries of several such recent studies focusing on techno-economic assessment of pressurized chemical looping combustion. Ogidiama et al. [127] conducted a detailed performance and economic comparison between the natural gas-fired CLC-based power plant with that of a conventional natural gas-fired combined cycle power plant with post-combustion CO_2 capture. A simple CLC cycle was employed with cycle pressure of 15 bar and NiO as the OC. The CO_2 capture costs shown in Table 6 are low compared to a review of CCS costs by Rubin et al [7], 48 - 111 $/ton.

Zhu et al. [128] presented the techno-economic performance of a CLC plant employing different OCs (Figure 26). The net electrical efficiencies reported were in the range 45 to 50% due to difference in turbine inlet temperature (TIT). The corresponding levelized cost of electricity ranged from 75 to 89 $/MWh, in which nickel has the lowest LCOE (due to its ability to facilitate high temperature operation) followed by ilmenite and copper. It was reported that an increase in pressure (6-18 bar) initially decreased the cost of electricity (105.3–74.5$/MWh). With a further increase in pressure, the cost of electricity increased indicating the requirement of an optimal pressure ratio that resulted in maximum power output at a specific TIT.

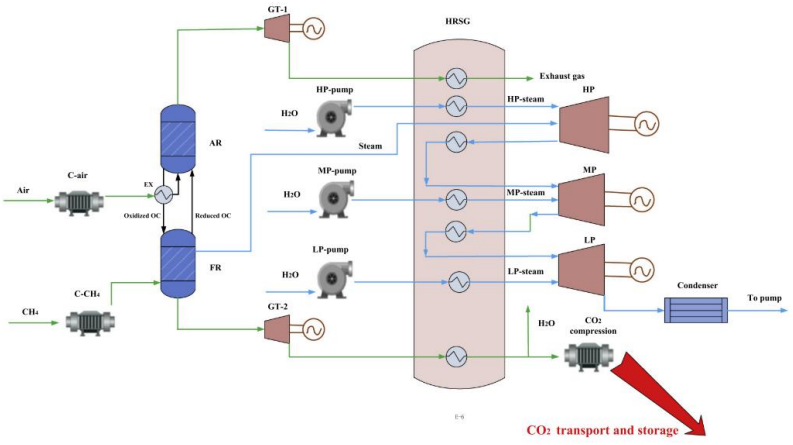

Figure 26. Configuration of chemical looping combustion for power generation [128], "Adapted with permission, Copyright (2018) Elsevier BV".

Porrazzo et al. [129] developed a system level model of the CLC process integrated with a combined cycle power plant. Detailed fluidized bed models considering the kinetics and hydrodynamics were implemented for the CLC reactors in the plant model. Nickel-based OC was used and the cycle was operated at a pressure of 10 bar. The net electrical efficiency was 1%-point better than the reference plant with 20% less LCOE.

Ogidiama et al. [130] used the chemical looping concept to utilize waste heat effectively. A CLC cycle integrated with a combined cycle plant was compared with a CLC cycle integrated with an absorption chiller plant. In both configurations, the CLC plant was operated at a pressure of 15 bar. A parabolic trough solar system was used to direct solar energy onto the fuel reactor, acting as an additional heat source for the endothermic fuel reaction. The results showed that by integrating with an absorption chiller and waste heat utilization potential of 49%, the overall plant efficiency can be significantly increased.

Diglio et al. [131] proposed a fixed bed CLC reactor network for small-scale power generation (Figure 27). The proposed configuration consisted of four fixed bed reactors in parallel operated at 20 bar. A copper-based OC was used in the fixed beds which allowed an exothermic reaction in both the oxidation and reduction stages. The reactors were arranged in a way such that two separate gas streams were obtained continuously, similar to that in conventional CLC system. The air stream was expanded for power generation while the CO_2 stream was used to preheat the fuel.

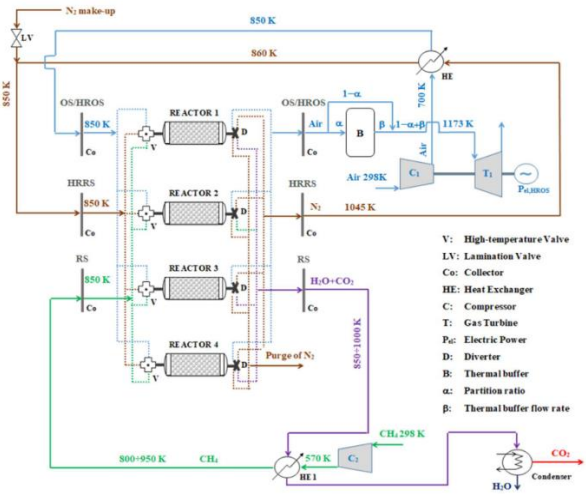

Figure 27. Layout of the CLC process integrated with stationary power plant [131], "Adapted with permission, Copyright (2018) ACS".

Iloeje et al. [132] developed a rotary CLC reactor which comprises of the OC in the form of closely packed microchannels. The objective of this design was to minimize the losses in efficiency associated with heat transfer in the reactor. The base case reactor configuration was operated at 5 bar and was integrated with a recuperative Brayton cycle plant. By varying the pressure ratio from 3 to 7 bar, it was reported that the net thermal efficiencies were increased by more than 2%-points with significant reduction in LCOE.

The natural gas-fired CLC configurations reviewed thus far all suffer from a fundamental problem: the maximum achievable reactor temperature is far below the firing temperature of modern gas turbines. Thus, although CLC imposes almost no direct energy penalty for CO_2 capture, the indirect energy penalty involved in running the combined power cycle from a lower starting temperature is considerable. Depending on the CLC reactor temperature selected and the reference plant TIT, the resulting power plant efficiency can be well below that of NGCC benchmarks with post-combustion CO_2 capture [148]. This problem can be mitigated by including an additional combustor downstream of the CLC reactors to increase the stream temperature to the operating level of the gas turbine. Khan et al. [133] recently conducted a techno-economic assessment of such a power plant configuration (Figure 28), finding that added firing with natural gas results in significantly lower CO_2 avoidance costs than a benchmark NGCC plant with post-combustion CO_2 capture. However, CO_2 avoidance is only 52.4% due to emissions from the added firing. When hydrogen firing is used instead, the cost of hydrogen production is very important to power plant economics. The study also confirmed that a CLC plant without added firing is less attractive than conventional NGCC with post-combustion CO_2 capture.

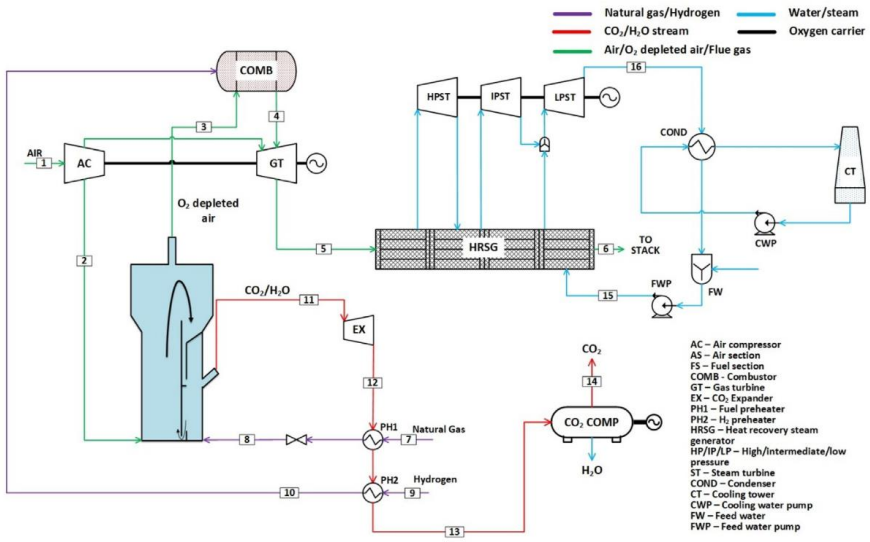

Figure 28. Layout of the CLC process integrated with stationary power plant [133], "Adapted with permission, Copyright (2020) Elsevier BV ".

The attractiveness of chemical looping concepts can be further increased by integrating them with coal-fired plants or integrated gasification combined cycle plant. Mancuso et al. [134] conducted a comprehensive economic-assessment on integrated gasification combined cycle (IGCC) and supercritical-pulverized coal plants with different configurations. The IGCC plant with CLC was based on the packed bed reactor concept. The syngas produced from the gasification was fed to the reduction reactor of the packed bed CLC process. The CLC cycle was operated at a pressure of 17 bar with ilmenite as an OC. An increase in net electrical efficiency by 5%-points and a reduction in LCOE by 9% with respect to the reference plant (IGCC plant with conventional pre-combustion CO_2 capture) was reported.

The aforementioned packed-bed CLC plant was integrated with a chemical looping oxygen production (CLOP) unit to increase the efficiency by 2.3 %-points [27]. The use of hot gas clean-up technology offered a further 2 %-point efficiency gain for a final efficiency of 45.3%. Despite the good thermodynamic performance, a subsequent economic assessment [135] found limited improvements in cost from including the CLOP unit due to the increase in size of the gasifier and gas clean-up units resulting from the lower heating value of the syngas produced. However, the LCOE still compared favorably against other clean energy technologies (nuclear, wind and solar). The benefits of operating this plant with biomass for negative emissions in a scenario with high CO_2 prices was also illustrated.

As was the case with natural gas-fired combined cycles, substantial gains in efficiency can be achieved in a CLC-IGCC power plant by including an added combustor to raise the TIT to that of the benchmark plant. In addition, a recuperator recovering the heat form the reduction stage to pre-heat the air can provide further efficiency gains. When these improvements are combined with the ability of the CLC plant to recover some heat from steam condensation and the potential to remove pre-combustion gas treatment, a very high efficiency could be achieved eliminating the CO_2 capture energy penalty [149]. In this case, natural gas was used in the added combustor to raise the temperature from 1165°C to 1370°C.

An important fundamental limitation of IGCC power plant configurations is the low flexibility of the gasification train, making such plants incompatible with future power systems containing large shares of fluctuating wind and solar power. In this respect, the OC can be exploited as an energy storage medium enabling variable power output from a constant stream of syngas input and CO_2 output. Such a plant requires complete uncoupling of the gasification train and the power cycle to allow for flexible operation and was recently proposed based on GSC reactors integrated with a HAT power cycle [150]. When a low-cost slurry-fed gasifier was employed, the plant could achieve 41.6% efficiency with high CO_2 capture.

2.4.2 Chemical looping reforming

Chemical looping reforming for syngas generation has also been extensively studied for pressurized operations. Generally, for hydrogen production, the syngas generated is subjected to water-gas shift reactors followed by pre-combustion CO_2 capture by conventional monoethanolamine systems. The hydrogen rich gas is then burned in a combined cycle power plant.

Farooqui et al. [136] compared the performance of an oxy-fuel combined cycle plant integrated with chemical looping syngas production (OXY-CC-CL) with a conventional NGCC and a natural gas-based oxyfuel combined cycle (OXY-CC) plants (Figure 29). In the fuel reactor, CO_2/H_2O dissociation was considered to produce syngas through partial oxidation of the reduced OC. The plant was operated at a lower pressure (2 bar) which increased the investment costs and the energy consumption for CO_2 compression to high pressures. Consequently, the LCOE reported was significantly higher than the conventional technologies.

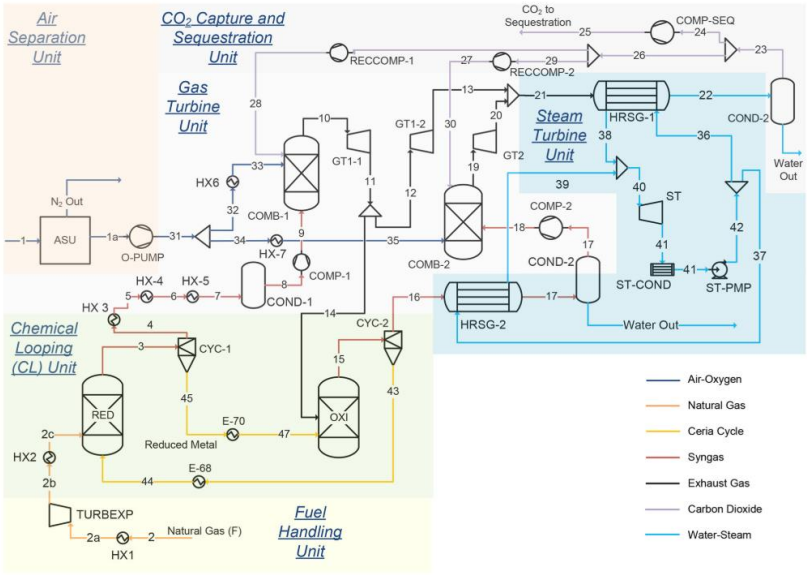

Figure 29. Process simulation flowsheet of OXY−CC-CL unit [136], "Adapted with permission, Copyright (2018) Elsevier BV".

Nazir et al. [137] investigated a CLR unit integrated with a combined cycle power plant. A nickel-based OC was used and the plant was operated at 18 bar pressure. In this work, the syngas produced in the CLR unit was subjected to water gas shift reaction before capturing the CO_2 in a methyl diethanolamine capture system (MDEA). The outlet stream mostly consisting of hydrogen was compressed and preheated before burning in the gas turbine. Subsequently, the exhaust gas heat is recovered in a steam cycle. A comprehensive sensitivity study reported that the net electrical efficiencies ranged between 40 - 43.4% while the LCOE varied between 132.7 and 145.9 $/MWh.

In another study Nazir et al. [138] investigated a novel reactor concept called as gas switching reforming (GSR) (Figure 30) [151] (as discussed in section (2.3.1.2)). Contrary to the chemical looping approach, in this concept, the OC was confined to one reactor with alternate switching of the feed gas to compete the GSR cycle. The reactor was operated at pressurized conditions of 18 bar at different OC utilization levels and steam to carbon ratios. It was also reported that by eliminating the WGS step the efficiency and the LCOE can be improved considerably by ~1%-points and 3% reduction, respectively.

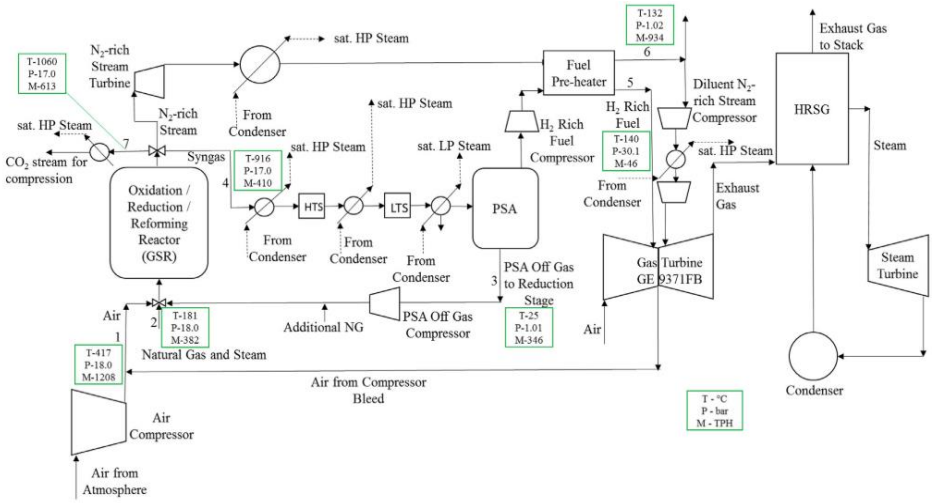

Figure 30. Schematic of a GSR-CC process [138], "Adapted with permission, Copyright (2018) Elsevier BV".

The ability of GSR to efficiently integrate a PSA unit for pure H_2 production is an important advantage that can be exploited for flexible operation to balance variable renewable energy (VRE). When VRE output is low, the plant is operated as outlined above to produce power with CO_2 capture. However, when VRE output is high, the power cycle is deactivated and pure H_2 is exported instead. This allows most of the plant capital (the GSR reactors, WGS reactors, PSA unit and CO_2 compressors) as well as the downstream CO_2 transport and storage infrastructure to operate continuously, while variable electricity output is provided to balance VRE and H_2 is produced to decarbonize other sectors of the economy. A recent work [152] showed that such flexible power and H_2 production can strongly improve the economic performance of GSR-CC when operating as a mid-load plant to balance VRE. Even though the LCOE of GSR-CC was similar to an NGCC plant with post-combustion CO_2 capture under baseload conditions, a 5% better annualized investment return was calculated under mid-load conditions. This conclusion was subsequently confirmed in a power system simulation study [153] showing that flexible GSR can reduce total power system costs by 8% and emissions by 41 kg/MWh, while increasing the optimal share of variable renewables by 50% relative to a system with conventional CCS plants. The GSR scenario also supplied a large amount of clean hydrogen to decarbonize sectors other than electricity. Such a flexible power and hydrogen plant would also be possible using coal or biomass as fuel, offering greater fuel flexibility to the power system. A coal-fired flexible power and hydrogen configuration was recently evaluated, showing that electric efficiencies exceeding 50% are possible with almost complete

CO_2 capture [154]. Future economic and system-scale assessments are necessary to confirm the potential of this configuration to reduce energy system costs and emissions.

When deployed as a dedicated hydrogen production facility, GSR also holds great promise. Nazir et al. [155] showed how the hydrogen production efficiency can be optimized with respect to process pressure and further improved using added thermal mass (metal rods) in the reactor to limit temperature variations across the cycle. This work was subsequently extended to include an economic assessment [139], showing that GSR can produce clean hydrogen for a CO_2 avoidance cost as low as $15/ton. A promising commercialization pathway was also proposed where GSR plants are first constructed without CO_2 capture by expanding and venting the concentrated CO_2 stream, in which case produced hydrogen is cheaper than conventional SMR, and easily retrofitted for almost complete CO_2 avoidance when CO_2 prices rise and CO_2 transport and storage networks become available.

Gas switching reforming has also been studied for hydrogen generation using membranes for hydrogen extraction. Wassie et al. [140] combined the GSR reactor concept with the H_2 perm-selective membranes (MA-GSR). Given the intermittent nature of the GSR concept, a cluster of five reactors operated at 50 bar was considered undergoing cycles consisting of oxidation, reduction and reforming stages. The Pd-based membranes were inserted in each of the reactors in the cluster. The membranes are expected to work only in the reforming stage, causing a relatively low utilization rate that negatively affects process economic performance.

This work was inspired by Spallina et al. [141] who performed a techno-economic assessment of a membrane-based chemical looping reforming (MA-CLR) plant integrated with CO_2 capture (Figure 31). The plant was operated at different pressures ranging from 32-50 bar. Simultaneous OC reduction and methane reforming to syngas occur in the fuel reactor, while the hydrogen produced is continuously extracted by the Pd-membranes. The results showed that the H_2 yield by this configuration is about 20% higher than the conventional plants. This plant also offers low energy cost for CO_2 separation and compression which makes the overall reforming efficiency up to 20% higher than the conventional FTR (fired tubular reforming) with CO_2 scrubbing.

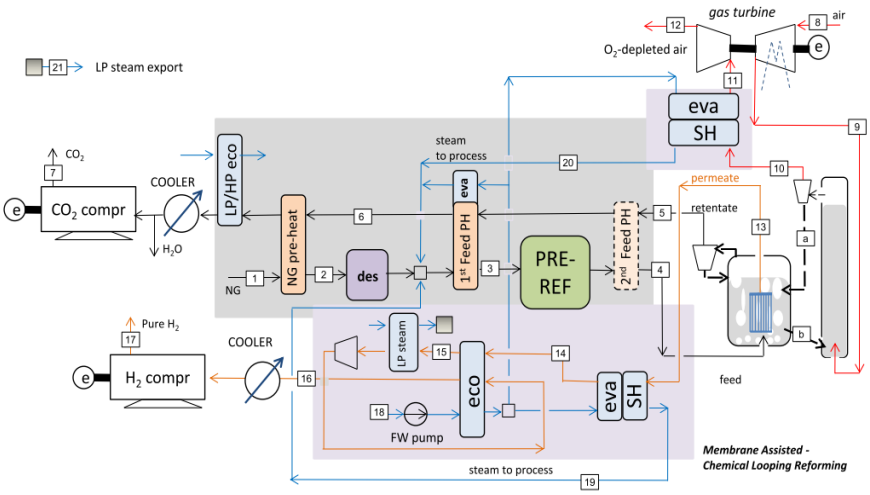

Figure 31. Plant layout considered for the MA-CLR [141].

Prior to that study, Spallina et al. [142] carried out as similar study on CLR system. The process flow schematic shown in Figure 32 consisted of a FR operating at 20 bar pressure. An increase in hydrogen efficiency by 8%-points and a slight reduction in LCOH was reported when compared to SMR plant with CO_2 capture. The lower efficiency was due to the lower hydrogen yield and higher electric power consumption. The critical challenge in this configuration was the operation of dual fluidized bed reactors at elevated pressures.

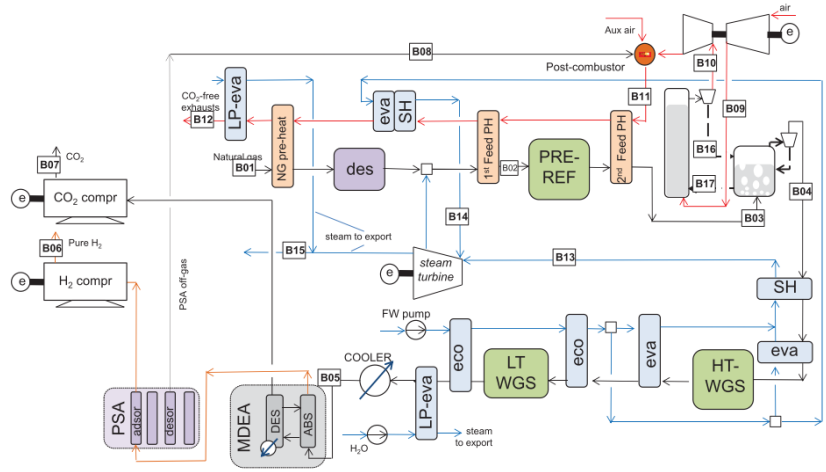

Figure 32. Process simulation flowsheet of chemical looping reforming [142], "Adapted with permission, Copyright (2019) Elsevier BV".

Cloete et al. [143] proposed an alternative to the (MA-CLR) system studied by Spallina et al. [141]. The so-called membrane-assisted autothermal reforming (MA-ATR) consisted of an ASU providing oxygen to the reduced OC, replacing the air reactor of MA-CLR (Figure 33). This was to avoid the challenge of maintaining reliable solids circulation between the air and fuel reactors at large scale under the very high pressures (50 bar or higher) required to maximize process efficiency. The very high operating pressure also means that the energy penalty of the ASU may not be so large compared to the losses involved in the compression and expansion of air to feed the MA-CLR air reactor. The economic assessment showed that hydrogen production by MA-ATR is only 1.5% more expensive than MA-CLR, which could be attractive given the significant process simplification. The cost of hydrogen production was lower than the MA-CLR plant discussed earlier mainly because of lower assumed natural gas prices. The MA-ATR concept was also evaluated for ammonia production [156], capitalizing on the possibility to feed N_2 from the ASU as a sweep gas through the membranes to increase the achievable permeate pressure, thus reducing downstream compression work before the ammonia synthesis loop. This process configuration returned 11% lower ammonia costs than the conventional benchmark process without CO_2 capture.

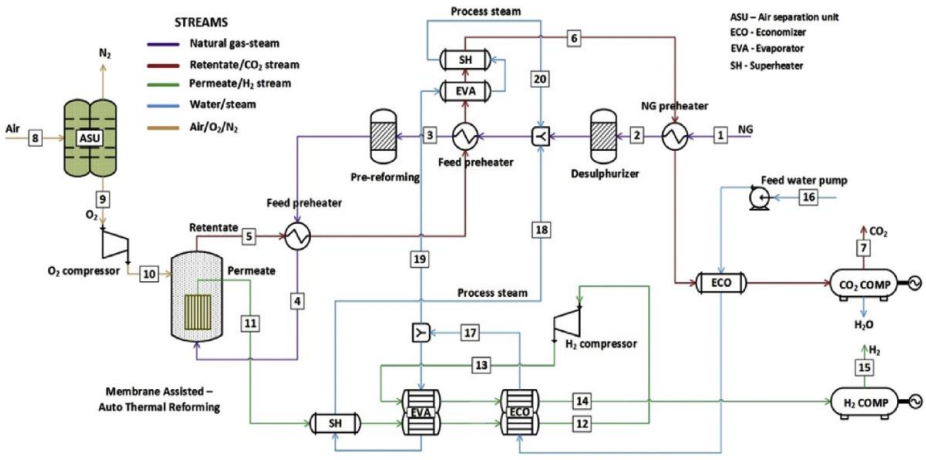

Figure 33. Schematic of membrane assisted autothermal reforming plant [143], "Adapted with permission, Copyright (2019) Elsevier BV".

Pressurized chemical looping process in packed bed reactors was also used for ammonia production by Pereira et al. [157]. A three packed-beds (each for oxidation, reduction and reforming) were operated at pressure above 30 bar. The ammonia yield reported was ~1.9%

more than the reference ammonia synthesis plant with CO_2 capture and with equally more equivalent specific energy consumption. The total plant cost was reduced by 19% owing to the pressurized reforming unit and CO_2 separation. The ammonia production cost estimated was ~5% less than the reference plant with negative CO_2 avoidance cost (-5 $/ton$_{CO2}$). A similar setup of three dynamically operated packed-bed reactors was also used for methanol production by Spallina et al. [158]. In this process, the reactors were operated at a pressure above 25 bar. An autothermal reforming process for syngas production was assumed as a reference plant without CO_2 capture. The equivalent methanol production efficiency for the CL plant was slightly less than the reference plant (~0.5%-points). The methanol production costs estimated was 17% lower than the reference plant with negative CO_2 avoidance costs (-303 $/ton$_{CO2}$); due to significantly lower investment costs associated with CL plant.

2.4.3 Chemical looping water splitting

In the chemical looping water splitting process, steam is split into hydrogen and oxygen that oxidizes the OC. A concept involving three reactors, basically combining the chemical looping combustion and chemical looping water splitting processes is called a three-reactor chemical looping hydrogen (CLH) production. Khan and Shamim [144] referred to the process as reforming due to similarity of the overall reaction to the SMR process after the oxidation of the carbon monoxide to CO_2. However, this is misleading and should be referred to as water splitting. The configuration consisted of three reactors: the fuel reactor where the natural gas was converted into CO_2 and H_2O, the steam reactor where the water was split into H_2, and the air reactor where the reduced OC was re-oxidized. Iron-based OCs were used in the plant operated at 20 bar. Heat was recovered from the three outlet streams for power generation using a complex network of heat exchangers. The cost of hydrogen production reported was significantly lower compared to the case of SMR with CO_2 capture (about 2.7 $/kg). In a similar study, Khan and Shamim [145] compared the performance of a similar plant using an iron-based and tungsten-based OCs (Figure 34). It was reported that the tungsten-based plant performed 4%-points better than the iron-based plant in terms of hydrogen production efficiency. As W-based oxides have a higher oxygen potential, they tend to absorb more oxygen when reacting with steam, consequently, producing more H_2, but the high cost of tungsten makes these OCs unaffordable. However, it was also reported that if the very high cost of tungsten-based OC were to be equal to that of the iron-based carrier, then the cost of hydrogen production would come down to 1.5 $/kg. Although the price of a tungsten OC can never approach that of an iron

OC, this result indicates the ultimate potential of developing a cheap OC with similar characteristics to the tungsten OC.

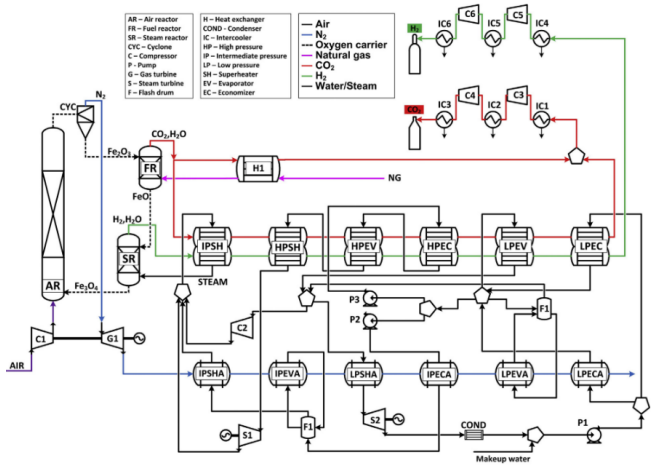

Figure 34. Process flow diagram of TRCLR plant [145], "Adapted with permission, Copyright (2019) Elsevier BV".

Xiang and Zhou [147] proposed a process design which comprises of CLH generation unit which utilizes coke oven gas as the fuel and iron-based OC (Figure 35). Part of the hydrogen produced was synthesized with nitrogen from an ASU to produce ammonia. In another configuration, a PSA unit was used to extract hydrogen from the coke oven gas before introducing it into the CLH unit. This ensured an increase in hydrogen production and also offered flexibility in the production of both hydrogen and ammonia depending on the market demand. The CLH unit was operated at 10 bar and was integrated as a mean of hydrogen source for the ammonia production, which was mostly used in the production of fertilizers. The results indicated that it was more efficient H_2 source than a conventional SMR.

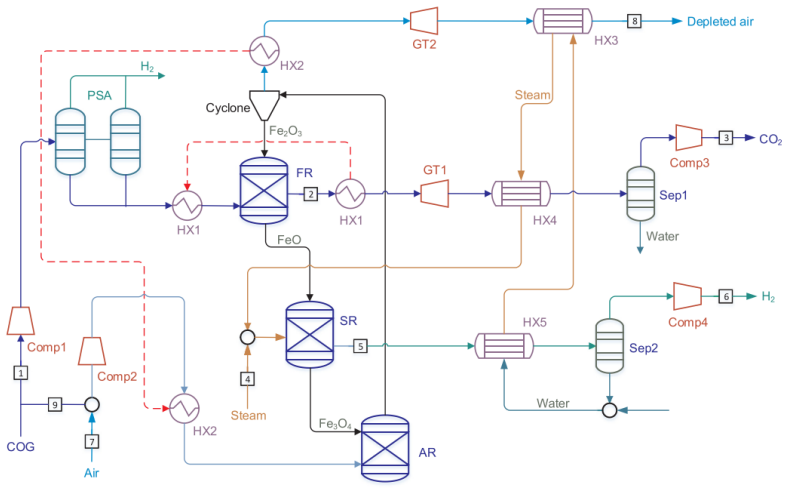

Figure 35. Process diagram of the CG_{PSA}-CLH1 [147], "Adapted with permission, Copyright (2018) Elsevier BV".

2.4.4 Discussion of techno-economic assessment findings

The primary finding from this review of techno-economic assessment studies is that pressurized chemical looping processes are more attractive for hydrogen (or other chemicals) production than power production. This is because the maximum chemical looping reactor temperature severely constrains combined power cycle efficiency relative to modern NGCC plants with very high TIT, but good reforming efficiency can still be achieved at achievable reactor temperatures.

This reactor temperature limitation can be mitigated in CLC combined cycle plants by using an additional combustor after the CLC reactor or by firing the combined power cycle with hydrogen produced via CLR. However, both options impose significant added costs or emissions. In the case of added firing, emissions are introduced if natural gas is used and costs are increased if hydrogen is used. In the case of a hydrogen-fired combined cycle, the conversion losses in the reforming process are augmented by the additional conversion losses in the combined cycle. Such strategies can still achieve reasonable techno-economic performance, but the superiority relative to benchmark post-combustion solutions is marginal.

For hydrogen production, on the other hand, the most efficient chemical looping configurations can approach the techno-economic performance of benchmark processes without any CO_2 capture, easily outperforming conventional CO_2 capture benchmarks. Several promising

pathways exist, each with unique advantages relative to the conventional steam methane reforming hydrogen production pathway. For GSR, the perfect heat transfer of the combustion heat to the reforming reaction via the oxygen carrier material allows the reforming to be completed at higher temperatures, leading to good methane conversion at lower S/C ratios. This reduces the heat required to raise steam, improving efficiency. For membrane-assisted reforming and water splitting, the downstream hydrogen separation processes are avoided, saving significant capital costs and efficiency losses. All three of these hydrogen production pathways show great promise to produce hydrogen and other chemicals with minimal or even negative CO_2 avoidance costs.

Finally, emerging studies of flexible power and hydrogen production plants for balancing variable renewable energy shows promise, given the large momentum behind wind and solar power and the hydrogen economy. Such processes capitalize on the high attractiveness of chemical looping for hydrogen production, while concentrating power production only during times of high electricity prices (low wind and solar output) to compensate for the marginal competitiveness of combustion discussed earlier.

2.5 Pressurized calcium looping process

Calcium looping (CaL) is a promising energy efficient CO_2 capture technology. It is largely applied as a post combustion technology for capturing CO_2 from the flue gas following an equilibrium reaction between calcium oxide and CO_2 to form calcium carbonate ($CaO + CO_2 \rightarrow CaCO_3$). At atmospheric pressure, the carbonation takes place at temperatures of ~700°C while the regeneration takes place above 900°C. Most of post combustion studies have been completed at atmospheric pressure demonstrating the technology up to TRL6. Abanades et al. [159] provides a good overview on the technology development up to 2015 building up on previous reviews from Harrison in 2008 [160] (focused on applying CaL in for sorbent enhanced hydrogen production) and Anthony et al. in 2011 [161] for CaL technology in general.

Pressurized operation of this technology can bring several advantages to the carbonation reaction such as improved kinetics, shifting the equilibrium in a positive direction and enhanced hydrodynamics and heat/mass transfer rates [162]. However, it makes the regeneration challenging, negatively affecting the equilibrium, and requiring temperatures beyond 1000°C to achieve satisfying conversion rates. Abanades et al. [159] identified this as the key challenge to solve to unlock the full potential of CaL technology when targeting pressurized pre-

combustion for production of an H_2 rich gas stream in methane reforming or gasification of biomass (or coal) intensified by CO_2 adsorption on CaO.

Most of recent studies continued focusing on the positive effect of pressure on CaO enhanced hydrogen production. CaO was reported to enhance the selectivity to hydrogen in coal [163] and biomass gasification [164]. High pressure operation using CaO was applied to In-situ biomass combustion and has shown to successfully reduce tar yield [164]. Gas–solid trickle flow reactor packed experiments have shown that hydrogen rich flue gas could be produced using sorbent enhanced SMR at temperatures as low as 500-600°C and a pressure of 4 bar [165].

Other studies focused on optimizing the carbonation reaction attempting to enhance the kinetics in specific applications. Steam addition was found to promote CO_2 adsorption via the formation of surface OH groups on the CaO surface [166]. K_2CO_3 catalyst addition was found to significantly improve coal gasification reactivity while the CaO sorbent mainly played the role of CO_2 absorbent and heat carrier [167]. The same study has reported that the reaction heat calculation results indicated that the catalytic calcium looping hydrogen generation process could shift from endothermic to exothermic as the pressure increases beyond 2.0 MPa.

An interesting alternative technology based on CaL for decarbonizing natural gas to hydrogen with integrated CO_2 capture is the Ca-Cu process. This technology uses the heat generated from the exothermic reaction of Cu-based oxygen carrier reduction to regenerate the $CaCO_3$ sorbent [146]. Methane reforming occurs similarly to the sorbent enhanced methane reforming process where the produced CO_2 adsorbs on the CaO sorbent shifting the equilibrium reaction for maximizing conversion to H_2 (the WGS reaction occurs simultaneously yielding to high purity H_2 after CO_2 removal by the sorbent). This process is receiving increased interest due to the predicted high energy efficiency and lower product costs compared to benchmarking CO_2 capture technologies [168]. Experimental development studies were completed, mainly focusing on the Ca-Cu material and its performance, testing under the main critical step of the process which combines reduction of CuO and calcination $CaCO_3$ [169–171]. A recent review by Fernández et al. [172] on the technology provides a complete overview of the progress both on process development, modelling and integration.

CaL technology was also applied for intensifying the Water-Gas-Shift reaction (WGS) through removing the produced CO_2 in the process using the calcium-based sorbent. The process is known as sorbent enhanced water-gas-shift (SEWGS). A recent study on this process has

demonstrated the possibility of experimentally achieving high-purity H_2 (99.4% in dry basis) in the SEWGS process at 573 K, 12 atm and an initial H_2O/CO molar ratio of 1.5 with a three catalyst/sorbent layered configuration [173]. Another study combined WGS Cu-based catalyst and K-doped hydrotalcite for CO_2 capture in the SEWGS process at different pressures. It has been shown that if steam is used during the regeneration step, all sites can be effectively regenerated, achieving a stable working sorption capacity [174].

2.6 Conclusion and Outlook

This paper reviews pressurized chemical looping studies addressing the different aspects that affect reactor performance, the different reactor configurations proposed, and the costs of CO_2 capture at elevated pressure. The effect of pressure on the thermodynamic equilibrium depends on the reactions involved in the process, governed by Le Chatelier's principle. As for the kinetics, the pressure was found to negatively affect the reaction rate when the partial pressure of the fuel is maintained constant, which was attributed to the increase in the external mass transfer resistance. At constant fuel molar fraction, contradicting findings were reported showing both negative and positive effects of the pressure on the reaction rate. Results suggest that keeping the gas space velocity constant counteracted the negative effect of the external mass transfer resistance. Pressurized reactor experimental results confirm this interpretation. This implies that the negative effect of pressure on kinetics in real reactors could be much smaller than suggested by most TGA studies, making pressurization an effective pathway for process intensification of chemical looping processes. This is an important finding for the future of pressurized chemical looping because the ability to leverage high reaction rates for downsizing pressurized reactors is important for controlling capital costs. The effect of pressure on the oxygen carrier morphology and durability is not widely studied yet; therefore, we highly recommend future research in this important aspect to assess the durability of various oxygen carriers at elevated pressure conditions.

A limited number of studies have been reported on experimental testing of reactor configurations under pressurized conditions, distributed between gas switching both under fluidized and packed bed modes (for gaseous fuel), interconnected fluidized bed reactors (mainly for solid fuel), and moving bed reactors (for the steam-iron process). All pressurized demonstration studies remain at lab and pre-pilot scales (up to 50 kW_{th} capacity). A summarized comparison of six different reactor configurations is also presented. Relative to

the conventional dual fluidized bed chemical looping reactor configuration, several concepts are available to simplify operation under pressurized conditions, although these involve trade-offs with respect to reactor footprint, thermochemical stresses on the oxygen carrier, and CO_2 capture ratio.

Techno-economic assessment studies on pressurized chemical looping have reported a wide range of energy penalties and associated CO_2 avoidance costs for different chemical looping processes, reactor configurations and process integrations. The wide variation in the assumptions employed hampers direct comparisons between studies, but most benchmarking works reported that chemical looping outperforms conventional CO_2 capture processes. Pressurized CLC faces a fundamental challenge from the maximum achievable reactor temperature that is far below the firing temperature of modern gas turbines. Recent works have proposed added firing after the CLC reactors to mitigate this challenge. Other chemical looping processes are not hampered by this limitation. In particular, hydrogen production concepts based on chemical looping reforming and chemical looping water splitting promise techno-economic performance approaching benchmarks without any CO_2 capture. Another important aspect recently studied is flexible power output to balance variable renewable energy, either through energy storage in the oxygen carrier or flexible output of power and hydrogen. Large energy system benefits have been found for the flexible power and hydrogen pathway.

The promising results from the techno-economic assessment studies present a strong case for further experimental demonstration of the promising chemical looping technologies in the reactor configurations that were identified to be suitable for pressurized operation. Thorough testing of these reactor configurations at operating temperatures and pressures relevant to industrial conditions for the specific processes is needed to identify and solve the technical challenges hindering their successful and safe operation with good performance in terms of fuel conversion and separation efficiency. Once demonstrated under these conditions, reactor concepts designed especially for pressurized operation should be relatively simple to scale up for commercialization, allowing chemical looping technology to accelerate the global energy transition via clean power, hydrogen and system flexibility.

Nomenclature

Acronyms

AR	Air reactor
ASU	Air separation unit
CCUS	Carbon Capture, Utilization and Storage
CGSM	Changing Grain Size Model
CLC	Chemical looping combustion
CLH	Chemical looping hydrogen
CLR	Chemical looping reforming
CLAS	Chemical looping air separation
CLOP	Chemical looping oxygen production
CLOU	Chemical looping with oxygen uncoupling
CFB	Circulating fluidized-bed
FR	Fuel reactor
FTR	Fired tubular reforming
GSR	Gas switching reforming
HAT	Humid air turbine
ICR	Internally circulating reactor
IGCC	Integrated gasification combined cycle
OC	Oxygen carrier
LHV	Lower heating value
LCOE	Levelized Cost of Electricity
LCOH	Levelized Cost of Hydrogen
MA-ATR	Membrane-Assisted Autothermal Reforming
MA-CLR	Membrane-Assisted Chemical looping reforming
MA-GSR	Membrane-Assisted Gas Switching Reforming
MDEA	Methyl diethanolamine
MSB	Magnetic suspension balance
NGCC	Natural Gas Fired Combined Cycle
OXY-CC	Oxyfuel combined cycle
PCLC	Pressurized Chemical looping combustion
PSD	Particle size distribution
PTGA	Pressurized thermogravimetric analysis
SCL	Syngas chemical looping
TGA	Thermogravimetric Analysis
TIT	Turbine inlet temperature
TRL	Technology readiness level
VRE	Variable renewable energy
WGS	Water gas shift
Symbols	
A	pre-exponential factor (s^{-1})
b	stoichiometric factor, mol of solid reacting (mol of gas)$^{-1}$
C	gas concentration, mol m^{-3}
C_{eq}	gas concentration at equilibrium conditions, mol m^{-3}
$C_{CO,b}$	The concentration of CO at the surface of the particle, mol m^{-3}
D	diffusivity, m^2/s
d	Fitted parameter for pressurized kinetics
E	activation energy, J mol^{-1}
ΔG	Gibbs free energy
ΔH	reaction enthalpy (kJ/mol)
k_0	pre-exponential factor of the chemical reaction rate constant, $mol^{1-n}\ m^{3n-2}\ s^{-1}$
$k_{0,P}$	pre-exponential factor of the chemical reaction rate constant for pressurized conditions, $mol^{1-n}\ m^{3n-2}\ s^{-1}$
k	chemical reaction rate constant, $mol^{1-n}\ m^{3n-2}\ s^{-1}$
k'	The overall rate constant, $m^3/(g\ s)$

L	layer thickness of the reacting solid for the platelike geometry, m
M	Molecular weight
m	mass of sample, g
m_{ox}	mass of the fully oxidized oxygen carrier, g
n	reaction order
P	total pressure, atm
P_p	partial pressure, atm
P_G	partial pressure of reacting gas G
P_T	Total pressure
R	ideal gas constant, J mol^{-1} K^{-1}
R_0	oxygen transport capacity of the oxygen carrier
r	grain radius, m
S	specific surface area of the particle
S_o	The initial reaction surface area, m^{-1}
t	time, s
T	Temperature, K
u	Fluidization velocity (m/s)
u_{mf}	Minimum fluidizing velocity (m/s)
X	solid conversion
w	mass fraction, kg/kg
Greek letters	
ρ_m	Molar density of the reacting material, mol m^{-3}
τ	Time for complete solid conversion, s
ε	Porosity, m^3/m^3
ε_{mf}	Porosity at minimal fluidizing velocity, m^3/m^3
ε_{mb}	Porosity at minimal bubbling velocity, m^3/m^3
ψ	Structure parameter (calculated from pore structure measurements and BET surface area)

Chapter 3 Initial experimental insight of the ICR concept

This chapter is based on the following paper:

Internally circulating fluidized-bed reactor for syngas production using chemical looping reforming

Mogahid Osman, Abdelghafour Zaabout, Schalk Cloete, Shahriar Amini

Chem. Eng. J. 377 (2019) 120076

Abstract

Chemical looping reforming (CLR) is a promising method for achieving autothermal methane reforming without the energy penalty of an air separation unit that is required for partial oxidation (POX) or oxygen-blown autothermal reforming (ATR). Scale-up of the conventional dual circulating fluidized bed CLR configuration is challenging, however, especially under the pressurized operating conditions required for high process efficiency. The internally circulating reactor (ICR) concept has previously been proposed as a simplified solution for chemical looping, especially under pressurized operation. It assembles the chemical looping process into a single reactor with two sections connected by specially designed ports for oxygen carrier circulation. This study has successfully demonstrated CLR operation in a dedicated ICR test unit with a NiO oxygen carrier. Up to 3 kW of methane feed was reformed to syngas, achieving conversion efficiencies as high as 98%. The reactor behaved largely as expected over a range of CH_4/O_2 ratios and in a case with steam addition. Autothermal reactor operation could also be achieved, illustrating the practicality of the ICR concept. Based on this positive first demonstration study, further study of the ICR concept is recommended.

Mogahid Osman planned the experiments with cooperation with other authors. Mogahid conducted the experimental tests with guidance from Abdelghafour Zaabout. All co-authors contributed on analyzing the results and writing the paper.

3.1 Introduction

Natural gas reforming to syngas is the main commercial process for the production of hydrogen, ammonia, methanol and other important chemicals [175]. Catalytic steam methane reforming (SMR) is the most widely used approach in industry for syngas production [176,177]. SMR reactions are highly endothermic and reaction heat is generally supplied by external combustion of a fossil fuel with air, leading to significant CO_2 emissions [176,177]. Other technologies for syngas production has also been applied in industry in the last decade, including partial oxidation (POX) and autothermal reforming (ATR) [178]. POX produces syngas by partially oxidizing a hydrocarbon fuel with pure oxygen in a catalytic or non-catalytic reactor vessel. The main advantages of POX are its ability to reform higher hydrocarbons and avoid the need for external combustion. However, a large quantity of pure oxygen is required, thus demanding substantial investment and energy costs to construct and operate an air separation unit (ASU). ATR is a combination of SMR and POX technologies, in which pure oxygen or air co-feed with natural gas and steam. The exothermic POX reaction provides the necessary heat for the endothermic reforming reactions. However, ATR requires an ASU to supply a high quality syngas (high fraction of CO and H_2). If air used directly, the product gas will be diluted with nitrogen, imposing additional costs and efficiency penalties unless nitrogen is required as in ammonia production.

Chemical looping reforming (CLR) has emerged as a promising technology for syngas production with the potential to address the key shortcomings mentioned above for the conventional techniques. CLR can achieve autothermal methane reforming without external combustion reaction or an ASU, and obtain a N_2 free syngas stream without an ASU [10,11]. Moreover, CLR reduces the energy penalty associated with an SMR plant with post-combustion CO_2 capture. A techno-economical study of different natural gas reforming technologies has shown that CLR with CO_2 capture is the most financially attractive option with a CO_2 avoidance cost of only \$5/tonne CO_2 relative to conventional SMR. SMR and ATR with CO_2 capture need CO_2 prices more than \$100 and \$50/tonne CO_2, respectively, to be a feasible option [179]. The study also found that CLR without CO_2 capture can be cheaper than conventional SMR.

The typical CLR system involves circulation of an oxygen-carrier (a metal-oxide material) between two interconnected reactors, namely the air reactor and the fuel reactor [22]. The material acts as an oxygen and heat transfer medium as well as a catalyst [11,22,23]. In the fuel

reactor, the fuel reacts with the metal oxide to form the reformer gas (a mixture of H_2, CO, H_2O and CO_2) where the reduced metal also acts as a catalyst and heat supply for the reforming reactions, (Figure 36 shows a simplified scheme of the working principle of the CLR process). In the air reactor, the reduced metal is oxidized and heated by the highly exothermic reaction before being transferred to the fuel reactor for continuous cyclic operation. Steam or CO_2 could be introduced with the fuel to enhance the reforming reaction and control the desired H_2/CO ratio in the produced syngas. It should be mentioned though, that steam or CO_2 addition is not a requirement because the part of the fuel being combusted during the autothermal reforming process will directly supply H_2O and CO_2 in the fuel reactor.

The CLR concept have been demonstrated at atmospheric pressure in a laboratory and pilot plant scale up to 140 kW (while natural gas CLR is the most widely studied [11,12,17,22,180], also liquid and solid fuel have been used for syngas production [181–185]). The performance of CLR under pressurized conditions was studied by Ortiz et al. [23] in a semi-continuous fluidized-bed reactor. The effect of total pressure on the CLR process using methane as fuel and nickel based oxygen-carriers was investigated. The results showed high conversion of methane and no effect of increasing the pressure on the products distributions. Extensive review of the recent CLR operational experiences can be found elsewhere [67,186].

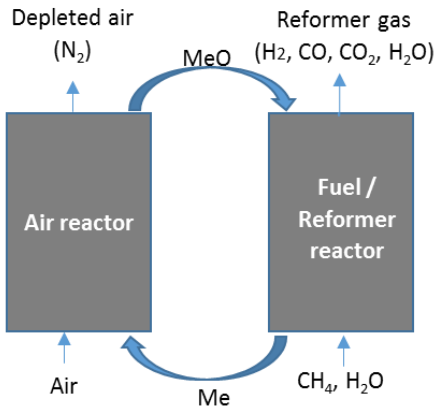

Figure 36. Schematic diagram of the CLR process.

Pressurized operation of the CLR process is essential to maximize thermodynamic and economic performance. In the case of hydrogen production, pressurized operation minimizes the energy and capital cost related to hydrogen separation and compression. Syngas to liquids

processes also require a pressurized syngas to maximize conversion efficiency. Furthermore, pressurized operation significantly reduces the plant footprint. A thermodynamic assessment has indeed shown that a 5% increase in energy efficiency could be achieved if CLR is operated under pressurized conditions, mainly gained from the energy saving made in H_2 and CO_2 compression [67]. The benefits of pressurized CLR operation addressed in the literature in various aspects including thermodynamic analysis, techno-economic studies, kinetic analysis and lab and pilot scale demonstration [23,67,187,188].

However, most experimental studies on chemical looping are based on operation at atmospheric pressure, as a circulating fluidized-bed reactor is the most widely studied reactor type for the CLR system. This configuration has been demonstrated experimentally at lab [10–12] and pilot scales [22]. To the best knowledge of the authors, only two studies have so far reported on pressurized interconnected fluidized beds for CLC. Wang et al. [75] carried out a pressurized CLC for coke-oven gas, where the operational pressure of the system was 3 bar and the maximum operating temperature was 950°C. More recently, Xiao et al. conducted solid fuel CLC at three pressure levels (1, 3 and 5 bar) [189]. The results showed that pressurized operation improved carbon conversion as well as CO_2 capture purity and combustion efficiency. However, higher losses of oxygen-carrier particles were reported with increasing pressure due to a decrease in the fuel reactor cyclone capture efficiency at elevated pressure. In this type of configuration, the system consists of two reactors, two loop seals and two cyclones to avoid gas leakage between the fuel and air reactors and achieve high gas-solid separation at the reactor outlets. Tightly controlled solids circulation between the two interconnected reactors, required to fulfill the heat and mass balance of the chemical looping process, presents a significant scale-up challenge, especially under pressurized conditions.

The need for pressurized CLR operation has inspired research into alternative reactor configurations that avoid external solids circulation. One such reactor configuration is the gas-switching concept, where the oxygen carrier material is stationary in one compact unit and exposed to alternate streams of air and fuel [82,190]. This arrangement greatly simplifies the reactor design and scale-up, but a coordinated cluster of reactors is required to achieve steady operation. The gas switching concept has been studied using packed-bed [100,190] and fluidized-bed configurations [80,191]. The packed bed system imposes several challenges including the requirement for pelletized oxygen-carrier materials, more pronounced carbon deposition, large thermo-chemical stresses on the oxygen carrier, and the requirement for reactor shutdown for replacement of the spent oxygen carrier material [192]. The fluidized bed configuration

circumvents these material-related challenges but suffers moderate losses in process and CO_2 capture due to the good mixing taking place in the reactor [192]. The most important technical uncertainty related to the gas switching technology at present is the need for high temperature outlet valves [192]. CLR typically operates at lower temperatures than CLC, thus minimizing this challenge. Other reactor concepts proposed in the literature are the moving bed [193] and rotating reactor [118,119].

However, the steady-state nature and high gas throughput rates of the dual circulating fluidized-bed configuration remains attractive even when considering the challenges of pressurized operation. Simplifying the solids circulation mechanism for this reactor setup promises to accelerate scale-up and eventual commercialization. For this reason, this paper investigates the recently proposed internally circulating reactor (ICR) where the loop seals involved in the conventional configuration are replaced by simple ports between two sections in a single vessel [20], with a freeboard on the top replacing the cyclones. ICR can operate similarly to the interconnected configuration, where solids circulation between the two sections is achieved by feeding gasses into the two sections at different velocities. The high velocity gas feed in the fast section transports solids to the freeboard. The decelerated solids in the freeboard (due to the larger section area) fall into the upper port to circulate to the second section operating at low velocity (the slow section). Accumulation of solids in this section leads to static pressure building up, hence forcing the solids to circulate back to the fast section through the port at the bottom.

Combining the functionality of both reactors, cyclones and loop seals into a single unit is expected to simplify operation and design and reduce costs under pressurized conditions. The ICR unit can be designed as a single pressure vessel, whereas the conventional dual circulating fluidized bed configuration requires a separate pressure shell for each component. In addition, the short and simple ports will simplify control of the high solids circulation rates required under pressurized operation, relative to the much more elaborate system of cyclones, loop seals and relatively long solids transport lines connecting the reactors in the dual circulating fluidized bed configuration. Due to the simplified solids circulation mechanism, pressure imbalances between the reactors will be less likely and a wider range of operating conditions should be achievable.

The most important trade-off the ICR configuration is however, the gas leakage when using the simple ports instead of dedicated loop seals. A hydrodynamic investigation on a pseudo-

2D cold-flow unit has revealed that a stable solids circulation and minimum gas leakage could be achieved with the ICR over a wide range of operating conditions [20]. This conclusion was confirmed by reactive multiphase flow modelling of a large-scale ICR unit (100 MWth) reactor [21]. Such a reactor configuration, based on internally circulating fluidized bed, was first proposed as an oil shale retort in 1986 [13] and was later widely used as a simplified version of the interconnected fluidized bed to evaluate the performance of different oxygen carrier materials under CLC and CLR process conditions on an atmospheric small lab scale [11,16–18,181,194–196].

In light of the promising results from the hydrodynamic study and the reactive simulations, the ICR unit shown in Figure 37 has been constructed and commissioned to operate under fully reactive high temperature pressurized conditions. The aim of this study is to experimentally study the feasibility of the ICR concept for chemical looping reforming of methane, as well as to obtain insights about this type of reactor configuration in terms of ability of autothermal operation, achieving minimal leakage between the reactor sections and stable solids circulation under reactive conditions. This study represents the first demonstration of our proposed ICR concept under reactive conditions.

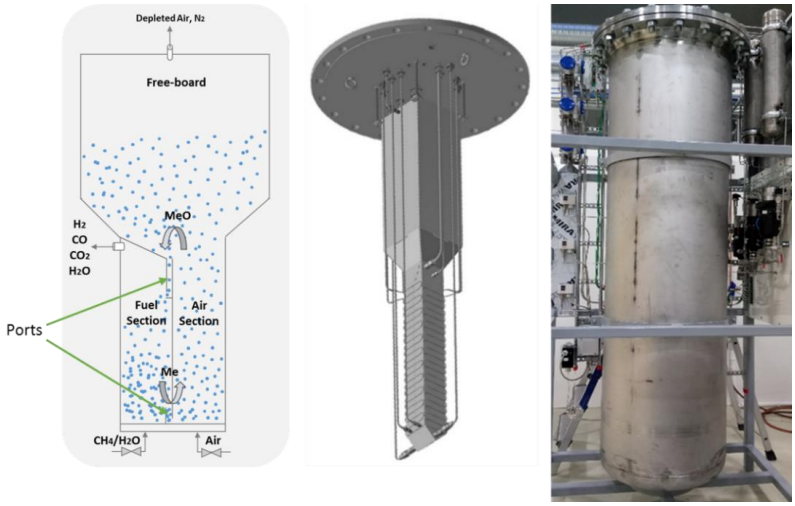

Figure 37. Simplified scheme of the ICR design, CAD drawing of the ICR unit, and the ICR unit under operation inside the shell.

3.2 Methodology

3.2.1 ICR unit

A lab scale ICR shown in Figure 37 has been constructed and commissioned. The reactor was made of Inconel material (Inconel Alloy 625) to withstand high temperature conditions. It has a square section of 10 cm width and 70 cm height, divided into two sections (air reactor and fuel reactor) by a vertical partition, with connecting ports in between, at the top and the bottom, for solids circulation. An expanding freeboard region is added to the air reactor (AR) where the depleted air transporting oxygen carrier from the AR is decelerated to avoid particle elutriation, thereby allowing the oxygen carrier to fall into the upper port and circulates to the fuel reactor (FR). With this configuration, fast and bubbling fluidization regimes can be established in the air and fuel reactor respectively. The gas feed to each reactor section is completed using a perforated cylindrical tube at the bottom of each section. This relatively concentrated injection mechanism may reduce the quality of gas-solid contact in the lower regions of the reactor compared to a conventional porous plate but was selected due to substantial simplification offered in terms of reactor design and construction. The ports connecting the two sections are L-type connection ports, which were adopted instead of a simple orifice to create conditions with solids flowing close to maximum packing. Such a flow condition creates a physical plug that minimizes undesired gas leakage through the port.

The reactor was placed in a cylindrical shell designed to withstand pressures up to 12 bar. The reactor can be heated up to the target operating temperature using external electrical heaters surrounding the bottom part of the reactor body. Insulating material (glass wool) was placed around the reactor to minimize heat losses. The pressures inside the reactor and the shell were controlled using back-pressure regulators placed on the outlet of each reactor section and the shell. The reactor exhaust stream was cooled with a water cooler installed on the outlet of each section. A low temperature filter (40 μm pore size) was installed after the cooler to prevent fine particles elutriation to the environment. The feed flow rate to each section was controlled by Bronkhorst mass flow controllers. The dry gas composition (sampled after the back-pressure valve) was measured at 1 Hz frequency using a syngas analyzer type MCA 100 Syn-P from ETG Risorse e Tecnologia.

The experimental set up was equipped with different additional devices (DP cells, pressure sensors, thermocouple etc.) to monitor the reactor operation (solids circulation, temperature and pressure inside the reactor, etc., in addition to devices used for safety). Figure 38 gives an

overview of the reactor design and shell and the P&ID showing the different parts forming the set-up.

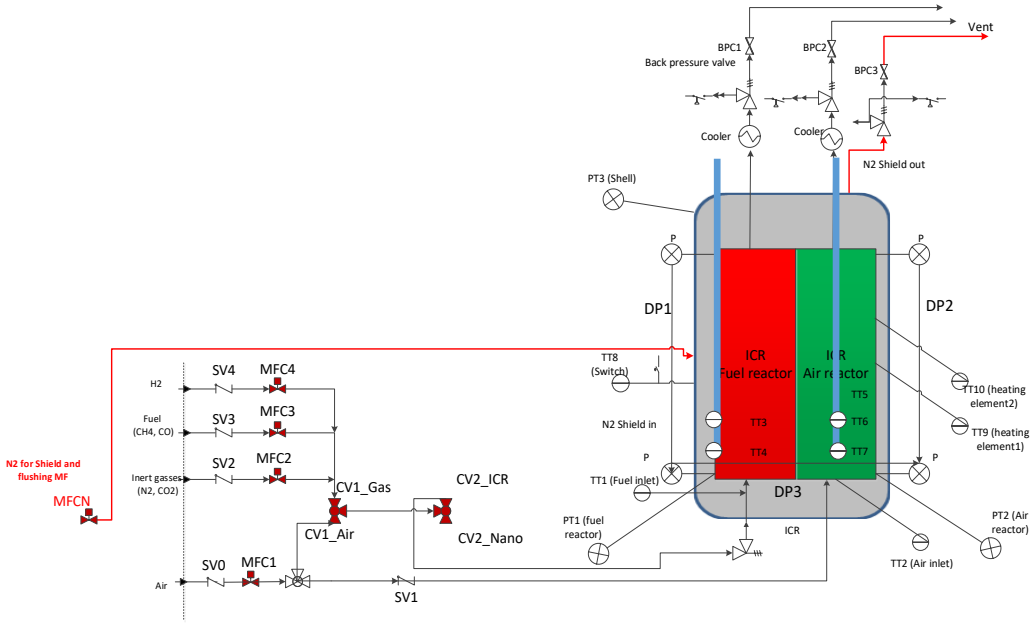

Figure 38. P&ID diagram of the ICR unit.

3.2.2 Oxygen carrier

In this study, a highly active oxygen carrier manufactured by VITO, was used. The oxygen carrier is based on NiO particles supported on Al_2O_3; the NiO/Al_2O_3 ratio was 65/35, but resulted in around 37% free NiO (based on weight) sites which are available for reaction, while the rest reacted to $NiAl_2O_4$ during heat treatment used in the spray drying manufacturing process [197]. The particle size cut-offs D10, D50, and D90 were measured to be 117.4, 161.7 and 231.3 mm respectively. The oxygen carrier had a loosely packed density of 1950 kg/m^3 and a tapped density of 2166 kg/m^3. This oxygen carrier was selected because it has been successfully used in previous studies, and showed high reactivity and durability [198,199]. It should however be emphasized that the selection of an optimal oxygen carrier is out of the scope of this study; the main aim is to demonstrate the experimental feasibility of the ICR concept applied to CLR.

3.2.3 Fuel

Methane was used as fuel in most experiments, although CO was also used initially to verify that good solids circulation is achieved. Steam could be added with the fuel by a steam generator at a temperature of 200°C. The steam is fed to the reactor in a heated tube to prevent condensation. When desired, it was also possible to dilute the fuel with CO_2 or N_2.

3.2.4 Experimental procedure

The experience and knowledge gained from operation of a pseudo-2D cold unit built in our previous studies [20], were used to design a safe operating window of the ICR reactor. The link between solids circulation rate and the gas leakage between the two sections was quantified and understood in the pseudo 2D experiments. Similar methodology was followed in the constructed 3D reactor, operated under cold and hot (electrical heating) conditions with feeding of non-reactive gasses, to identify feed conditions that result in minimal gas leakage and steady solids circulation between the reactor sections. For all experiments, a total mass of 2 kg of NiO/Al_2O_3 particles was used (corresponding to 10 cm static bed-height). The reactor was electrically heated to 650 °C before feeding reactive gases. During the reactive experiments, the power of the heater was adjusted between 0 to 100% depending on the operating conditions. For autothermal operation, the heater power was set to 0%. Due to technical limitation, the set point temperature of the heating elements surrounding the reactor is limited to a maximum value of 820 °C. For this reason, all the experiments presented on this paper were carried out below this limit.

Before conducting the reactive experiments, initial tests were carried out to define an operating window in which solids circulation is achieved. The tests were completed by feeding a reactive gas, CO, to the fuel reactor (FR) and N_2 to the air reactor (AR), into a fully oxidized bed of oxygen carrier material. CO is highly reactive with NiO, and the CO breakthrough curves can therefore be used to clearly see whether circulation is transferring additional fully oxidized oxygen carrier from the AR to the FR under different gas feed rates to the air section. The outlet gas flowrates from each section were adjusted to be equal to the respective inlet gas flowrates by means of a manual needle valve placed on the outlet of the FR, while a rotameter was placed on the outlet of the AR. It should be noted that controlling flow rates at the outlets of the ICR sections affects the amounts of occurring gas leakage and solids circulation [20,21].

After defining operating conditions in which stable solids circulation is achieved, another set of experiments was conducted to quantify the gas leakage between the two ICR sections. This

test was done by feeding CO_2 to FR and air to AR under external heating. CO_2 recovery and purity were calculated based on the amount of measured gas leakage from each section to the other.

In the CLR tests, seven experimental cases were considered in the current study. The main objective of the CLR process is to selectively produce syngas, which can be achieved by controlling various parameters in the system. The main operating variable is the CH_4/O_2 ratio in the FR, which can be altered by three parameters: solids circulation rate, oxygen feed to the AR and CH_4 feed to the FR. In all cases, the solids circulation was kept constant using constant fluidization velocities to both sections at a constant loading of the OC. At these conditions, bubbling and fast fluidization regimes in the FR and AR, respectively, were established. The fuel side fluidization velocity was estimated by assuming that methane will expand in volume by a factor of three after reacting to form syngas (with assuming full methane conversion).

Four cases were completed by changing CH_4 concentration in FR and two cases by changing O_2 concentration in AR for comparison. N_2 was used for dilution of the feed in both sections to maintain the total flow rate constant. One additional case was carried out with co-feeding steam with CH_4. A summary of the experimental cases is given in Table 8 and

Table 9 . It should be noted that all experiments were carried out at 1.7 bara pressure and that the experimental results represent an average over at least 10 minutes of steady state operation. It is worth mentioning that approximately 3% of the total solids loading was lost as fines after all CLR operation. The lost fines were mainly recovered on the water trap in the heat exchanger after the FR and the on the filter after the AR. The ones collected on AR mainly originated from the fines in the fresh solids placed initially in the reactor before experiments, while the ones collected on FR contained larger particles that seem been elutriated from the bed, possibly due to sudden large bursts of gas that leaked from AR to FR.

Table 8. Summary of the experimental cases conducted in this study.

Experimental cases	Fuel-reactor (flowrate Nl/min)					Air-reactor (flowrate Nl/min)	
	CH_4	N_2	Steam	CO	CO_2	Air	N_2
Case-1	-	-	-	20	-	-	0, 70, 80, 90
Case-2	-	-	-	-	15	80	-
Case-3	3	6	-	-	-	80	-
Case-4	3.5	4.5	-	-	-	80	-

Case-5	4	3	-	-	-	80	-
Case-6	5	-	-	-	-	80	-
Case-7	4	3	-	-	-	25	55
Case-8	5	-	-	-	-	20	60
Case-9	4	-	3	-	-	80	-

Table 9. Summary of CLR operating conditions

Fuel	CH_4
Oxygen carrier	NiO/Al_2O_3
Particle size	~161.7 μm
Particle loading	2 kg (10 cm static bed-height)
Temperature	650 °C (initial temperature)
Pressure	1.7 bara
Flow rate in AR	80 Nl/min
Flow rate in FR	15 Nl/min

3.2.5 Data evaluation

Reactivity of fuel with OC particle are expressed by γ_{CH_4}, the carbon conversion of methane, which is defined as in Eq. (3-1):

$$\gamma_{CH_4} = \frac{x_{CO_2} + x_{CO}}{x_{CH_4} + x_{CO_2} + x_{CO}} \tag{3-1}$$

where x_i is the volume fraction of compound i in the dry gas leaving the FR.

In the non-reactive gas leakage experiments, CO_2 recovery was calculated as the ratio between the CO_2 leaking from the FR and the total amount of CO_2 in the FR (Eq. (3-2)). Similarly, CO_2 purity was calculated as the ratio between the air leaking from the AR and the total amount of CO_2 in the FR (Eq. (3-3)):

$$\mathrm{CO_2\ recovery} = \left(1 - \frac{\mathrm{CO_2\ flowrate\ at\ AR\ outlet}}{\mathrm{CO_2\ flowrate\ at\ FR\ inlet}}\right) \times 100 \tag{3-2}$$

$$\mathrm{CO_2\ purity} = \left(\frac{\mathrm{CO_2\ flowrate\ at\ FR\ outlet}}{\mathrm{Total\ flowrate\ at\ FR\ outlet}}\right) \times 100 \tag{3-3}$$

Similarly, for the gas leakage during CLR experiments, the syngas recovery is obtained as the ratio between the syngas leaks from the FR to the AR and the total amount of syngas produced in the FR. Syngas purity calculated based on the N_2 leaking from the AR to the FR and the total amount of syngas produced in the FR.

The following reactions are involved in the CLR process. It is noted that R1 and R2 occur primarily as combinations of R3-R6.

Fuel reactor:

$$CH_4 + NiO \leftrightarrow CO + 2H_2 + Ni \quad R1$$

$$CH_4 + 4NiO \leftrightarrow CO_2 + 2H_2O + 4Ni \quad R2$$

$$CH_4 + H_2O \leftrightarrow CO + 3H_2 \quad R3$$

$$CO + H_2O \leftrightarrow CO_2 + H_2 \quad R4$$

$$H_2 + NiO \rightarrow Ni + H_2O \quad R5$$

$$CO + NiO \rightarrow Ni + CO_2 \quad R6$$

Air reactor:

$$O_2 + 2Ni \leftrightarrow 2NiO \quad R7$$

3.3 Results and Discussions

The results will be presented and discussed in three parts: 1) Solids circulation, 2) Gas leakage, 3) CLR of methane. Table 10 summarizes the main results of the CLR experimental campaigns which will be disused in the following sections.

Table 10. Summary of the main results of the CLR experimental campaigns.

	Product compositions (vol%)					Fuel Reactor		Air Reactor		Syngas recovery %	Syngas purity %	T-FR (°C)	T-AR (°C)
	CH_4	CO_2	CO	H_2	N_2	CH_4 Conv %	H_2/CO	O_2 Conv %	CO_2 vol %				
Case-3	1.7	29.2	0.4	0.0	68.7	94.7	0.0	28.8	0.43	88.6	90.7	764	800
Case-4	0.8	30.3	5.7	10.5	52.6	97.8	1.83	30.0	0.51	88.9	90.9	760	810
Case-5	0.9	31.1	10.8	22.9	34.4	98.1	2.13	34.3	0.46	91.3	93.0	745	785
Case-6	2.0	31.8	19.7	41.3	5.3	96.3	2.09	33.8	0.38	94.1	95.2	753	793
Case-7	1.5	19.4	14.0	31.2	33.9	95.8	2.22	96.4	0.31	93.9	94.9	746	765
Case-8	3.4	13.9	23.7	51.1	7.9	91.7	2.16	100.0	1.14	81.2	84.1	740	765
Case-9	3.7	19.2	15.3	51.5	10.3	90.3	3.36	23.8	0.61	87.2	89.1	721	753

3.3.1 Solids circulation

The solids circulation rate is a critical operating variable for the chemical looping reforming process. Estimating the solids circulation rate in a hot, pressurized ICR system is a challenging task because no direct measurement technique is possible. In this study, we follow the indirect approach described in Section 2.4 to define an operating window where solids circulation is sufficient for CLR process.

Figure 39. shows the profile of CO conversion with time for different N_2 flowrates in the AR. Complete CO conversion was observed for all cases during the first minute of operation before gradually reducing with time as the oxidized oxygen carrier is consumed in absence of an air feed for re-oxidation. The test was stopped at a certain level of CO conversion (~20%) to avoid carbon deposition in the existence of highly reduced oxygen carrier as metallic Ni is well known to catalyze CO decomposition. The case of not feeding N_2 to the AR shows that the oxygen carrier in the fuel reactor can be reduced in about 160 s if no solids circulation takes place. With introducing N_2 to the AS, the time almost doubled, implying successful solids circulation and reduction of all the OC loaded in the reactor. Only minor differences were observed between the three N_2 feed rates investigated, implying that the range of 70-90 Nl/min feed to the AR is safe for achieving good solids circulation in the reactor.

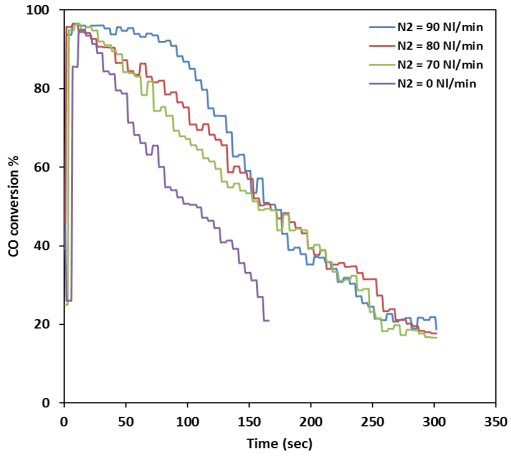

Figure 39. Temporal evolution of CO conversion for different N_2 flowrates in the AR, Case-1.

3.3.2 Gas leakage

Gas leakage between FR and AR is undesirable in CLR process because it lowers syngas recovery and purity. In the pseudo-2D ICR cold study, we have shown that gas leakage can be controlled by ensuring that the gas outflow is equivalent to the gas inflow in each section [20]. In the non-reactive gas leakage study described in Section 2.4, analysis from the outlets of the FR and AR shows that 1.7 vol% of the air feed bypassed to the FR and 9 vol% of CO_2 feed bypassed to the AR. This corresponds to 91 % CO_2 recovery and purity.

In a similar ICR concept, Kronberger et, al. [16] carried out a cold flow study of a two compartment fluidized-bed reactor with different slots design connecting the two beds. A slot design with a height of 1.2 mm and an 8 mm wide was found to be the best in achieving a minimum gas leakage. This design has also the possibility of fluidization with inert gas below the slot, which is further reduce the gas leakage. Subsequent studies for CLC and CLR process in a 300 W unit showed that the leakage from the FR to the AR was about 5% of the added carbon, whereas the leakage flow in the opposite direction was 0-0.2% of the added air [200]. Herguido et, al. [19] also applied ICR concept for hydrogen separation using the steam-iron process. They studied the effect of several parameters on gas leakage and solid circulation. Fluidization velocity in both sections and design of the orifice connected the reactor sections found to be the key parameters for controlling gas leakage and solid circulation rate. An orifice diameter of 0.3 cm was found to be an optimal in achieving sufficient solid circulation rate while minimizing the gas leakage.

All fully reactive CLR tests in the following sections were completed with identical operating conditions (temperature, fluidization velocity and solids loading), so it is expected that similar gas leakage will be observed. It is expected that gas leakage occurs mainly through the top port as this port will not be completely filled with particles due to the small quantity of oxygen carrier used in these tests. A filled port is important to restrict uncontrolled gas slippage between the two reactor sections [20]. The possibility for further decreases in gas leakage will be further investigated in future works with different oxygen carrier loadings and fluidization velocities.

3.3.3 Chemical looping reforming of methane (excess air)

The ICR unit used in this study was designed to test a number of different chemical looping concepts, hence the equal cross sections of the AR and FR of the reactor (Figure 37). In CLR, the air requirement is much smaller than in CLC, implying that a feed of pure air to the AR at

the high flowrate required to achieve solids circulation will provide excess oxygen. In this case, however, the oxygen transport to the FR was limited by the oxygen carrier circulation rate, not by the amount of oxygen fed to the AR. This allowed the CH_4/O_2 ratio to be controlled by simply varying the degree of fuel dilution, while feeding an excess of air to the AR (cases 3-6 in Table 8). The CH_4/O_2 ratio in the FR controls the tendency towards reforming or combustion. Gas concentration measurements at the AR outlet showed that only about a third of the incoming oxygen (~5.6 Nl/min) was consumed in these cases. This results in CH_4/O_2 ratios of 0.54-0.89 for the four cases investigated in this section.

Figure 40 and Figure 41 show the results from this experimental campaign. Case-3 showed near complete combustion of CH_4 to CO_2 and H_2O, which implies an excess of NiO in the fuel reactor (R2). A minor amount of CO was also detected, although H_2 is completely consumed due to its very high reactivity with NiO. This may be expected given that the CH_4/O_2 ratio is close to the stoichiometric ratio of 0.5 for methane combustion. Increasing the methane flowrate from 3 Nl/min to 5 Nl/min increases the CH_4/O_2 ratio and therefore shifts the reaction further towards reforming instead of combustion, producing more H_2 and CO (R1). For case 5 and 6, an H_2/CO ratio of 2 was obtained, which is desirable for the Fischer-Tropsch process [201].

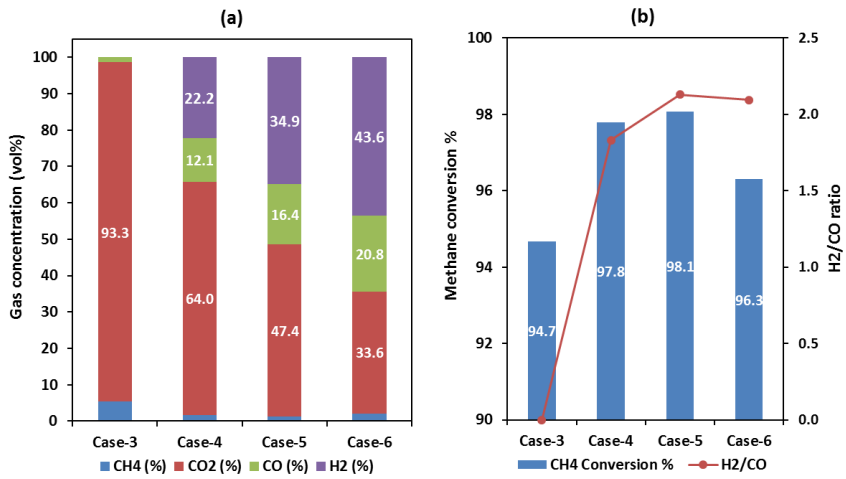

Figure 40. Products distribution (a) and methane conversion and H_2/CO ratio (b) for cases 3-6.

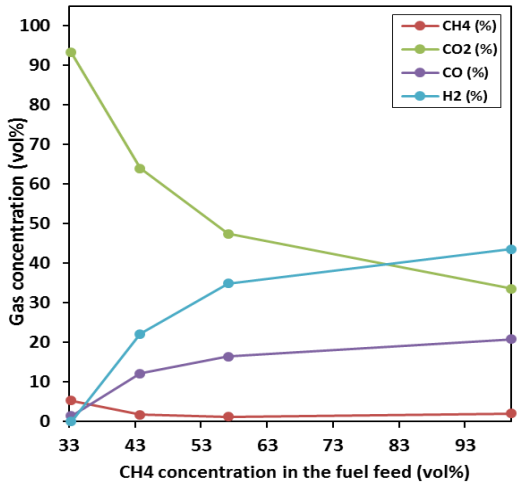

Figure 41. Effects of methane concentration on the products compositions.

Figure 40b shows the methane conversion level for cases 3-6. The first observation is that methane conversion is higher than 94% in all cases. This is testament to the extremely high reactivity of the NiO oxygen carrier used in this study. It is worthwhile to keep in mind that the bed height in the FR is only 10 cm and that the gas is injected in a relatively concentrated manner, imposing significant bubble-to-emulsion mass transfer limitations. Under similar conditions, a larger reactor will therefore easily achieve complete equilibrium conversion.

The second observation is that maximum methane conversion is reached at intermediate CH_4/O_2 ratios. This trend of methane conversion over NiO is associated with the degree of oxygen carrier reduction and the presence of H_2O and CO_2 in the FR. With a fixed solids circulation rate, increasing the fuel concentration in the FR will affect the OC reduction level and hence its activity and selectivity for methane reactions. A similar trend was revealed by several studies on CLC and CLR [17,202–206]. A study of methane CLC over NiO in a fixed bed reactor observed methane slippage during the first part of the reduction when the particles were fully oxidized, which disappeared as the particles became more reduced, i.e. the content of Ni increased [206]. Thus, at lower CH_4/O_2 ratios, the oxygen carrier was not sufficiently reduced to rapidly catalyze the reforming reaction on free Ni sites, resulting in reaction rate-limited methane conversion. At high CH_4/O_2 ratios, on the other hand, the lower fraction of CH_4 combustion produced a lower concentration of H_2O and CO_2 in the reactor, results in equilibrium limitations for the methane reforming reactions. When only CH_4 is fed to the

reactor, a large portion of this fuel must be combusted to H_2O and CO_2 to promote the Ni-catalyzed steam and dry reforming reactions, otherwise the degree of methane conversion will be thermodynamically limited.

Autothermal operation of ICR was investigated for these cases. Case 5 and 6 achieved autothermal operation successfully. Figure 42. shows the temperature profile for case 5: the temperature was constant in both sections for about 20 min of continuous operation without external heating. The temperature difference was 40°C between the two sections. Circulation of the OC and the heat transfer through the wall separating the two sections were the only source of heat for the reforming reactions during this investigation.

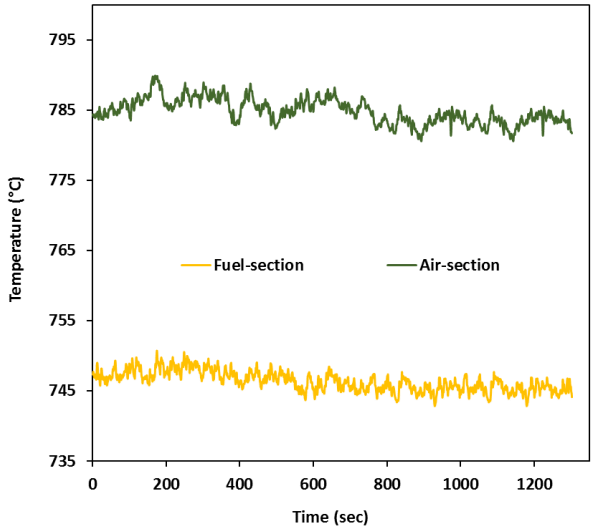

Figure 42. Temperature of FR and AR during autothermal chemical looping reforming of methane (case-5).

3.3.4 Chemical looping reforming of methane (diluted air)

In a second series of experiments, the oxygen supply to the AR was limited by N_2 dilution (case 7 and 8). In both cases, almost complete oxygen conversion was achieved (Table 10), which represents more realistic CLR behavior where the oxygen carrier circulation rate is not the limiting factor in oxygen transport between reactor sections as was the case in the previous section. Consequently, the oxygen added to the AR in cases 7 and 8 is not sufficient to reoxidize the OC completely. The OC flowing from the AR to the FR is therefore in a less oxidized form,

leading to higher reforming activity and, assuming a constant solids circulation rate, a lower flow of oxidized oxygen carrier to the FR.

The comparison between case 5 and case 7 was designed to achieve roughly the same CH_4/O_2 ratio in the FR. However, a significant difference in FR outlet gas composition and methane conversion is observed between these two cases because of the aforementioned factors. The increased presence of Ni and the lower presence of NiO in case 7 caused a higher fraction of H_2 and CO, but lower methane conversion relative to case 5 (Figure 43).

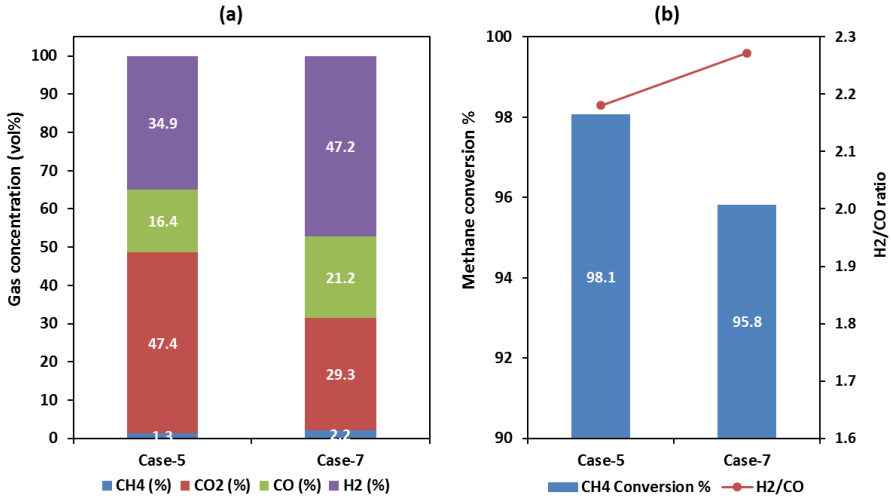

Figure 43. Products distribution (a) and methane conversion and H_2/CO ratio (b) for cases 5 and 7.

Case 8 was designed to achieve a substantially higher CH_4/O_2 ratio than case 6 (Figure 44). Naturally, this further increased the degree of reduction of the oxygen carrier entering the FR from the AR, leading to a greater shift towards H_2 and CO as well as a lower degree of methane conversion (thermodynamically limited due to the relatively low fraction of CH_4 combusted to H_2O and CO_2).

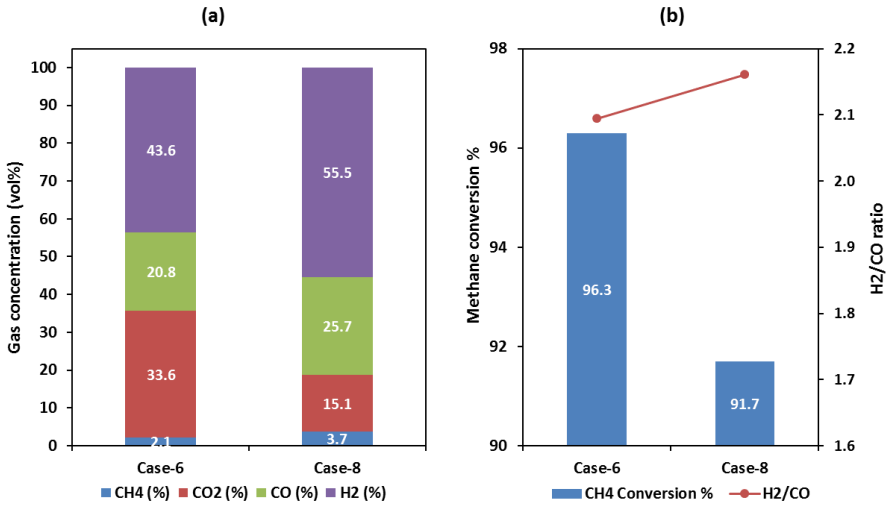

Figure 44. Products distribution (a) and methane conversion and H_2/CO ratio (b) for cases 6 and 8.

Further insight is provided by comparing the observed reactor performance to equilibrium calculations. These results were obtained using the equilibrium module of the HSC chemistry software 9.2, which is based on the method of minimization of the Gibbs free energy [207]. Figure 45 shows the comparison of the gaseous products obtained in case-5 to case-8 and the equilibrium compositions as a function of the CH_4/O_2 ratio for a reaction temperature of 746°C, and pressure of 1.7 bara. The temperature selected as an average temperature between case-5, case-6, case-7 and case-8, whereas the CH_4/O_2 ratio for these cases are 0.69, 0.88, 0.79 and 1.19, respectively.

Despite some scatter in the experimental results, it follows the same trend as the equilibrium calculations. The equilibrium composition of methane increases with increasing CH_4/O_2 ratio, which validates the drop of methane conversion in case-7 and case-8 compared to case-5 and case-6, respectively. Equilibrium is not reached mainly because of CH_4 slippage. This is attributed to a reaction rate limitation caused by the short bed height in the FR and the concentrated gas injection mechanism that limits gas-solid contact. Furthermore, the experimental H_2 and CO concentrations are lower than the equilibrium calculations because these gases react more rapidly than CH_4 with NiO. For instance, Wassie et al. [191] showed that CH_4 fed to a bed of NiO results in substantial fuel slippage, whereas a feed of H_2 results in complete fuel conversion. NiO enters from the top of the FR, while most reforming occurs over

the reduced OC at the bottom of the FR. Therefore, NiO is primarily reduced to Ni in the upper regions of the bed by H_2 and CO resulting from steam-methane reforming in the lower regions of the bed. If the FR was perfectly mixed, the experimental observations would be even closer to the equilibrium calculations.

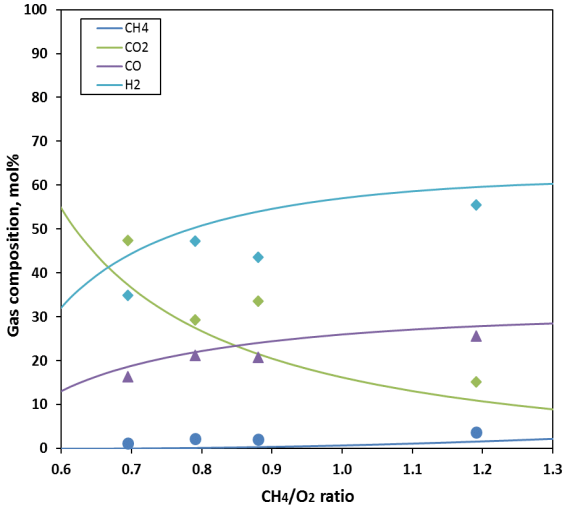

Figure 45. Dry gas compositions according to cases (5)-(8) compared to thermodynamic equilibrium for CLR of methane at 746°C and 1.7 bara.

3.3.5 Chemical looping reforming of methane (steam addition)

Partial oxidation of methane typically produces syngas with H_2/CO ratio of 2, as observed in the previous cases (case 4-8). Addition of steam with methane into the FR is the most suitable approach to increase the H_2 content in the syngas and prevent carbon formation. Steam boosts the catalytic methane reforming over metallic Ni (R3), which increases the H_2/CO ratio in the syngas produced. This process would be the most suitable one for H_2 production. Furthermore, additional steam will alleviate the equilibrium limitations on methane conversion observed when only CH_4 is fed to the reactor at a high CH_4/O_2 ratio (e.g. case 8).

In the current study, addition of steam with the fuel feed was investigated (case-9). An S/C ratio of 1.33 was chosen to keep the total flowrate constant and hence compare all results under similar hydrodynamic conditions. As shown in Figure 46, addition of steam enhances the methane reforming reactions, producing more H_2 and less CO_2, 57 vol% H_2 (dry basis) was produced compared to 35 vol% for the dry fuel feed (case-5). The H_2/CO ratio increases from 2.1 to 3.4 upon steam co-feeding.

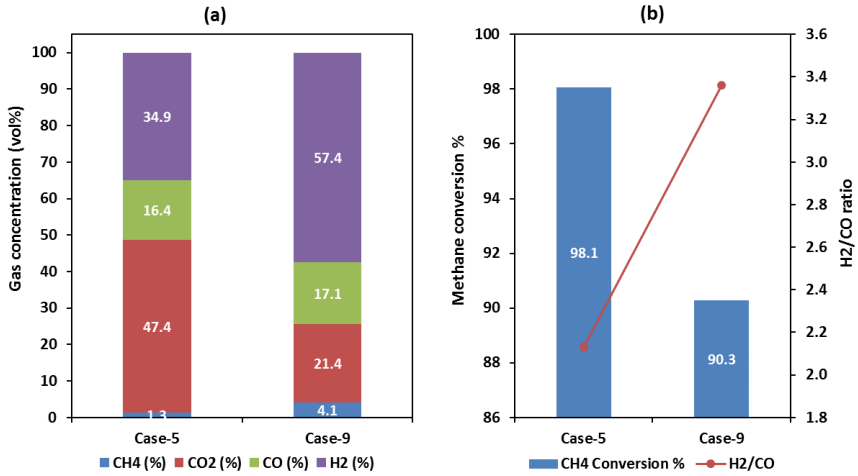

Figure 46. Products distribution (a), Methane conversion and H_2/CO ratio (b). comparing case 5 and 9.

Surprisingly, methane conversion dropped to 90% compared to 98% in case-5. Methane conversion is expected to increase with steam addition due to a favorable shift in the equilibrium of the steam reforming reaction (R3). The FR temperature is lower by 24°C in case-9 compared to case-5 (see Table 10) due to the strong endothermicity of the steam reforming reaction. Thermodynamic calculations showed a drop of less than 1.0% of methane conversion due to the lower reactor temperature in case-9. The lower reactor temperature will also lead to lower reaction rates, limiting methane conversion further below the equilibrium prediction. Another contributing factor could be the difference of the oxidation/reduction state of the oxygen carrier in the FR for case-5 and case-9. In case-9, the oxygen consumption in the AR was lower compared to case-5 (as in Table 10) since part of methane in the FR is involved in the steam reforming R3. This led to lower solids conversion and hence a lower Ni/NiO ratio in the FR limiting the catalytic activity of the oxygen carrier. This phenomenon has been revealed by the current study in case-3 to case-6, also in earlier studies [17,202–206,208,209].

Overall, the results presented in this study are comparable with findings reported by other CLR experimental studies. Diego et al [12,210] conducted CLR operation in a 900 W dual circulating fluidized bed reactor using methane as fuel and a total of 1.5 kg of a nickel based oxygen carrier. They reported a high methane conversion over a wide range of operating conditions. The solid circulation rate (NiO/CH_4 molar ratio) was the most influential variable on the products distribution. Autothermal operation could be achieved with a NiO/CH_4 molar ratio of 1.25, and the product composition at this condition was 65 vol.% H_2, 25 vol.% CO, 9 vol.%

CO_2, and 1-1.5 vol.% CH_4. A maximum of 25% steam added with methane slightly changed the products distribution and reduced the carbon deposition. Comparable results were also observed by Rydèn et.al [11] in a 300 W two compartment fluidized beds reactor.

3.3.6 Gas leakage during CLR operation

The gas leakage between the two sections is a critical parameter in ICR, and should be minimized to maximize syngas recovery and purity. If there is a leakage from the FR to the AR, the syngas recovery will decrease since part of the produced syngas will be lost through the AR. Gas leakage into the other direction will cause the syngas stream to be diluted with nitrogen reducing the syngas purity. During the CLR tests, the air leakage from the AR to the FR can be estimated based on the N_2 concentration in the FR exhaust gas. The O_2 leaked from the AR to the FR will either react with the oxygen carrier or combust part of the syngas. The leakage of the syngas from the FR to the AR can be estimated from the CO_2 concentration at the AR outlet. A minor amount of CO_2 could also form in the AR as a result of carbon deposition in the FR. Table 10 shows the calculated syngas recovery and purity in each case. One can observe that the syngas recovery and purity is in the range of 81% to 95%. The values are rather scattered, but in a similar range compared to the non-reactive leakage test, which showed a CO_2 recovery and purity of 91%. This similarity is expected, given that variations in the solids circulation were minimized by aiming for constant fluidization velocities in both sections (under the assumption that all CH_4 is converted) and constant solids loading in all cases. The deviation occurs in the CLR tests mainly due to reduction of the air flowrate after O_2 consumption in the AR, the incomplete methane conversion in the FR, and the variation in the gas composition (and therefore the gas density and viscosity) in the FR.

Case-8 showed the highest CO_2 concentration in the AR (Table 10) compared to other cases, this could be due to carbon deposition in the FR, which led to extra CO_2 release when the deposited carbon is oxidized in the AR. In this specific case, insufficient oxygen was supplied to the AR to fully oxidize the oxygen carrier (no O_2 was observed in the AR outlet), so the OC flowing from the AR to the FR was in less oxidized form. This will result in a higher Ni/NiO ratio compared to other cases, which promotes methane decomposition to C and H_2 over the Ni catalyst. Therefore, the calculated syngas recovery in this case should be higher than the reported value (81%) after excluding part of the CO_2 that released due to carbon combustion.

3.4 Summary and conclusion

This study has successfully demonstrated chemical looping reforming (CLR) of methane in a novel internally circulating reactor (ICR). The reactor was especially designed to simplify scale up of the conventional dual circulating fluidized bed chemical looping configuration, especially under pressurized conditions. In ICR, the functionality of two reactors, two cyclones and two loop seals is packaged into a single unit, which can be designed and operated in a single pressure shell. The large degree of process simplification offered by the ICR concept comes with a trade-off in the form of increased gas leakage between the two reactor sections. In this study, CO_2 leakage to the air reactor and dilution of the syngas by N_2 leaking from the air reactor was about 9% on average, although substantial improvements are expected as more operating experience is gained.

CLR operation was conducted in three separate studies. Firstly, air was fed in excess to the AR. It was found that oxygen transport to the FR was limited by the oxygen carrier circulation rate, allowing for a modification of the CH_4/O_2 ratio by only changing the amount of methane feed to the FR. The reactor behaved largely as expected, showing almost no syngas production when the CH_4/O_2 ratio was close to 0.5 (stoichiometric ratio for combustion), but steadily increasing syngas production when the CH_4/O_2 ratio was increased. Low CH_4/O_2 ratios experienced reaction rate limitations and high CH_4/O_2 ratios experienced thermodynamic limitations, resulting in an optimal methane conversion of 98% at intermediate CH_4/O_2 ratios.

Subsequently, the O_2 feed to the AR was reduced so that the oxygen carrier circulation rate was no longer the limiting factor in oxygen transport to the FR. As expected, this led to higher CH_4/O_2 ratios, resulting in more reforming activity, but also lower, thermodynamically limited methane conversions. Finally, a case with additional steam feed to the FR was completed to demonstrate how the H_2/CO ratio of the produced syngas could be increased from 2 in the cases with only methane feed to higher values that are more applicable to hydrogen production.

Autothermal operation could be achieved in some of the cases, further illustrating the functionality of the ICR concept. Overall, this first concept demonstration study was successful and further study of the ICR concept applied to different chemical looping concepts over a wider range of temperatures and pressures is strongly recommended.

Chapter 4 Mapping the operating performance of the ICR at atmospheric pressure

This chapter is based on the following paper:

Mapping the operating performance of a novel internally circulating fluidized bed reactor applied to chemical looping combustion

Mogahid Osman, Abdelghafour Zaabout, Schalk Cloete, Shahriar Amini

Fuel Process. Technol. 197 (2020) 106183

Abstract

Chemical looping combustion is a promising technology for minimizing the energy penalty of CO_2 capture. To accelerate the scale-up and commercialization of this technology for pressurized operation, the internally circulating reactor (ICR) was recently proposed. ICR integrates the two reactors, cyclones, loop seals and solids transport lines of the conventional chemical looping configuration into a single unit that simplifies design and operation. This chapter reports the ICR operating performance over a range of operating parameters applied to chemical looping combustion (CLC). The concept proved relatively simple to operate, allowing the oxygen-carrier circulation rate to be controlled over a wide range by varying the bed loading and the air reactor feed rate. Fully autothermal CLC operation was demonstrated as an illustration of the ease of ICR operation. Gas leakage between the two reactor chambers decreased strongly with decreasing solids loading, resulting in CO_2 capture and purity up to 94% for the lowest bed loading. The data showed that significant room for further optimization of the solids transport ports in the reactor exists, which will further increase the CO_2 separation performance. These results demonstrate the promise of ICR concept and provide valuable insights for the design of larger-scale units in future work.

Mogahid Osman planned the experiments with cooperation with other authors. Mogahid conducted the experimental tests with guidance from Abdelghafour Zaabout. All co-authors contributed on analyzing the results and writing the paper.

4.1 Introduction

The global energy demand projected to rise by 25% by 2040 (according to the 2018 Energy Outlook issued by the international energy agency IEA [3]) and hence fossil fuels will most likely remain the backbone of the global energy system for the coming decades [3]. Carbon capture and storage CCS has the potential to reduce CO_2 emissions from fossil fuel utilization in order to fulfil the ambitions of Paris agreement in limiting future temperature increases to 2°C [3]. Among the different alternative technologies for CCS, chemical looping combustion (CLC) is viewed as a promising technology that allows generation of cleaner energy from fossil fuel with inherent CO_2 capture and high overall power plant efficiency [211]. The CLC system avoids direct air and fuel contact by utilizing an oxygen-carrier martial circulated between two interconnected reactors, namely the air reactor and the fuel reactor [212,213]. In the fuel reactor, the fuel reacts with the metal oxide to form CO_2 and H_2O, from which a pure CO_2 stream can easily be produced by condensing the water. In the air reactor, the reduced metal is oxidized and heated by the highly exothermic reaction before being transferred to the fuel reactor for continuous cyclic operation. The large stream of hot CO_2-free gas from the air reactor can drive a power cycle.

To achieve competitive power plant efficiencies with gaseous fuels, pressurized operation of the CLC process is essential to enable integration with a combined power cycle. A thermodynamic assessment has shown that a pressurized CLC (PCLC) system integrated with a natural gas combined cycle (NGCC) resulted in a power efficiency of 52-55% (LHV), which is about 3-5 %-points more efficient than NGCC with post-combustion CO_2 capture [33,34]. Nevertheless, the CLC process has mostly been studied at atmospheric pressure operation, given that the dual circulating fluidized-bed reactor is the most widely used reactor configuration for CLC system. Extensive investigations using this configuration had been conducted using lab [10–12] and pilot scales [22,214]. The conventional dual-circulating fluidized-bed configuration combined two interconnected reactors and a gas-solid separation system (loop seals and cyclones) to avoid gas leakage between the fuel and air reactors. To achieve a pressurized CLC, this configuration requires a separate pressure shell for each of these interconnected components and careful management of the pressure in each unit to ensure reliable solids circulation. Thus far, gas-fueled CLC scale-up has been slow, even though almost all studies were done under atmospheric pressure [211]. Accelerating this scale-up

process while adding the significant complexity of pressurized operation requires a different approach.

Alternative reactor configurations have been proposed by many researchers to avoid external solids circulation and ease pressurized operation. The gas-switching concept is one of such reactor configurations, where alternate streams of air and fuel are introduced to one fluidized-bed reactor that contains the oxygen carrier material [82,86]. This concept greatly simplifies the reactor design and scale-up, but a coordinated cluster of reactors is required to achieve steady operation. Other reactor concepts proposed in the literature are the moving bed [116,193] and rotating bed reactor [119,126].

However, the circulating fluidized-bed configuration remains an attractive option considering its steady-state nature, high gas throughput rates and excellent intra-particle and interphase heat and mass transfer. It is possible, however, that the solids circulation mechanism will have to be simplified considerably for this reactor configuration to achieve successful scale-up and eventual commercialization for pressurized CLC. For this reason, this paper investigates the recently proposed internally circulating fluidized-bed reactor (ICR) where the loop seals involved in the conventional configuration are replaced by simple ports between two chambers in a single vessel, with a freeboard on the top replacing the cyclones [20,90]. The ICR concept (as shown in Figure 47) was especially designed to simplify scale up of the conventional dual circulating fluidized bed chemical looping configuration for pressurized operation.

In ICR, the functionality of two reactors, two cyclones and two loop seals are combined into a single unit, which can be designed and operated in a single pressure shell. The ICR operates in a similar way as the conventional interconnected CLC reactor configuration; where gaseous fuel and air are fed at different velocities to separate chambers containing a bed of oxygen carrier initially placed in the reactor. The high velocity gas feed in the fast chamber transports solids to the freeboard. The decelerated solids in the freeboard (due to the larger chamber area) fall into the upper port to circulate to the second chamber operating at low velocity (the slow chamber). Accumulation of solids in this chamber leads to static pressure build-up, forcing the solids to circulate back to the fast chamber through the port at the bottom.

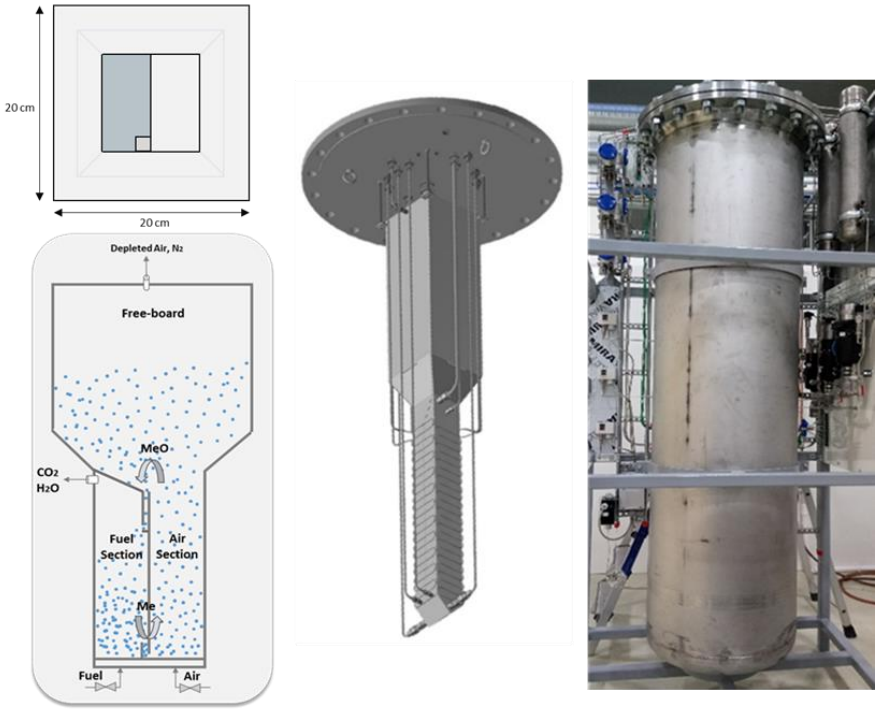

Figure 47. From left to right; a simplified scheme of the ICR design showing top view and front side view of ICR, CAD drawing of the ICR unit, and the ICR unit under operation inside the shell (Modified from Osman et al. [90]).

The compactness of the ICR concept comes at the expense of gas leakage, which takes place between the two reactor chambers through the connecting ports. A hydrodynamic investigation on a pseudo-2D cold-flow ICR unit has revealed that stable solids circulation and minimum gas leakage could be achieved over a wide range of operating conditions [20], and they can be controlled by adjusting the ratio of the gas velocities in the air and fuel champers, in addition to the solids loading in the reactor. This conclusion was confirmed by reactive multiphase flow modelling of a large-scale ICR unit (100 MW_{th}) reactor [21]. In light of the promising results from the hydrodynamic study and the reactive simulations, the ICR unit (as shown in Figure 47) has been constructed and commissioned to operate under fully reactive high temperature pressurized conditions. The unit had been successfully demonstrated for chemical looping methane reforming to syngas under atmospheric operation [90].

The aim of this study is to gain a full understanding on the process parameters that affect the ICR performance in terms of solids circulation rate, gas leakage between the chambers and fuel

conversion under atmospheric conditions. A comprehensive experimental campaign has been conducted with various solids loadings and fluidization velocities in the two reactor chambers. These experiments were completed under chemical looping combustion mode using a $CaMnO_{3-\delta}$-based oxygen carrier and CO as a fuel. To isolate the effect of reaction kinetics, all experiments were completed at nearly constant operating temperature of ~840°C at which high conversion of CO was achieved over $CaMnO_{3-\delta}$-based oxygen carrier [81]. The campaign was carried out at atmospheric pressure to minimize the complexity and cost of carrying out the large number of experiments reported in this study. Accordingly, an operating window maximizing the overall reactor performance was defined for future pressurized operation and further scale-up.

4.2 Methodology

4.2.1 ICR unit

The ICR system consists of a single reactor vessel with partitions creating two interconnected chambers with two connected ports at the top and the bottom, as well as a freeboard region for minimizing particle elutriation (Figure 47). The chambers have equal cross-sectional areas (0.05×0.1 m^2) and heights of 70 cm. One of the chamber (the air reactor AR) is connected to an expanding freeboard for decelerating the gas so that solids can fall into the top port for transport to the another chamber (the fuel reactor FR). The mechanisms by which solids circulation between the chambers occurs is as follows: by feeding the gas at a sufficiently high velocity into the AR, the solid particles will transport to the freeboard where the gas velocity decelerates causing the solids to fall down into the FR through the top connecting port. The accumulation of solids in the FR, which is operated with a lower gas velocity, will create a static pressure build up, forcing the solids to circulate back to the AR through the connecting port at the bottom. It should be noted that the freeboard was made large enough to enable the flexibility of running a wide range of operating conditions needed in this research phase of the concept, while maintaining minimal solids elutriation. Further refinement of the design of the different components of the reactor could be implemented when the process behavior is well understood.

The gas feed to each reactor chamber is introduced using a perforated cylindrical tube at the bottom of each chamber. The ports connecting the two chambers are L-type connection ports, which were adopted instead of a simple orifice to create conditions with solids flowing close to maximum packing. Such a flow condition creates a physical plug that minimizes undesired

gas leakage through the port. The top port connects the freeboard and the FR at the corner opposite to the FR gas outlet as shown in the top view of ICR in Figure 47. More details about the unit design and specifications can be found in a previous study where this ICR system was used for chemical looping reforming of methane using a NiO-based oxygen carrier [90].

Figure 48 gives the layout of the unit and its different auxiliary components. In addition to the reactor, the experimental setup includes heat exchangers placed on the outlet of each chamber for cooling down the exhaust streams before being sent to the atmosphere. Low temperature filters (5 µm pore size) installed after the coolers were used to collect elutriated fine particles. The dry gas composition (sampled after the filters) was measured using an analyzer (MCA 100 Syn-P from ETG Risorse e Tecnologia). Additional devices were used for controlling and monitoring reactor operation and for safety measures, including mass flow controllers for gas feed, thermocouples, pressure sensors and valves.

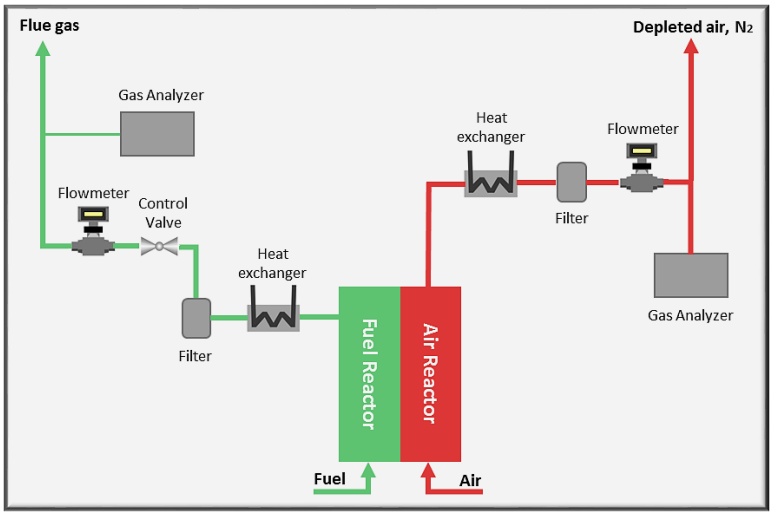

Figure 48. Simplified illustration of the ICR auxiliary components.

4.2.2 Oxygen carrier

In this study, an oxygen carrier (OC) based on calcium manganite with a perovskite structure was used. The oxygen carrier has a nominal composition of ($CaMn_{0.775}Ti_{0.125}Mg_{0.1}O_{3-\delta}$), and was manufactured by VITO (Flemish institute for technological research) through the spray-drying method. Ti and Mg were added to the structure to improve fuel conversion, fluidization properties and mechanical stability [215]. The δ-factor describes the oxygen deficiency in the

perovskite structure, where O_2 is released in the fuel reactor (FR) in a low O_2 partial pressure environment leading to increased oxygen deficiency, while δ decreases in the air reactor (AR) due to the O_2 rich environment leading to oxygen uptake [215–217]. Zaabout et al. [81] calculated the oxygen carrying capacity of this OC as 2.92% at 810°C while higher values were reported at operating temperatures of 950°C showing the high sensitivity to temperature of the CLOU effect of this oxygen carrier [217]. The physical properties of this OC are presented in Table 11. This OC was selected as it showed great promise for CLC application due to its high chemical performance and stability, in addition to the low attrition rate shown in prolonged lab and pilot scale experiments [215,218]. It should however be emphasized that the selection of an optimal oxygen carrier is out of the scope of this study; the main aim is to demonstrate the experimental feasibility of the ICR concept applied to CLC and map out its performance in terms of solids circulation rate, and CO_2 purity and capture efficiency.

Table 11 – Properties of the $CaMn_{0.775}Ti_{0.125}Mg_{0.1}O_{3-\delta}$ oxygen carrier used in this study

Parameter	Value
Bulk density (kg/m^3)	1600
Particle size distribution in μm (D10; D50; D90)	94.2; 134.2; 187.6
Sintering temperature (°C)	1350
Crushing strength (N)	2.44
Minimum fluidization velocity at operating conditions for AR (m/s)	0.013
Minimum fluidization velocity at operating conditions for FR (m/s)	0.014
Terminal velocity at operating conditions for AR (m/s)	0.59

4.2.3 Experimental procedure

CO was used as fuel in all experiments conducted in this study due to its good reactivity and simple reaction mechanism with the oxygen carrier, keeping the focus of the study on the separation performance and the solids circulation characteristics of the ICR. The fuel was diluted with N_2 in most cases to control the heat generation in the system so that all experiments could be carried out at similar temperatures while maintaining the fluidization velocity in the fuel reactor high enough to achieve enough bed expansion for the solids to circulate back to the air chamber through the bottom port. Additionally, this prevents full OC reduction in the fuel reactor, thus minimizing the risk of carbon deposition and large fuel slip.

The solids inventory in the unit was varied as 1.5, 2.5, and 3.5 kg, corresponding to 9.4, 15.6, and 21.8 cm static-bed height, respectively. A total of 16 experimental cases was conducted in this study varying the solids inventory, AR flowrate and FR flowrate (Table 2). The flowrate in the FR was varied from 7 to 15 Nl/min and the flowrate in the AR from 30 to 110 Nl/min. At these conditions, bubbling and fast fluidization regimes were established in the FR and AR, respectively. Each case was designed to elucidate the effect of one parameter while maintaining the others constant. For instance, cases 1, 5 and 6 were designed to investigate the effect of FR flowrate while keeping the AR flowrate and solids inventory constant.

The reactor was electrically heated to 700°C before feeding air and fuel for pushing the temperature up to the target reaction temperature. During the reactive CLC experiments, this target FR bed temperature was kept constant at 840°C for all the cases; hence, the power of the heater was adjusted between 0 to 100% depending on the operating conditions. For autothermal operation, the heater power was set to 0% so that the system temperature is maintained solely through the redox reactions taking place in the CLC process. All experiments were carried out at atmospheric pressure and the experimental results from each case were averaged over at least 30 minutes of steady state operation. Table 13 summarizes the main operating conditions investigated in the current study.

Table 12 - Experimental cases investigated in this study

Experimental cases	Solids Inventory (kg)	Flowrate (Nl/min)			
		AR	FR		
		air	CO	N_2	Total
1	1.5	50	5	5	10
2		70			
3		90			
4		110			
5		50		2	7
6		50		10	15
7		60	10	0	10
8		70			
9	2.5	30	5	5	10
10		50			
11		70			
12		50		2	7
13	3.5	30	5	2	7
14		40			
15		50			
16		70			

Table 13 - The operating conditions investigated in this study

Parameter	Value
FR bed temperature (°C)	840
Pressure (bara)	1.0
Solids inventory (kg)	1.5, 2.5, 3.5
Bed height (cm)	9.4, 15.6, 21.8
Fluidization velocity in AR (m/s)	0.40 - 1.34
Fluidization velocity in FR (m/s)	0.09 - 0.20
Volumetric flowrate in AR (Nl/min)	30 - 110
Volumetric flowrate in FR (Nl/min)	7 - 15
Thermal power of the fuel input	1 to 2.1 kW

4.2.4 Data evaluation

4.2.4.1 Fuel conversion

Reactivity of CO with the OC was expressed by γ_{CO}, the conversion of CO, which is defined as in Eq. (4-1):

$$\gamma_{CO} = \frac{F_{i_{CO}} - F_{o_{CO}}}{F_{i_{CO}}} \times 100 \tag{4-1}$$

4.2.4.2 CO_2 capture efficiency and purity

Gas leakage between the FR and AR is undesirable because it lowers CO_2 capture efficiency and purity. The CO_2 capture efficiency can be calculated from the amount of CO_2 exiting at the AR outlet according to Eq. (4-2). Similarly, CO_2 purity can be calculated as the percentage of the measured impurities in the CO_2 stream at FR outlet (Eq.(4-3)). Note that the N_2 diluting the fuel for the purpose of achieving consistent reactor performance over all the experiments is subtracted from the total FR outlet flowrate in the denominator of Eq. (3-3).

$$CO_2 \text{ capture effiency} = \left(1 - \frac{F_{AR,o_{CO_2}}}{F_{FR,i_{CO}}}\right) \times 100 \tag{4-2}$$

$$CO_2 \text{ purity} = \left(\frac{F_{FR,o_{CO_2}}}{F_{FR,o_{tot}} - F_{FR,i_{N_2}}}\right) \times 100 \tag{4-3}$$

4.2.4.3 Solids circulation rate

The solids circulation rate is a critical operating variable for the CLC process. Solids circulation between FR and AR is required to transfer oxygen and heat between the two reactors in order to fulfil the mass and heat balance of the system. Estimating the solids circulation rate in a hot ICR system is a challenging task because no direct measurement technique is possible. An indirect approach was adopted in this study, by considering the correlation between the solids circulation rate with the solids conversion difference between the AR and the FR. By re-oxidation of the OC after a steady state CLC experiment, it is possible to estimate the degree of reduction/oxidation of the particles placed in the reactor from the amount of the O_2 consumed. Hence the average solids conversion difference between the AR and the FR in the steady state operation can be estimated, which is directly linked to the magnitude of the solids circulation rate during the CLC process. This methodology has been proposed by many CLC studies carried out in a circulating fluidize-bed reactor [17,180,194,212,219–222].

The following procedure was used for the re-oxidation test in the current study, after at least one hour of steady state CLC operation. Fuel feed was replaced with N_2 in the FR, while air was kept in the AR. During this experiment, the O_2 measurement from the AR outlet provides the O_2 consumption by the reduced OC in the reactor. Figure 49 and Figure 50 show an example of the AR oxygen profile during the re-oxidation test for selected cases. In these cases, the re-oxidation tests was carried out using the same flowrates in AR and FR (50 and 10 Nl/min in the AR and FR, respectively) after steady state operations completed with varying the FR feed at constant AR feed (Figure 49) and varying the AR feed at constant FR feed (Figure 50). Figure 49 reveals that the O_2 consumption was insensitive to the FR feed, whereas Figure 50 shows a clear effect of the AR feed. This means that the FR feed rate had no effect on the solids circulation rate, but the AR feed rate had a significant effect.

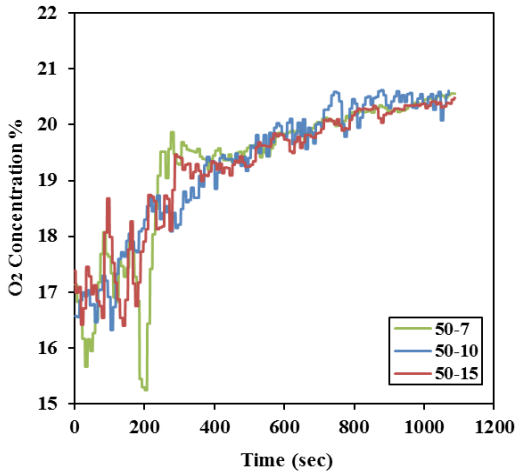

Figure 49. Transient oxygen concentration at the AR outlet during the re-oxidation test for three CLC cases. The gas flowrate in AR was maintained at 50 Nl/min while the FR flowrate was varied between 7, 10, 15 Nl/min. A1.5 kg solids inventory was used.

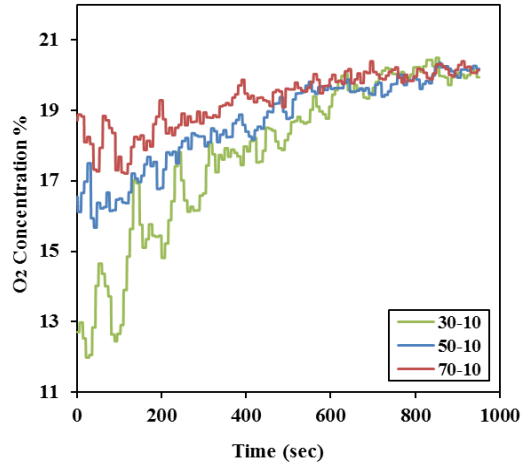

Figure 50. Transient oxygen concentration at the AR outlet during the re-oxidation test for three CLC cases. The gas flowrate in FR was maintained at 10 Nl/min while the AR flowrate was varied between 30, 50, 70 Nl/min. A 2.5 kg solids inventory was used.

The total O_2 consumption $\left(m_{O_2}\right)$ is calculated using the O_2 profiles of the re-oxidation tests, which is used for calculating the solids conversion difference as follows:

$$\Delta X_s = X_{s,AR} - X_{s,FR} \tag{4-4}$$

$$X_s = \frac{m_{OC} - m_{OC_{ox}}(1 - R_o)}{m_{OC_{ox}} R_o} \tag{4-5}$$

$$m_{OC} = m_{OC_{ox}} - m_{O_2} \quad (4\text{-}6)$$

Two assumptions were considered to estimate the solids conversion difference:

1) The OC was fully oxidized in the AR ($X_{s,AR} = 1$), because air was supplied to the AR in excess. This implies that the O_2 consumption during the re-oxidation test was only from the OC in the FR at the start of the test.
2) The mass of the OC was equally distributed between the FR and the AR during the CLC operation. This assumption was considered due to the absence of accurate measurement technique to estimate the actual amount of solids placed in each chamber during the CLC operation.

By combining Eqs. (4-4), (4-5) and (4-6) under the two assumptions given above, the solids conversion difference can be calculated. With the estimate of the solids conversion difference, the solids circulation rate can be calculated using the oxygen balance in the AR: the oxygen consumed in the AR is equal to the oxygen taken by the OC in the AR as in Eq. (4-7):

$$F_{O_{2,AR,in}} x_{O_2} M_{O_2} = \dot{m}_s R_o \Delta X_s \quad (4\text{-}8)$$

The calculated solids circulation rate should only be considered as a rough estimation, given the considered assumptions.

4.2.4.4 Solids elutriation

In the current study, an oxygen carrier with high stability and low attrition rate was used based on previous prolonged lab and pilot scale experiments [8,9]. Particle elutriation in the current study is therefore mainly due to hydrodynamics in the bed, which will limit the maximum achievable gas feed rates and bed loading. The procedure for estimating solids elutriation was based on collecting the solids found on the filters and the coolers after each experimental case, which corresponds to around 1 hour of a steady state CLC operation. The collected solids were then weighted and sieved. This approach reveals the effect of AR flowrate, FR flowrate and solids inventory on the solids elutriation rate.

4.2.5 Scope of the study

There are two main categories of parameters that affect the performance of a given ICR when applied to the CLC process; the oxygen carrier properties and the operating conditions. Among

the different parameters, the focus in this study was on the role played by the solids inventory and the fluidization velocity in AR and FR on various ICR performance measures, which include CO_2 capture efficiency and purity, fuel conversion, solids circulation rate and solids elutriation rate. The aim is to find an operating window that maximizes the overall reactor performance by achieving high fuel conversion and CO_2 separation performance and low solids elutriation. Based on this knowledge, future pressurized operation will be carried out using the best-defined operating conditions.

4.3 Results and Discussion

The results will be presented and discussed in three parts: 1) Effect of AR flowrate and solids inventory, 2) Effect of FR flowrate, and 3) Autothermal CLC operation. Four performance measures will be evaluated: 1) Fuel conversion, 2) Solids circulation rates, 3) CO_2 capture efficiency and purity, and 4) Solids elutriation. Table 14 summarizes the main results of all the CLC experimental campaigns which will be discussed in the following sections.

An example of the concentration of the outlet gas from the FR and AR for a typical CLC operation is shown in Figure 51. It could be seen that steady state operation was achieved for a prolonged period resulting in relatively constant CO_2 production in the FR and stable consumption of O_2 in the AR. This demonstrates the ability of the ICR reactor in establishing stable solids circulation between the chambers, transferring oxygen from AR to oxidize the fuel fed to the FR. Traces of CO_2 was measured in the AR outlet indicating presence of gas leakage between the chambers. It should be emphasized that the high oxygen excess in the AR, as shown in Figure 51 and Table 14 for the other cases, is due to the use of a limited fuel input in this study to avoid excessive temperature rise in the AR in the cases with lower air flowrates (less air to remove heat from the system). Such a temperature rise had to be prevented to ensure that all cases were operated at a constant temperature. However, in a real CLC process the air to fuel ratio should be adjusted to maximize the system performance.

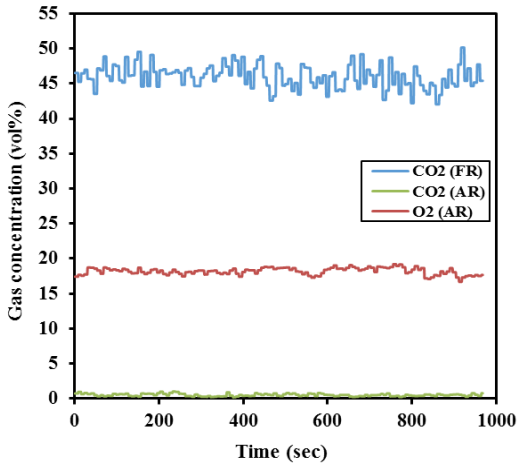

Figure 51. Gas product distribution obtained at the outlet of FR and AR during CLC tests for case 2 in Table 14.

Table 14 - Summary of the main results of the CLC experimental campaigns

Experimental cases	Solids Inventory (kg)	Flowrate Nl/min			Products Concentration (vol%)						CO Conversion %	CO_2 Capture Efficiency %	CO_2 Purity %	Solids circulation rate (g/s)	Solids elutriation (g)
		AR	FR		FR				AR						
		air	CO	N_2	CO	CO_2	O_2	N_2	CO_2	O_2					
1	**1.5**	50	5	5	0.90	45.30	0.29	53.51	0.84	16.99	98.2	92.0	92.4	2.8	6
2		70			0.52	46.05	0.31	53.12	0.51	18.20	99.0	93.1	93.1	3.6	8
3		90			0.31	46.47	0.38	52.83	0.38	18.85	99.4	93.3	93.6	6.1	15
4		110			0.00	45.58	0.60	53.82	0.35	18.98	100.0	92.4	91.2	7.0	54
5		50		2	0.15	65.09	1.12	33.65	0.92	17.02	99.8	91.2	91.3	2.7	-
6		50		10	1.21	30.06	0.15	68.58	0.60	17.04	96.4	94.2	93.8	2.7	11
7		60	10	0	2.92	89.25	0.56	7.27	1.32	14.16	97.1	92.7	92.2	-	-
8		70			3.08	89.18	0.58	7.17	1.21	15.23	96.9	92.2	92.3	-	-
9	**2.5**	30	5	5	0.3	43.8	0.2	55.7	2.7	13.3	99.4	85.0	87.5	2.6	6
10		50			0.0	41.6	0.4	58.1	1.9	17.0	100.0	81.5	83.1	4.3	14
11		70			0.0	41.2	0.6	58.2	1.5	18.2	100.0	79.1	82.4	6.9	25
12		50		2	0.0	58.4	0.8	40.9	2.2	17.0	100.0	78.6	81.7	4.4	11
13	**3.5**	30	5	2	0.0	53.7	0.8	45.4	4.7	13.9	100.0	73.5	75.2	4.7	7
14		40			0.0	53.0	1.3	45.7	3.4	15.9	100.0	74.5	74.2	6.5	20
15		50			0.0	52.6	1.3	46.1	2.7	17.0	100.0	74.2	73.7	8.1	28
16		70			0.0	51.9	2.0	46.1	2.0	18.3	100.0	73.1	72.7	10.2	44

4.3.1 Effect of AR flowrate and solids inventory

In this section, the impact of AR flowrate and solids inventory on ICR performance will be presented and discussed. Cases (1-4, 9-11, and 13-16) were designed to study the effect of the AR flowrates for three different solids inventories. CO flowrate was maintained the same for all cases (5 Nl/min), while the total FR flowrate was lowered for the case with the highest bed loading. Specifically, for the 1.5 and 2.5 kg solids inventory cases, 10 Nl/min was used as a total flow rate, while 7 Nl/min was used for 3.5 kg solids inventory cases to minimize solids elutriation due to large bed expansion.

4.3.2 Solids circulation rate

The solids circulation rate was estimated based on the procedure described in section (4.2.4.3) by re-oxidation of the OC after a steady state CLC test. Figure 52 shows the effect of the AR flowrate on the solids circulation rate and the solids conversion difference for the different solids inventories considered in this study. It was observed that the solids circulation rate increases with the AR flowrate and the solids inventory. This result is expected given that the AR flowrate and the solids inventory are the main controlling parameters of solids circulation in the ICR system as observed in our previous study on a pseudo-2D ICR cold flow unit [20]. In this previous study, solids circulation rate was found to be tightly linked to the pressure difference between the FR and AR chambers where a larger pressure difference drives larger quantities of solids to circulate from the FR to the AR [20].

Specifically, a larger AR flowrate and solids inventory result in greater bed expansion in the AR, transporting more solids to the freeboard to gain access to the top port for transport to the FR. The resulting larger accumulation of solids in the FR results in a larger static pressure build-up, the driving force for solids transport through the bottom port. This is also in line with findings in previous studies that reported similar mechanisms controlling solids circulation in interconnected fluidized bed reactors and confirmed the tight correlation between the solids circulation rate and the two independent parameters which are the AR flowrate and solids inventory [20,220,223–227]. It is also important to emphasize that, in the ICR system, a sufficiently large AR flowrate or solids inventory (or both) is needed for achieving acceptable solids circulation rates. For instance, in the present study the case of the 1.5 kg solids inventory, very little or no solids circulation was observed at AR flowrate below 50 Nl/min.

Figure 52 also shows that larger solids circulation rates, when the AR flowrate or solids inventory (or both) are increased, decreases the solids conversion difference between the

chambers. This result is expected because the amount of oxygen transport required to oxidize the fuel stays constant in all cases due to the constant fuel feed rate. Larger solids circulation rates require a lower degree of conversion to transport oxygen from the AR to the FR at a constant rate.

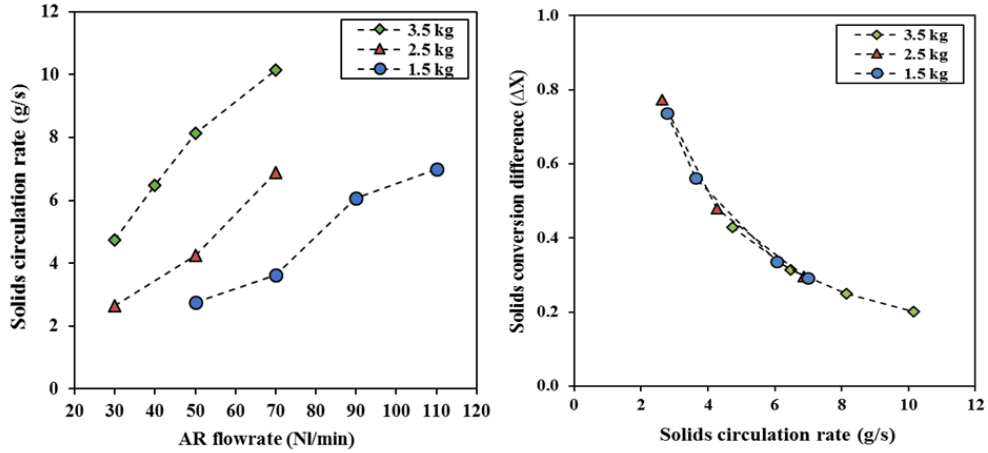

Figure 52. Solids circulation rate and solids conversion difference with various AR flowrates for different solids inventory, FR flowrate = 7.0 Nl/min (for 3.5 kg solids inventory) and 10 Nl/min (for 1.5, 2.5 kg solids inventory), Cases (1-4, 9-11, and 13-16).

4.3.3 Fuel conversion

Figure 53 shows the effect of the solids circulation rate on CO conversion for the three studied solids inventories. Complete CO conversion is observed for the 3.5 kg solids inventory for all solids circulation rate, while small CO slippage was detected for the 1.5 kg solids inventory (the poorest achieved CO conversion was 98% that improved with feeding larger AR flowrates). Fuel slippage with the lower solids inventory could be explained either by the lower solids circulation rate or by the shorter bed height. At constant FR flowrate, short bed heights lead to smaller gas residence time in the bed, which reduces the gas-solids contact quality, thus negatively affecting CO conversion. This effect is accentuated in the current ICR setup because the gas is injected using a perforated cylindrical tube in a relatively concentrated manner, imposing significant bubble-to-emulsion mass transfer limitations.

Another explanation for the fuel slippage could be originated from the correlation between the reaction rate and the solids circulation rate. A lower solids circulation rate increases the OC conversion difference between the AR and FR as illustrated in Figure 52. If the AR oxygen

carrier conversion is assumed to be 1 and the highest solids conversion differences approach 0.8 in Figure 52, the OC conversion in the FR is only about 0.2 (implying it is about 80% reduced). The reaction rate of the reduction reaction decreases significantly at lower OC conversions because less oxidized oxygen carrier is available for reaction, and this could explain the greater fuel slip with higher degrees of solids conversion difference at lower solids circulation rate and the lowest solids loading as observed in Figure 52 and Figure 53.

In this case, given the short bed heights and the concentrated fuel injection, the low fuel slippage observed for the cases with low solids circulation is testament to the high reactivity of the OC used in this study. In a larger scale ICR reactor, the greater gas residence time should easily ensure full conversion of the fuel, even at high degrees of OC reduction.

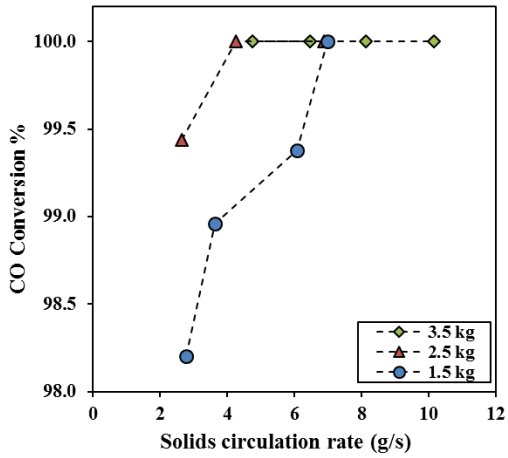

Figure 53. CO conversion with various solids circulation rate for different solids inventory, FR flowrate = 7.0 Nl/min (for 3.5 kg solids inventory) and 10 Nl/min (for 1.5, 2.5 kg solids inventory), Cases (1-3, 9-11, and 13-16).

4.3.4 CO_2 capture efficiency and purity

The gas leakage between the two reactor chambers is a critical parameter in ICR performance and should be minimized to maximize CO_2 capture efficiency and purity. Gas leakage can be controlled by ensuring that the gas outflow is equivalent to the gas inflow in each chamber. The gas leakage mainly occurs as a result of the gas being dragged with the circulated solids or as a result of pressure-induced flow. If there is a gas leak from the FR to the AR, the CO_2 capture efficiency will decrease since part of the combusted gas will leak to the AR where the

slipped CO_2 is vented to the atmosphere. Gas leakage in the other direction will cause the CO_2 stream to be diluted with nitrogen from AR, reducing the CO_2 purity.

Figure 54 shows the calculated CO_2 capture efficiency and purity with different solids circulation rates for the various solids inventories studied. One can observe that the solids circulation rate slightly affects the CO_2 capture efficiency and purity, while the solids inventory has a much larger effect. Figure 55 isolates the effect of solids inventory at fixed AR and FR feed rates, showing that the larger solids circulation rates allowed by larger solids inventories comes at the cost of more gas mixing and reduced CO_2 separation performance. However, this large trade-off between solids circulation rate and CO_2 separation performance seems to be much smaller when the solids circulation rate is changed by changing the AR flowrate (Figure 54). Despite the large increase in solids circulation with AR flowrate for all bed loadings (Figure 52), the CO_2 separation performance showed only small sensitivities. In the 1.5 kg bed loading, larger solid circulation rates allowed by higher AR flowrates even slightly improved CO_2 capture and purity (Figure 54).

This implies that there are other factors affecting this leakage phenomenon, which is mostly related to design and hydrodynamic characteristic of the ICR system. As has been stated in section (4.3.2), increasing the solids inventory increases the pressure difference at the bottom of the two chambers, and the pressure drop especially in the FR chamber operating at dense bed conditions. This causes larger resistance for the gas to flow through the bed and enhances the driving force for the gas to leak mostly through the bottom port of ICR. Similar observation was revealed by Latif [223] using a cold model of an internally circulating fluidized-bed gasification system. They attributed the increase of the gas leakage with the solids inventory to the increase of the bed height in the combustor, which in turn increases the resistive force to the up-flowing gas. The study conducted on the pseudo-2D cold flow unit of the ICR system [20] also revealed the same trend of increased gas leakage with increasing the solids inventory, which was correlated to the increase of the pressure difference between the two chambers. The ICR pseudo-2D cold flow system has also revealed development of gas pocket leakage at the bottom port increased size as the solids inventory is increased [20]. Similar behavior should be expected in the hot ICR rig used in the present study that has a similar design as the cold flow unit used in [20].

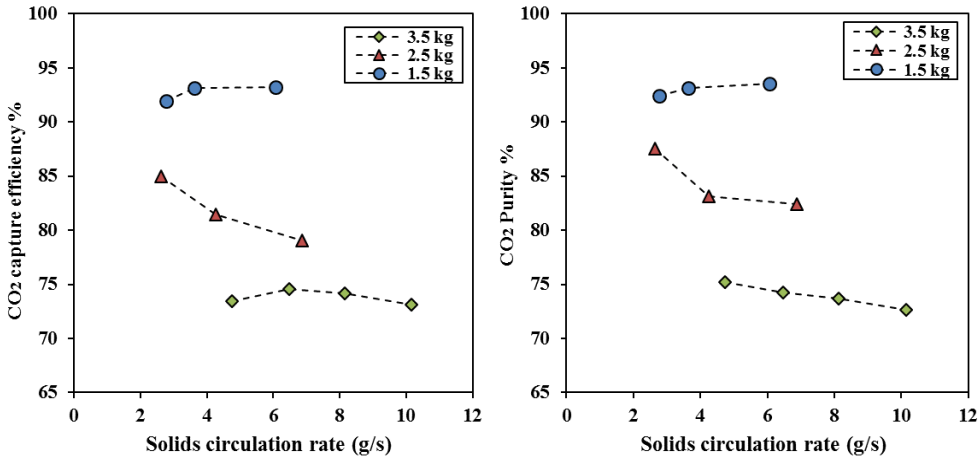

Figure 54. CO_2 capture efficiency and purity % as function of solids circulation rate for different solids inventory, FR flowrate = 7.0 Nl/min (for 3.5 kg solids inventory) and 10 Nl/min (for 1.5, 2.5 kg solids inventory), Cases (1-4, 9-13, and 13-16).

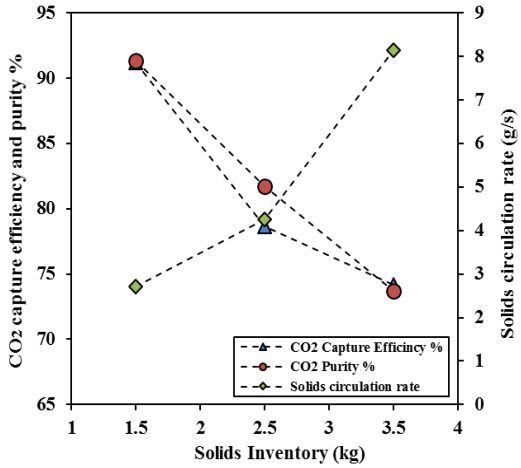

Figure 55. CO_2 capture efficiency and purity and solids circulation rate with various solids inventories, FR flowrate = 7.0 Nl/min, AR flowrate = 50 Nl/min, cases (5, 12 and 15).

In the present ICR setup, the measurements of O_2 concentration at the FR outlet (Table 14) allows for additional insight into the gas leakage behavior, specifically whether gas leakage from the AR to the FR occurred through the top or bottom port. O_2 in the gas leaking from the AR to the FR through the bottom port will be consumed by reaction with the fuel and oxygen

carrier at the bottom of the FR. On the other hand, O_2 leaking from the AR to the FR through the top port will experience minimal or no reaction and can therefore reach the FR outlet.

Figure 56 illustrates the large difference between the CO_2 purity calculated using Eq. (4-3) and the estimated CO_2 purity that would be observed with only gas leakage through the top port using the following equation:

$$CO_2 \text{ purity top port } = \left(1 - \frac{y_{FR,o_{O_2}} / y_{AR,o_{O_2}}}{y_{FR,o_{CO_2}} + y_{FR,o_{O_2}} / y_{AR,o_{O_2}}}\right) \times 100 \qquad (4\text{-}9)$$

In Eq. (4-9), the ratio of O_2 mole fractions at the FR and AR outlets $\left(y_{FR,o_{O_2}} / y_{AR,o_{O_2}}\right)$ represents the estimated mole fraction of all impurities at the FR outlet originating from gas leakage through the top port, assuming that N_2 will leak with O_2 in the same ratio with which they are present at the AR outlet. It should be noted that this estimation of gas leakage through the top port using O_2 mole fraction data is only valid for the cases where fuel conversion was complete (no possibility for O_2 slipping through the top port to react with slipped fuel above the bed). For this reason, only the two larger bed loadings are included in Figure 56.

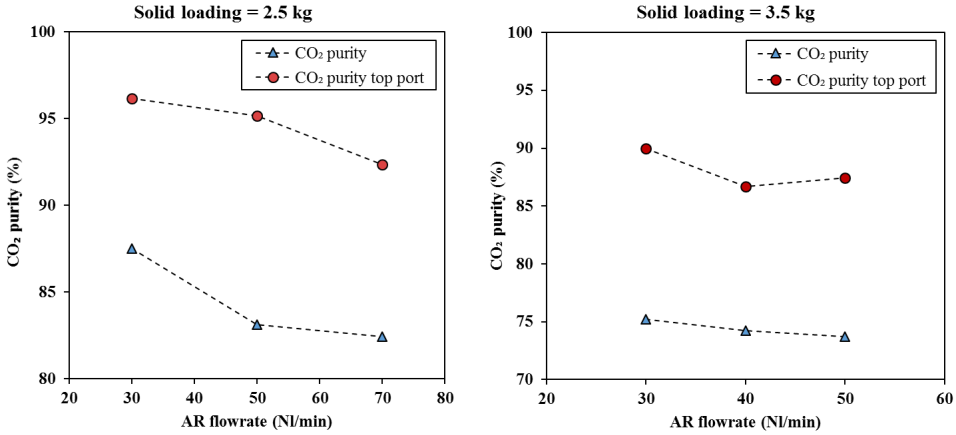

Figure 56. Comparison of the total CO_2 purity to the CO_2 purity that would be observed if gas leakage from the AR to the FR occurred only through the top port with the circulation of the OC.

Figure 56 shows that the CO_2 purity originating only from the top port is much better than the total CO_2 purity observed in the experiments from both ports. Under ideal ICR operation, all gas leakage from the AR to the FR would occur through the top port with the OC circulation. In this case, however, the data indicates that most gas leakage from AR to FR occurred through

the bottom port. The implication of this finding is that regular instances of reverse flow occur through the bottom port, which was also observed for taller beds in the aforementioned cold-flow experiments [20]. This effect is most likely driven by the dynamic nature of pressure fluctuations at the bottom of the two ICR chambers. Although the mean pressure at the bottom of the FR should be higher than the mean pressure at the bottom of the AR, the dynamic fluctuations of both pressure signals frequently create instances where the pressure at the bottom of the AR is higher than at the bottom of the FR, driving gas from the AR into the FR.

The design of the bottom port in ICR systems therefore appears to be very important to attenuate these backflows and minimize the resulting undesired gas leakage. For example, making the bottom port smaller will increase the flow resistance through the port, resulting in a larger solids accumulation in the FR and a larger average overpressure, reducing the likelihood of instantaneous reversals of the pressure gradient. A longer port will also reduce the likelihood that short-lived reversals of the pressure gradient will be able to force gas from the AR into the FR through the bottom port.

Naturally, the extent to which the port can be made smaller and longer is limited by the need to maintain a sufficiently high solids circulation rate to supply oxygen to the reduction reaction taking place in the FR. The present ICR setup was designed with conservatively large ports to ensure that sufficient solids circulation will be possible over a wide range of experimental tests, but future scaled-up ICR units should be designed with the minimum port size at which the required circulation rate can be achieved to minimize gas leakage. Another interesting topic for future work is the injection of a purge gas into the ports to further increase CO_2 capture and purity. Despite the sub-optimal nature of the bottom port in the present ICR reactor design, good CO_2 capture rates and purities can still be achieved for the lowest bed loading in Figure 55. Future optimizations of the ICR design will significantly improve this performance.

4.3.5 Solids elutriation

Following the procedure described in section (4.2.4.4), the solids elutriation was estimated as the mass of solids found in the filters and the coolers after 1 hour of a steady state CLC operation. The collected particles were mostly fine particles with a particle size below 80 μm. Figure 57 shows the solids elutriation with different AR flowrates for the various solids inventories studied. As expected, increasing AR flowrate increases the solids elutriation for all cases, and higher solids elutriation was observed with higher solids inventory. Case-4 in Table

14 shows that feeding 110 Nl/min to the AR results in the highest solids elutriation of 54 g/hr, which indicates that the fluidization velocity in this case was too high to allow the freeboard to decelerate the solids to prevent excessive elutriation. The resulted solids elutriation rate using ICR system is well within the tolerable limit for CLC process and expected to be improved further for long operation period using the current OC. Furthermore, the elutriation could further be minimized with a better design of the ICR reactor.

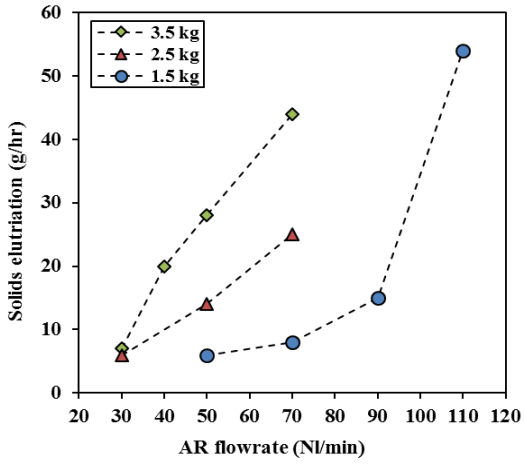

Figure 57. Solids elutriation with various AR flowrates for different solids inventory, FR flowrate = 7.0 Nl/min for 3.5 kg solids inventory and 10 Nl/min for 1.5, 2.5 kg solids inventory, Cases (1-4, 9-13, and 13-16).

4.3.6 Effect of FR flowrate

To investigate the effect of FR flowrate on ICR performance, experiments were performed with the same AR flowrate (50 Nl/min), solids inventory (1.5 kg) and CO flowrate (5 Nl/min) while varying the total FR flowrate (7, 10, and 15 Nl/min) by altering the amount of N_2 dilution to the FR. The three FR flowrates revealed the same solids circulation rate (Table 14), indicating that the solids circulation rate is independent of the FR flowrate. However, increasing the total FR flowrates reduces the CO conversion and increases CO_2 capture efficiency and purity as it can be seen in Figure 58. The reduction of CO conversion is expected since higher gas flowrate lowers the gas residence time in the FR. Also, the reduction of CO partial pressure from increasing N_2 dilution contributes to reduce the CO conversion.

The improvement in CO_2 capture efficiency and purity with the FR flowrate could be the result improved bed hydrodynamics that moves towards the turbulent regime at higher feed rates,

resulting in smoother fluidization behavior with lower pressure fluctuations, thus leading to lower gas leakage between the chambers. In addition, greater expansion of the bed in the FR will increase the mean pressure at the top of the bottom port, reducing the likelihood of backflow leakage from the AR to the FR. This combination of a higher mean pressure difference and a lower degree of pressure fluctuations cause better gas leakage performance through the bottom port. Increasing the FR flowrates also increases the solids elutriation (Table 14) and hence a trade-off between CO conversion, CO_2 capture efficiency and purity and solids elutriation should be made when selecting the optimum value of FR flowrate.

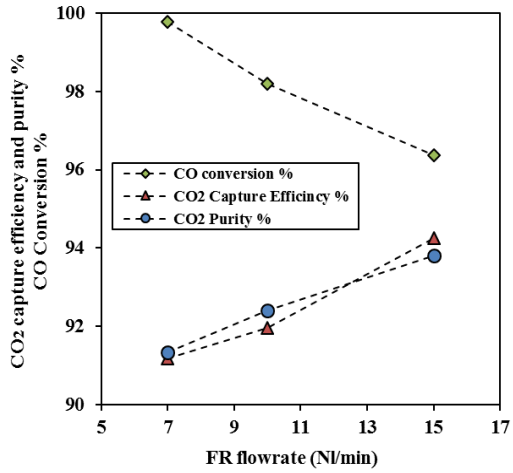

Figure 58. CO_2 capture efficiency and purity and CO conversion with various FR flowrates, at AR flowrate = 50 Nl/min and a solids inventory = 1.5 kg (cases 1, 5 and 6).

4.3.7 Autothermal CLC operation in ICR

All the experience gained in the parametric study was used for designing an autothermal operation of the ICR without any external heat supply, where all the heat duties of the system are fulfilled by the heat generated in the CLC process. The energy balance over the autothermal ICR system is dominated by heat generation from fuel combustion, heat removal by the gases being heated up in the system, and heat losses from the reactor (which are generally large in lab-scale units). A high degree of fuel conversion is required to maximize heat generation from fuel combustion and the air flowrate can be adjusted to determine the reactor temperature under autothermal operation, with lower air flowrates resulting in higher temperatures.

Feeding 10 Nl/min of CO to the FR and 60 Nl/min of air in the AR using 1.5 kg solids inventory was found to achieve autothermal operation at a similar temperature to the other experiments conducted in the study. As can be seen in Figure 59 stable temperatures were achieved in different measurement locations of the reactor without any external heating. Remarkably, the temperature at the bottom of the FR was higher than that in the AR despite the highly exothermic oxidation reaction taking place in the latter. This can be explained by the six times larger cold air feed to the AR than CO feed in the FR, in addition to the dilute solids flow nature in the AR chamber resulting in spatially distributed heat generation, in contrast to the concentrated heat generation in the FR due the dense solids flow (the employed OC has an exothermic reduction reaction with CO).

CO conversion was however only 97% (Case 7 in Table 14). To investigate the cause of CO slip, an additional experiment was conducted by increasing the AR flowrate to 70 Nl/min while keeping the same fuel input (case-8). Despite the increased solids circulation rate for 70 Nl/min (Table 14), CO conversion remained unchanged, which indicates that CO slip was due to the short-bed height in FR and not because of limitations in the solids circulation rate. Full conversion should be easily achievable in a larger-scale reactor with greater gas residence time.

Nevertheless, the ease and stability of ICR autothermal operation makes this configuration a prime candidate for replacing the interconnected fluidized bed reactor configuration for highly efficient chemical looping technology. However, the full potential of ICR configuration would only be proven if it demonstrates the ability of achieving acceptable levels of leakage between the ICR chambers at high pressure operation relevant to the foreseen industrial chemical looping conditions. This will be the scope of a future study.

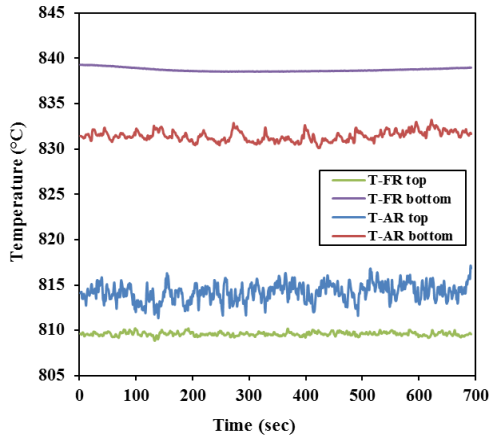

Figure 59. Temperature profile in FR and AR during autothermal CLC test, AR flowrate = 60 Nl/min, FR flowrate = 10 Nl/min, solids inventory = 1.5 kg (case-7).

4.4 Summary and Conclusion

The present work presents a detailed study of the operating behavior of the internally circulating reactor (ICR) applied to chemical looping combustion (CLC). ICR is a promising reactor concept that aims to simplify the design and operation of pressurized chemical looping processes by eliminating the need for cyclones, loop seals and long solids transport lines between interconnected fluidized bed reactors. Instead, a single reactor vessel is used with internal partitions to create different reaction chambers with simple interconnecting ports for oxygen carrier circulation.

Good oxygen carrier circulation is essential for successful CLC operation. The study found the expected trends of increased solids circulation with greater solids loadings and greater differences between the feed rates to the different ICR chambers. Overall, sufficient oxygen carrier circulation could easily be achieved over a wide range of operating conditions.

The primary trade-off for the simplicity offered by the ICR concept is the reduction in CO_2 capture and purity caused by undesired gas leakage through the connecting ports. Large gas leakage was observed for higher bed loadings, but good performance of up to 94% CO_2 capture and purity was achieved at the lowest bed loading investigated. Due to the short bed height in the fuel reactor for this bed loading, fuel conversion was only 97% in some cases, but 100% fuel conversion will be easily achievable in an upscaled reactor with greater gas residence time.

Results also showed that the CO_2 separation performance can be improved substantially in future studies by optimizing the bottom port. In an optimized unit, this port will be smaller and longer to minimize gas leakage resulting from instantaneous pressure difference reversals caused by dynamic pressure fluctuations from fluidization in the air and fuel reactors. However, the port must still be large enough to allow for sufficient solids circulation.

In conclusion, the ICR concept could be a promising candidate for accelerating scale-up and commercialization of pressurized chemical looping technologies. The reactor proved relatively simple to control over a range of operating conditions and showed predictable solids circulation and fuel conversion behavior. An autothermal experimental run was completed to demonstrate this ease of operation. Future investigation of the ICR concept is therefore strongly

recommended, particularly pressurized demonstration and reactor scale-up studies with more optimized design.

Nomenclature

AR	Air reactor
CLC	Chemical looping combustion
CLOU	Chemical looping oxygen uncoupling
FR	Fuel reactor
ICR	Internally circulating reactor
OC	Oxygen carrier
$F_{i_{CO}}$	CO molar flowrate at FR inlet (mol/min)
$F_{o_{CO}}$	CO molar flowrate at FR outlet (mol/min)
$F_{AR,o_{CO_2}}$	CO_2 flowrate at AR outlet (Nl/min)
$F_{FR,i_{CO}}$	CO flowrate at FR inlet (Nl/min)
$F_{FR,o_{CO_2}}$	CO_2 flowrate at FR outlet (Nl/min)
$F_{FR,o_{tot}}$	Total FR outlet flowrate (Nl/min)
$F_{FR,i_{N_2}}$	N_2 flowrate at FR inlet (Nl/min)
$F_{O_{2,AR,in}}$	Inlet molar flowrate of oxygen to the AR
m_{OC}	Actual mass of the OC in its partially oxidized state (g)
$m_{OC_{ox}}$	Mass of the fully oxidized OC (g)
m_{O_2}	Mass of O_2 consumed during the re-oxidation test (g)
$\dot{m}_s$	Solids circulation rate (g/s)
M_{O_2}	Molecular weight of oxygen
R_o	Oxygen transport capacity of the OC
$X_{s,FR}$	Solids conversion in FR
$X_{s,AR}$	Solids conversion in AR
x_{O_2}	Oxygen conversion at outlet of AR
ΔX_s	Solids conversion difference between AR and FR
γ_{CO}	Conversion of CO, %

Chapter 5 Pressurized chemical looping combustion

This chapter is based on the following paper:

Experimental demonstration of pressurized chemical looping combustion in an internally circulating reactor for power production with integrated CO_2 capture
Mogahid Osman, Abdelghafour Zaabout, Schalk Cloete, Shahriar Amini
Chem. Eng. J. 401 (2020) 125974

Abstract

This chapter presents an experimental demonstration of pressurized chemical looping combustion (CLC) in an internally circulating reactor (ICR). The ICR concept is a novel alternative to the conventional interconnected fluidized bed CLC configuration as it eliminates all cyclones, loop seals and solids transport lines, and it can be pressurized in a single pressure shell. Stable operation with high fuel conversion was established for about 40 hours of operation at pressures up to 6 bar, achieving reasonable CO_2 purity and capture efficiency (up to 97%). The solids circulation rate was found to increase with increasing the operating pressure at a constant fluidization velocity with no effect on CO_2 capture and purity. The experimental campaign also examined the effects of solids inventory and fluidization velocities in the air and fuel reactors. The CO_2 purity and capture efficiency were most sensitive to the solids inventory, whereas the solids circulation rate was most sensitive to the air reactor fluidization velocity and the solids inventory. A correlation for solids circulation rate was derived from the collected experimental data, thus providing a robust tool for designing an ICR system for pressurized operation. This correlation can assist in further scale-up and demonstration of the ICR concept in commercial scale.

Mogahid Osman planned the experiments with cooperation with other authors. Mogahid conducted the experimental tests with guidance from Abdelghafour Zaabout. All co-authors contributed on analyzing the results and writing the paper.

5.1 Introduction

Carbon capture and storage (CCS) has a great potential of reducing CO_2 emissions from the utilization of fossil fuels, which would play a significant role in fulfilling the ambitions of the Paris agreement to limit future temperature rise below 2°C [3]. Various technologies for CCS have been introduced in the last decades with a reduction in the energy penalty of CO_2 capture as one of the main objectives. Chemical looping combustion (CLC) is a promising technology for power production based on fossil fuels combustion with integrated CO_2 capture and with a reduced energy penalty. The CLC system carried out in two steps, in the fuel reactor the fuel interacts with an oxygen carrier (metal oxide) to fully oxidize to CO_2 and H_2O, the reduced metal oxide is re-oxidized in a flow of air in the air reactor, ready to start a new cycle and producing heat for power production [11,22,23]. If the CLC system is pressurized, the hot depleted air from the air reactor can be used for efficient power generation in a downstream combined cycle.

Pressurized chemical looping combustion (PCLC) therefore has the potential for maximizing the power plant efficiency by using a combined cycle instead of the steam cycle used with atmospheric pressure boilers. In addition, high pressure combustion increases the condensate temperature, hence, the condensate in the fuel reactor outlet stream can be utilized as a heat source within the process, which increases the thermal energy recovery from the fuel (the higher heating value instead of the lower heating value). This is especially magnified for CLC with natural gas given the high moisture content in the fuel reactor flue gas. Other benefits for high pressure CLC operation include: reduced power consumption for CO_2 compression and/or refrigeration steps, and increased heat transfer rates. Thermodynamic investigations has revealed that the integration of PCLC with a natural gas fired combined cycle (NGCC) can achieve a power efficiency of 52 to 55% (LHV), that is higher than NGCC with post-combustion CO_2 capture by 3-5% points [33,34]. Pressurized CLC is also applicable to solid fuels using integrated gasification combined cycle (IGCC) power plant configurations. Compared to conventional pre-combustion CO_2 capture, such CLC-IGCC plants can also improve power plant efficiency by 3-5% points [228]. The challenge of relatively low turbine inlet temperatures limited by the maximum operating temperature of the CLC reactors can be mitigated by using an added combustor after the CLC reactors as has been simulated for NGCC [133,229] and IGCC power plants [230]. Such added firing can almost eliminate the CO_2 capture energy penalty, but

it introduces additional costs when firing with hydrogen or additional emissions when firing with natural gas.

The circulating fluidized-bed reactor (CFB) is the mostly used reactor configuration for chemical looping processes at a lab [10–12] and pilot scales [22,214]. The CFB system consists of two separate reactors connected with a loop seals and cyclones for gas-solid separation. Pressurized operation in such a highly interconnected system will impose several challenges. First, each reactor, cyclone, loop seal and solids transport line must be designed in a separate pressure shell to ensure mechanical integrity under pressurized operation at very high temperatures. Second, any pressure imbalance can lead to significant instabilities in the solids circulation rate, and may lower the performance of loop seals and cyclones causing a high gas leakage between the two reactors. Third, the required fluidization steam for the loop seals will increase with increasing pressure, which would result in a higher energy penalty [148]. These challenges prompted research on different reactor configurations with the potential ability to operate under pressurized conditions. These configurations include gas switching concept [80,82,190], moving bed [116,193], rotating bed reactor [119,126] and the internally circulating fluidized-bed reactor (ICR) [20,90], which will be the focus of the current study.

The ICR incorporates many of the operational capabilities of the circulating fluidized-bed reactor, while eliminating the complex separation systems (i.e., cyclone and loop seals). Specifically, the ICR concept aims to simplify the design, ease the solids circulation, and operate at high pressure easily in a single pressurized vessel. The ICR concept (as shown in **Fig. 60**) is a single vessel unit with two chambers connected by ports (one in the top and the second at the bottom), and a freeboard. The two ports replace the loop seals involved in the CFB, while the freeboard replaces the cyclones making the ICR reactor design compact while maintaining the same benefits and functionalities of the CFB reactors. The oxygen carrier circulation in ICR attained through feeding higher gaseous velocity in the air reactor (AR) than in the fuel reactor (FR). The solids transported to the freeboard decelerate and falls to the FR through the top port. The accumulation of solids in FR led to static pressure build-up that forces the solids to circulate back to the AR through the bottom port. This simple solids circulation mechanism combined with the compact design make the ICR concept very suitable for pressurized operation. The use of a freeboard instead of cyclones for gas solid separation after the air reactor will also reduce particle elutriation.

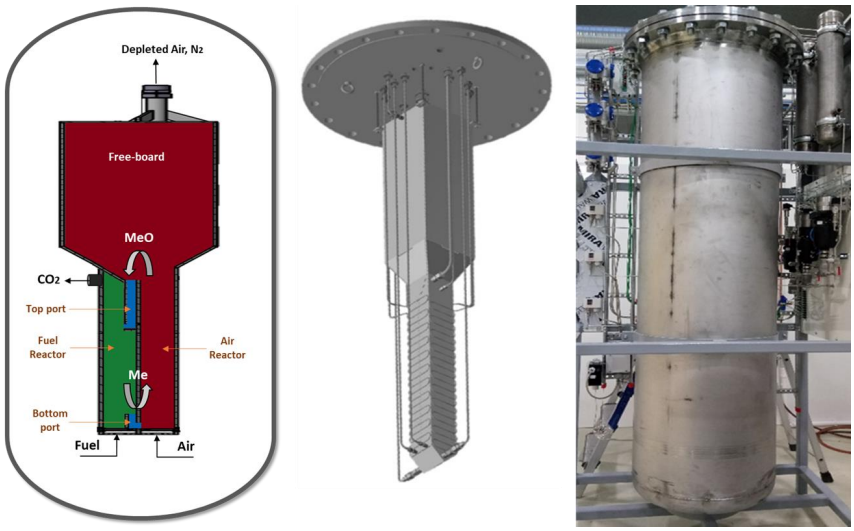

Fig. 60. From left to right; a simplified scheme of the ICR design, CAD drawing of the ICR unit, and the ICR unit under operation inside the shell.

The major trade-off of the simplicity obtained by the ICR concept is the gas leakage between the two reactor sections through the connecting ports, reducing CO_2 capture efficiency and purity. Large gas leakages could also raise safety concerns from direct contact of air and fuel. This is of lower concern in the lower port because any large heat release would be quickly absorbed by the high heat capacity of the particles. No particles are present to control a large heat release at the top port, but as long as complete fuel conversion is achieved in the fuel reactor, there is no risk. However, the demonstration of the current ICR for atmospheric CLC operation showed that the gas leakage can be easily minimized by controlling the fluidization velocity ratio of the two chambers and the solids inventory, attaining CO_2 capture efficiency and purity greater than 95% [91]. The current ICR unit had also been used for chemical looping reforming of methane at atmospheric operation [90]. The reactor showed promising performance in terms of gas leakage, solids circulation rate, fuel conversion and revealed a simple approach to control its performance over a wide range of operating conditions.

Following the successful operation of ICR under atmospheric operation, the current study aimed to experimentally investigate the ICR behavior for gaseous fuel CLC under pressurized operation. The largest focus of this study falls on re-evaluating the effect of process parameters such as solids loading and gas fluidization velocity under pressurized conditions on the ICR performance indicators such as gas leakage between the chambers, fuel conversion and solids

circulation rate. Given the importance of the latter in accurate design of large-scale pressurized ICR reactors, a correlation linking the solids circulation rate to the process parameters was extracted experimentally at an operating pressure range of 1 to 6 bar. NiO-based oxygen carrier and CO as a fuel were used for the chemical looping combustion experiments. This study represents the first demonstration of the ICR concept under pressurized conditions for CLC.

5.2 Methodology

5.2.1 ICR unit

The ICR unit is a single reactor vessel that consists of a two separate chambers; AR and FR (air and fuel reactors), connected through two ports at the top and the bottom and a freeboard (Fig. 60). The unit is enclosed in a cylindrical shell to enable operation at high pressure. The two connecting ports were designed to facilitate solids circulation between the two chambers while minimizing gas leakage and the freeboard aimed to deaccelerate the solids and minimize particle elutriation in the AR. Further details about the ICR unit design and specifications can be found in previous studies, in which this ICR unit was demonstrated for chemical looping combustion and reforming under atmospheric conditions [90,91].

Fig. 61 illustrates the layout of the various auxiliary components of the ICR unit beside the main reactor vessel. A water heat exchanger used for cooling down the exhaust gaseous from the AR and the FR before being vented to the atmosphere, followed by particle filters to collect any elutriated fine particles. A gas analyzer (from ETG Risorse e Tecnologia) used to measure the dry gas composition from the AR and the FR. The gas analyzer measures multiple gases with a single optical path platform using a non-dispersive infrared sensor for CO and CO_2 measurement and an electrochemical sensor for O_2 measurement. The measurement range for CO, CO_2 and O_2 is 0-30%, 0-50% and 0-25%, respectively. The outlet gas from the FR was diluted with N_2 a known feed rate, first to ensure accurate gas concentration measurement within the gas analyzer measurement range and secondly to determine the molar outlet flow rates of the different species. Back-pressure regulators were installed on the outlet of each reactor chambers and the shell to control the pressure inside the reactor and the shell. Other devices also used to control and monitor the reactor operation, including mass flow controllers for gas feed, flowmeter for gas outlet measurement, thermocouples, pressure sensors and valves. During operation, a small amount of elutriated solids was collected on the filters and the coolers after each section. It should be noted that the attrition rate was low as the selected oxygen carrier has high mechanical and thermochemical stability.

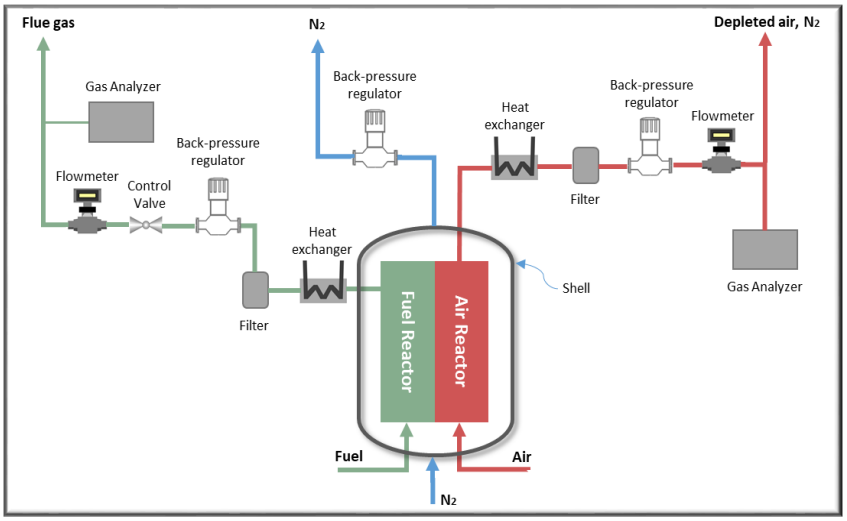

Fig. 61. A simplified illustration of the ICR auxiliary components.

5.2.2 Oxygen carrier

A NiO-based oxygen carrier was used in this study. The OC particles supported on Al_2O_3 with a NiO/Al_2O_3 ratio of 65/35 and consisted of around 37% free NiO which are available for reaction (the OC manufactured by VITO). This OC was selected as it revealed high chemical performance and stability for CLC application in many previous studies [90,231,232]. However, a major disadvantage of using a NiO-based OC is its high toxicity. Therefore, extensive health and safety measures are required when handling this OC.

5.2.3 Fuel

CO was the only gaseous fuel used for all PCLC experiments in this study, given its high reactivity with the NiO-based oxygen carrier with a simple reaction mechanism. Hence, the main focus of the study can be concentrated towards understanding the various performance measures of the ICR under high pressure operation. The fuel was also diluted with N_2 in some cases to maintain the flowrate in the FR at a certain level while maximizing fuel conversion. In several cases, particularly at elevated pressures, solids circulation was not sufficient to fully convert a pure fuel stream fed at a fluidization velocity required for good ICR operation, thus requiring the fuel to be diluted with N_2.

5.2.4 Experimental procedure

Experiments were conducted by altering four independent variables: solids inventory, pressure, air fluidization velocity in AR and fuel fluidization velocity in FR. Four dependent variables were determined from each experiment: solids circulation rate, CO conversion, CO_2 capture efficiency and CO_2 purity. The FR reactor temperature during CLC operation was maintained constant at around 840°C for all the cases by controlling the power output of the electrical heater surrounding the reactor. During autothermal PCLC operation, the electrical heater was switched off, hence the temperature inside the reactor was maintained only by the oxygen carrier circulation. Table 15 shows a summary of the main operating conditions examined in the current study. The experimental results for each case were averaged over at least one hour of steady state CLC operation.

Table 15 - Operating condition investigated in this study

Parameter	**Value**
Temperature (°C)	800 - 850
Pressure (bar)	1.0 - 6.0
Solids inventory (kg)	2.0 and 2.5
Fluidization velocity in AR (m/s)	0.45 - 0.80
Fluidization velocity in FR (m/s)	0.055 - 0.13
Volumetric flowrate in AR (Nl/min)	35 - 210
Volumetric flowrate in FR (Nl/min)	8.5 - 40
Total time of CLC operation (hr)	~40
Thermal power of the fuel input	1 - 4 kW

5.2.5 Data evaluation

5.2.5.1 Fuel conversion

CO conversion during CLC operation (γ_{CO}), was defined as in Eq. (5-1) where F_i and F_o refer to the inlet and outlet molar rates respectively:

$$\gamma_{CO} = \frac{F_{i_{CO}} - F_{o_{CO}}}{F_{i_{CO}}} \times 100 \qquad (5\text{-}1)$$

5.2.5.2 CO_2 capture efficiency and purity

The gas leakage between the AR and FR is characterize by the CO_2 capture efficiency and purity. CO_2 capture efficiency is calculated based the amount of CO_2 leaking to the AR outlet according to Eq. (5-2(3-2) and the CO_2 purity is calculated based on amount of air leaking to the FR outlet as in (Eq.(5-3)).

$$\mathrm{CO_2\ capture\ effiency} = \left(1 - \frac{F_{AR,o_{CO_2}}}{F_{FR,i_{CO}}}\right) \times 100 \tag{5-2}$$

$$\mathrm{CO_2\ purity} = \left(\frac{F_{FR,o_{CO_2}} + F_{FR,o_{CO}}}{F_{FR,o_{tot}} - F_{FR,i_{N_2}}}\right) \times 100 \tag{5-3}$$

5.2.5.3 Solids circulation rate

The solids circulation rate is the prime CLC criterion because the solids transfer oxygen and heat between AR and FR reactors fulfilling the required heat and mass balance. In the current study, the solids circulation rate was estimated by an indirect approach considering the correlation between the solids conversion difference between AR and FR and the solids circulation rate. After each steady state CLC operational case, the OC was re-oxidized by replacing the fuel feed on the FR by N_2, while measuring the O_2 concentration in the AR outlet. This strategy gives the O_2 consumption of the reduced OC in the reactor, which reveals the degree of reduction of the OC of the previous CLC operation, which is directly linked with the solids circulating rate.

The solids conversion difference was calculated based on the total O_2 consumption $\left(\mathrm{m_{O_2}}\right)$ from the re-oxidation test, as follows:

$$\Delta X_s = X_{s,AR} - X_{s,FR} \tag{5-4}$$

$$X_s = \frac{m_{OC} - m_{OC_{ox}}(1 - R_o)}{m_{OC_{ox}} R_o} \tag{5-5}$$

$$m_{OC} = m_{OC_{ox}} - m_{O_2} \tag{5-6}$$

The solids conversion difference (ΔX_s) was calculated combining Eqs. (5-4), (5-5), and (5-6) by assuming that the OC mass in the AR was equal to that in the FR, and the O_2 consumption from the re-oxidation test was only from the reduced OC placed in the FR, considering that the

OC placed in the AR was fully oxidized ($X_{s,AR} = 1$); since air was supplied to the AR in excess. Accordingly, the solids circulation rate calculated from the oxygen balance in the AR as in Eq. (5-7).

$$F_{O_{2,AR,in}} x_{O_2} M_{O_2} = \dot{m}_s R_o \Delta X_s \quad (5\text{-}7)$$

This approach was adopted by various CLC studies carried out in a circulating fluidize-bed reactor [17,180,194,212,219–222] and it was adopted in the previous ICR atmospheric operation study [91].

5.2.5.4 The oxygen carrier to fuel ratio (OC/fuel ratio, ϕ)

The oxygen carrier to fuel ratio, defined as the ratio between the flow of oxygen supplied by the oxygen carrier and the oxygen needed for complete CO conversion, is calculated by Eq. (5-8) as follows:

$$\phi = \frac{\dot{m}_s R_o X_{s,AR}}{0.5 \dot{n}_{CO} M_{O_2}} \quad (5\text{-}8)$$

5.2.5.5 The overall air equivalence ratio (λ)

The overall air equivalence ratio (λ) compares the oxygen fed to the AR with the oxygen demand for complete combustion of the fuel fed to the FR. Lowering the air equivalence ratio is done by reducing the amount of air fed to the AR. The definition of the air equivalence number is shown in Eq. (5-9):

$$\lambda = \frac{0.21 F_{air,in}}{0.5 F_{CO,in}} \quad (5\text{-}9)$$

5.2.6 Uncertainties of the measurements

The accuracies of the measuring devices used in this study (provided by the manufacturer) are as follows: ±0.5%, ±1%, <±0.5%, <±0.5%, and <±3% for mass flow controllers, gas flowmeters, thermocouples, pressure sensors and the gas analyzer, respectively. The highest uncertainty is associated with the gas concentration measurements. However, this uncertainty was mitigated by operating each experimental cases for at least 1 hr of steady state CLC operation, and average data of these measurements were taken as representative.

In addition, the methodology of estimating the solids circulation rate (described in Section 4.2.4.3) involves some important uncertainties, primarily the assumptions that the oxygen carrier is equally distributed between the two reactor sections and fully oxidized in the air section. It was not possible to accurately quantify this uncertainty, but it should be similar between the different cases, implying that the response of solids circulation rate to various independent variables reported in the results section should be reliable. Moreover, two of the experimental cases were repeated two times and resulted in a deviation no larger than 5%, confirming that the reported results are reliable.

5.2.7 Scope of the study

The focus in this study is on understanding the role played by the pressure, the solids inventory and the fluidization velocity in AR and FR on various ICR performance measures during chemical looping combustion condition. The ICR performance measures include CO_2 capture efficiency and purity, fuel conversion, and solids circulation rate. The collected data will also give the basis for designing an ICR pilot plant in the order of 0.1 to 1 MW at pressures relevant to real industrial conditions by extracting a correlation linking the solids circulation rate to the process variables such as the fluidization velocity in the two chambers, the operating pressure and the solids inventory.

5.3 Results and discussions

The results will be presented and discussed in two main parts: 1) the ICR operation performance under pressurized CLC conditions and its sensitivity to the process variables and 2) fitting the collected data into a correlation for solids circulation rate. Table 16 and Table 17 summarize the main results of the PCLC experimental campaigns for the operation with 2.5 kg and 2 kg solids loading, respectively, which will be discussed in the following sections.

5.3.1 Pressurized chemical looping combustion (PCLC)

Fig. 62 shows an example of the gas concentration profile of the outlet gases from the FR and AR during PCLC at 4 bar (case-11). A relatively constant CO_2 concentration in the FR and stable consumption of O_2 in the AR was attained during a steady state CLC operation. This demonstrates the ability of the ICR reactor in achieving a stable solids circulation between the two chambers.

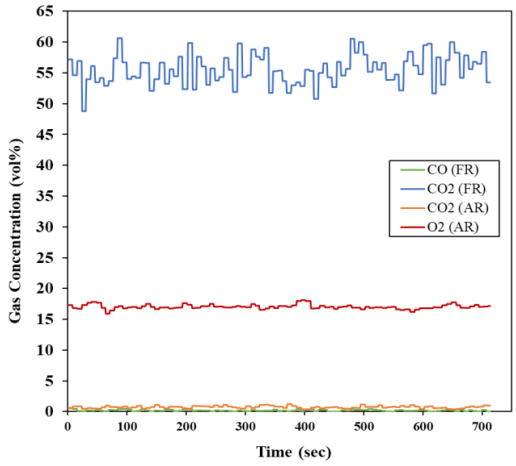

Fig. 62. Gas product concentration measured at the FR and AR outlet during PCLC tests (case-11).

Table 16- Summary of the main results of the CLC experimental campaigns using 2.5 kg of solids inventory

Experimental cases	Pressure	Flowrate Ln/min			Products Concentration vol%							CO conversion %	CO_2 Capture Efficiency %	CO_2 Purity %	Solids circulation g/s	The air equivalence ratio	The OC/Fuel ratio
		AR	FR		FR				AR								
		air	CO	N_2	CO	CO_2	O_2	N_2	CO_2	O_2	N_2						
1	1	35	10	0	0.27	92.24	1.31	6.19	2.36	8.07	89.58	99.73	92.92	92.5	2.78	1.47	1.81
2		40	10	0	0.21	92.63	1.09	6.06	2.24	9.97	87.79	99.79	92.15	92.84	2.96	1.68	1.93
3		60	10	0	0	91.98	1.05	6.97	1.34	13.96	84.7	100	92.66	91.98	3.81	2.52	2.49
4		73	5	3.5	0.03	54.17	0.9	44.9	0.56	18.22	81.22	99.95	92.15	92.14	4.36	6.13	5.70
5	2	80	15	0	5.99	86.48	0.39	7.14	1.63	13.55	84.82	94.01	92.06	92.47	3.18	2.24	1.38
6		100	15	0	0.2	92.74	0.64	6.43	1.22	14.68	84.11	99.8	92.5	92.94	3.68	2.80	1.60
7		110	8	5	0	56.55	0.55	42.9	0.58	18.04	81.38	100	92.32	91.89	3.91	5.78	3.19
8	3	120	15	5	1.29	68.09	0.69	29.93	1	15.85	83.16	98.27	92.5	92.51	3.42	3.36	1.49
9		105	15	5	5.1	64.17	0.61	30.12	1.19	15.43	83.37	93.19	92.2	92.36	3.14	2.94	1.36
10		140	15	5	0.12	69.02	0.7	30.16	0.89	16.54	82.57	99.84	92.12	92.19	3.73	3.92	1.62
11	4	160	15	10	0.22	55.52	0.46	43.8	0.78	17.1	82.12	99.63	92.09	92.9	3.60	4.48	1.57
12		160	15	25	0.92	33.37	0.52	65.19	0.74	17.26	81.99	97.55	92.43	91.45	3.37	4.48	1.47
13		165	12	8	0.05	55.17	0.7	44.08	0.57	18.06	81.37	99.92	92.46	92.03	3.73	5.78	2.03
14		165	20	0	8.87	83.96	0.91	6.27	1.01	16.39	82.6	91.13	92.11	92.83	3.73	3.47	1.22
15	5	200	15	10	0	55.46	1.19	43.35	0.63	17.91	81.46	100	91.86	92.43	3.77	5.60	1.64
16		200	15	0	0	92.29	0.89	6.82	0.6	17.88	81.52	100	92.32	92.29	3.98	5.60	1.73
17		175	15	10	1.89	53.4	0.71	44	0.72	17.56	81.72	96.85	91.93	92.15	3.48	4.90	1.52
18	6	210	15	10	0	55.48	1.09	43.43	0.55	18.06	81.39	100	92.58	92.47	3.66	5.88	1.59

Table 17- Summary of the main results of the CLC experimental campaigns using 2 kg of solids inventory

Experimental cases	Pressure	Flowrate (Ln/min)			Products Concentration (vol%)							CO conversion %	CO_2 Capture Efficiency %	CO_2 Purity %	Solids circulation g/s	The air equivalence ratio	The OC/Fuel ratio
		AR	FR		FR				AR								
		air	CO	N_2	CO	CO_2	O_2	N_2	CO_2	O_2	N_2						
19	1	40	7	3	0.25	67.39	0.38	31.97	0.47	13.5	86.03	99.64	97.54	96.63	2.37	2.40	2.41
20	2	80	8	7	1.32	50.76	0.27	47.65	0.3	17.01	82.68	97.52	97.11	97.66	2.55	4.20	2.27
21	3	120	8	12	0.37	38.48	0.22	60.93	0.22	18.36	81.42	99.09	96.84	97.12	2.76	6.30	2.46
22		120	8	7	0.51	51.06	0.23	48.2	0.21	18.3	81.49	99.04	96.89	96.69	2.89	6.30	2.57
23		120	9	11	0.9	43.01	0.25	55.84	0.23	18.01	81.76	98	97.04	97.58	-	5.60	-
24		130	9	11	0.1	43.83	0.28	55.8	0.19	18.17	81.64	99.78	97.34	97.61	2.92	6.07	2.31
25	4	160	9	16	0.36	34.62	0.36	64.66	0.18	18.73	81.1	99.01	96.96	97.17	3.12	7.47	2.47
26		160	11	14	2.59	40.3	0.45	56.66	0.2	18.47	81.33	94.11	97.18	97.5	-	6.11	-

Further sensitivity study of ICR performance under pressurized CLC conditions (PCLC) will be presented and discussed in this section, with the focus on the 2.5 kg of solids inventory. The respective experiments were conducted in a pressure range of 1 to 6 bar, where air flowrate to the AR was increased proportionally to the pressure in order to maintain the gas fluidization velocity constant. The volumetric gas flowrate to the FR was increased with pressure; however, the gas fluidization velocity was decreased to avoid solids elutriation due to large bed expansion. This decrease should however have a limited effect on the ICR performance as found in the atmospheric study [91]. This is also confirmed in the current study where an increase of 60-66% in the FR flow rate has barely resulted in 5-6% decrease in solids circulation rate (cases 11 and 12 at 4 bar and cases 15 and 16 at 5 bar; U_{AR} was maintained constant for each operating pressure). Increasing the fluidization velocity in the AR (U_{AR}) resulted in higher solids circulation rate at different pressure as illustrated in Fig. 63. As explained in the previous study [91], the increase in U_{AR} leads to larger bed expansion, thus resulting in larger solids entrainment to reach the freeboard and fall into the FR through the top port. The larger accumulation rate of solids in FR creates larger driving force for solids to flow back from the FR to the AR through the bottom port. The CO_2 separation performance remains relatively insensitive to both AR and FR flowrates (Table 17).

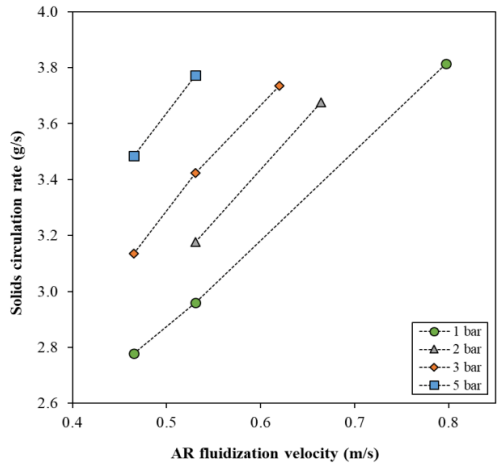

Fig. 63. Solids circulation rate as function of air fluidization velocity in AR at various pressure.

5.3.2 Effect of pressure

The understanding of the effects of pressure on fluidized-beds performance is essential for optimal design and operation. The operating pressure mainly affects the hydrodynamic behavior of the

fluidized-beds through the increase of the gas density, which increases the gas-solids drag [162]. Solid-solid interactions are not directly changed with elevated pressure due to the rigidity of the solids [68], but a denser gas increases the gas-particle drag, which also leads to fewer solid-solid collisions. As a result, it produces a more homogeneous fluidization and decreases the minimum fluidization velocity [233,234]. Increasing pressure also increases the bed-expansion and reduces the bubble size; as a result it leads to a better gas-solid contact and therefore higher interphase mass-transfer [235,236].

Fig. 64 shows the results of solids circulation rate, CO_2 capture efficiency and purity for the two AR fluidization velocities (U_{AR}= 0.53 and 0.46 m/s) as function of the operating pressure. The solids circulation rate was found to increase with the pressure. Similar observation for the increases of solids circulation rate with pressure have been reported by several studies on pressurized circulating fluidized-bed [237,238]. For instance, Horio et. al [237] carried out a hydrodynamic investigation on a pressurized circulating fluidized bed using FCC particles in a pressure range of 1 to 7 bar. They found that, keeping the gas velocity constant with pressure increases the solids circulation rate and that a lower gas velocity is required for the transition from bubbling to turbulent fluidization regimens when the pressure is increased. This result stems from the fact that the gas density increases with pressure, which increases the gas-solids drag [239,240].

Acceptably high CO_2 capture efficiency and purity were established (~92%) for all cases independently of the pressure for both tested AR fluidization velocities (Fig. 64). The insensitivity of undesired gas mixing to both the AR feed rate and the pressure supports previous findings that gas transport with the circulating solids between the two reactor sections is not the main gas mixing mechanism in this particular ICR setup [91]. In an optimal ICR system, as would be designed during further scale-up efforts toward commercial deployment, the gas would only leak with the circulating solids in a ratio of about 1:1 by volume, resulting in substantially lower leakage than observed in Fig. 64 (see previous large-scale simulation studies [21,241]). Considerable room for further reductions in gas leakage therefore exists by optimising the ICR port design and operating conditions. As discussed in the next section, the 2 kg inventory offers an indication of the good separation performance that can be achieved in an ICR. If required, the ports can be designed to act like loop seals by injecting steam into the ports to further reduce the gas leakages.

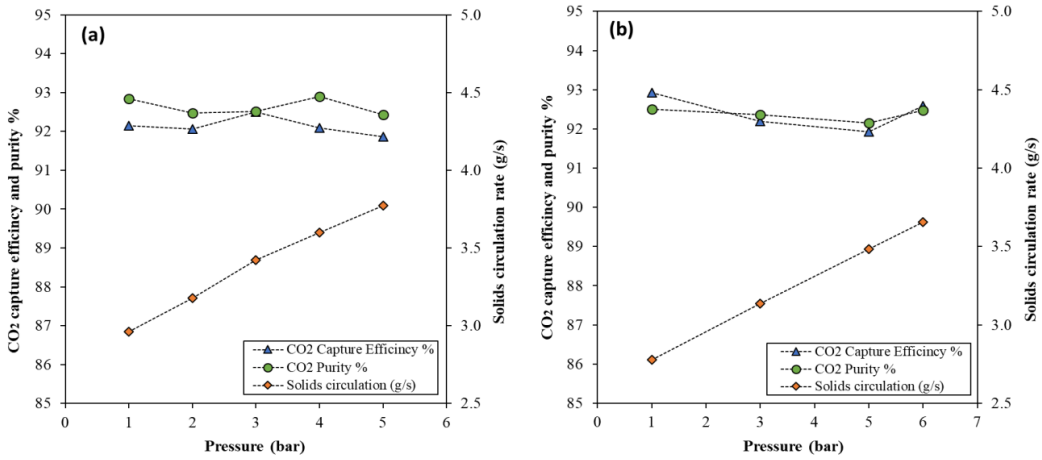

Fig. 64. Solids circulation rate and CO_2 capture efficiency and purity % as function of pressure, a) U_{AR}=0.53 m/s, case (2,5,8,11,15), b) U_{AR}=0.46 m/s, case (1,9,17,18).

To identify a condition at which similar hydrodynamic performance can be obtained at various pressures, additional experiments were conducted at lower pressures (1, 2, and 3 bar) with higher AR fluidization velocities (case-3, 6, and 10). Fig. 65a shows that both AR fluidization velocity and pressure led to an increase in the solids circulation rate. To obtain a similar solids circulation rate at various pressures, different AR fluidization velocities are needed. For instance, to achieve a solids circulation rate of 3.6 g/s, the required AR fluidization velocity can be interpolated from the data in Fig. 65a. Fig. 65b shows that the required air fluidization velocity for achieving a given solids circulation rate decreases with increasing the pressure.

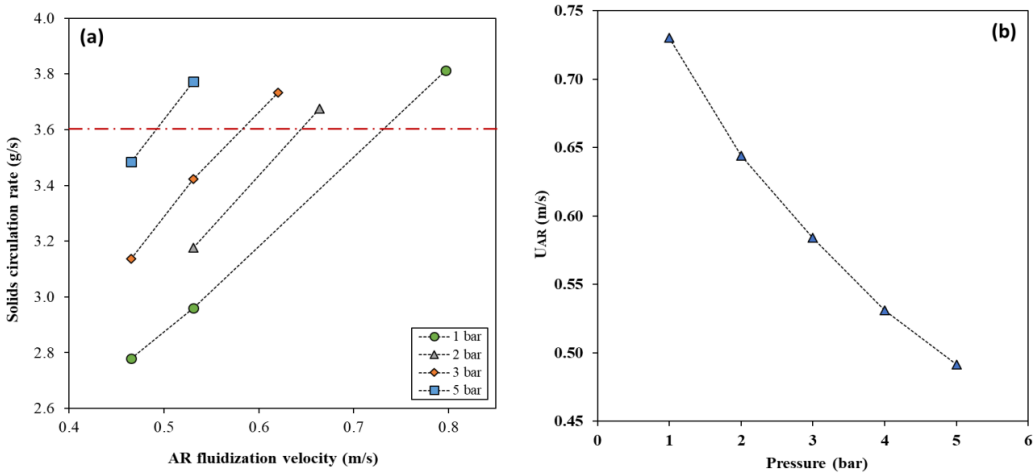

Fig. 65. a) Solids circulation rate as function of air fluidization velocity in AR at various pressure, b) the estimated air fluidization velocity in AR as function of pressure that keep solids circulation rate constant at 3.6 g/s.

5.3.3 Effect of solids inventory

The solids inventory is a critical operating variable for the CLC process. In CLC, the solids inventory must be high enough to achieve complete fuel conversion. A more reactive oxygen carrier is advantageous, since lower solids inventory can be used, which will reduce the required reactor size and pressure drop. For ICR, the solids inventory also has a strong influence on the hydrodynamic behaviour of the system [91].

To study the effects of the solids inventory on ICR performance, an additional experimental campaign was conducted using 2 kg of solids inventory over a pressure range of 1 to 4 bar (Table 17), to be compared with the results using 2.5 kg of solids inventory discussed in the previous sections. AR and FR flowrates were maintained similar to the experimental cases with 2.5 kg of solids inventory for each pressure, to focus the study on the effects of solids inventory.

Fig. 66 reveals the effect of increasing the solids inventory on the solids circulation rate at different pressures. Both solids inventories showed a similar trend of increasing the solids circulation rate with pressure. The addition of more solids to the ICR system leads to higher solids circulation rates (an increase of 25% in the solids inventory has resulted in a solids circulation increase of ~30%). The bed expansion in the AR is the main driving force for transporting the solids to the freeboard to reach the top port for circulation from the AR to the FR. A larger bed inventory allows for greater bed expansion, thus increasing the solids circulation rate.

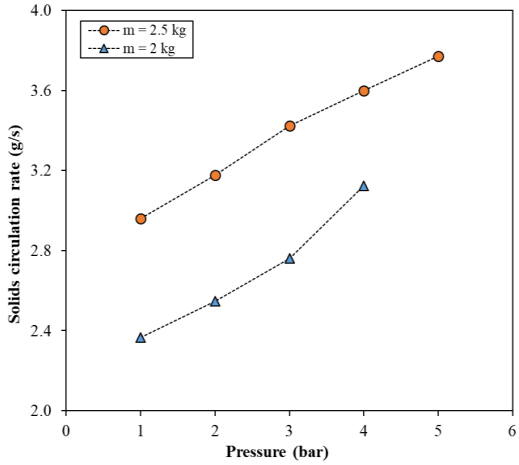

Fig. 66. Solids circulation rate as function of pressure for various solids inventories (2 and 2.5 kg), U_{AR} = 0.53 m/s, case (2,5,8,11,15) compared with case (19,20,21,25).

The effect of solids inventory and pressure on CO_2 capture efficiency and purity during CLC operation are shown in Fig. 67. It is shown that for both solids inventory the pressure has no effect on CO_2 capture efficacy and purity. However, high CO_2 capture efficiency and purity (~97%) was observed using lower solids inventory (2 kg), compared to around 92% for the higher solids inventory (2.5 kg). A similar effect of increasing gas leakage between the two chambers with increasing solids inventory was also observed at atmospheric pressure [91]. As outlined in that study [91], this effect is mainly due to design and hydrodynamic constrains of the ICR system. The most likely explanation is that higher solids inventories cause larger instantaneous pressure fluctuations at the bottom of the two reactor sections, resulting in short-lived backwards and forwards gas flows through the bottom port (in addition to the gas flowing from the FR to the AR with the solids). These results suggest that this mechanism for extra undesired gas mixing remains strong at 2.5 kg of solids inventory, but almost disappears at 2 kg of solids inventory. Improved design of the bottom port and optimal solids loading should therefore be prioritized during scale-up of the ICR concept.

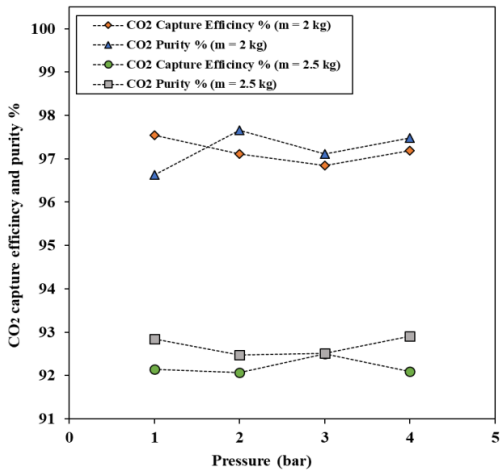

Fig. 67. CO_2 capture efficacy and purity % as function of pressure for various solids inventory (2 and 2.5 kg), U_{AR} = 0.53 m/s, case (2,5,8,11,15) compared with case (19,20,21,25).

5.3.4 Effect of the operating conditions on fuel conversion

In this section, the effect of various operating variables on the fuel conversion is discussed. Fig. 68 shows the effect of air flowrate and pressure on CO conversion, increasing both air flowrate and pressure improve the CO conversion as a result of increasing the solids circulation rate. Fig. 69a illustrates the effect of solids circulation rate and OC/fuel ratio on CO conversion for various cases at constant fuel feed (CO flowrate = 15 Nl/min) and solids inventory of 2.5 kg (overall specific inventory = 787 kg/MW). It can be seen that complete CO conversion was achieved with solids circulation rate higher than 3.6 g/s and OC/fuel ratio higher than 1.55. When using 2 kg of solids inventory, a higher OC/fuel ratio was required (higher than 2.3) to achieve complete CO conversion compared to the results of 2.5 kg of solids inventory (Fig. 69b). This effect is due to the short bed height that led to a smaller gas residence time in the bed, which reduces the gas-solids contact quality, thus negatively affecting CO conversion. The current ICR setup accentuates this effect because the gas is injected using a perforated cylindrical tube in a relatively concentrated manner, imposing significant bubble-to-emulsion mass transfer limitations. The specific solids inventory (937-1472 kg/MW) is higher than the cases with 2.5 kg solids inventory because a lower CO feed had to be used to get good conversion due to the lower solids circulation rates in the 2 kg solids inventory cases. However, the total fuel

reactor flowrate was kept similar using greater N_2 dilution, explaining the higher OC/fuel ratio required for full conversion despite the higher specific solids inventory.

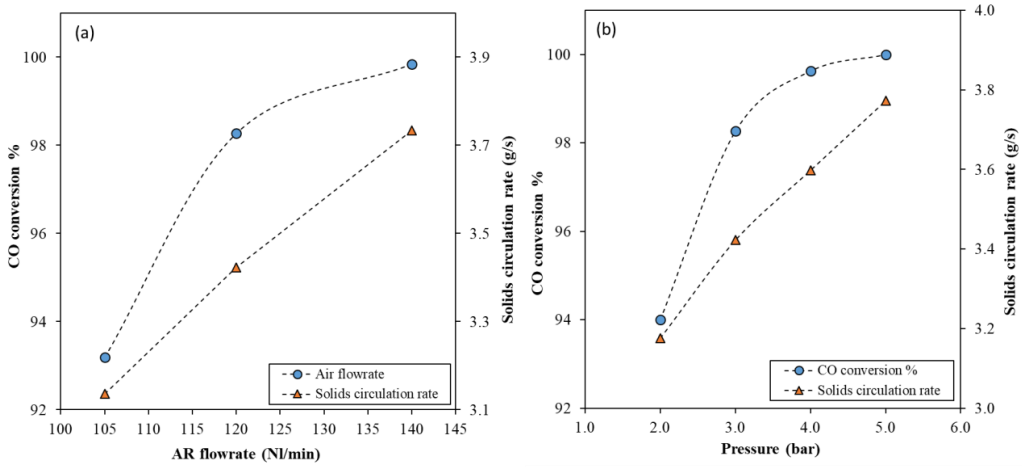

Fig. 68. a) Effect of AR flowrate on CO conversion and solids circulation rate, (Pressure = 3 bar). b) Effect of pressure on CO conversion and solids circulation rate, (FR specific inventory = 393 kg/MW).

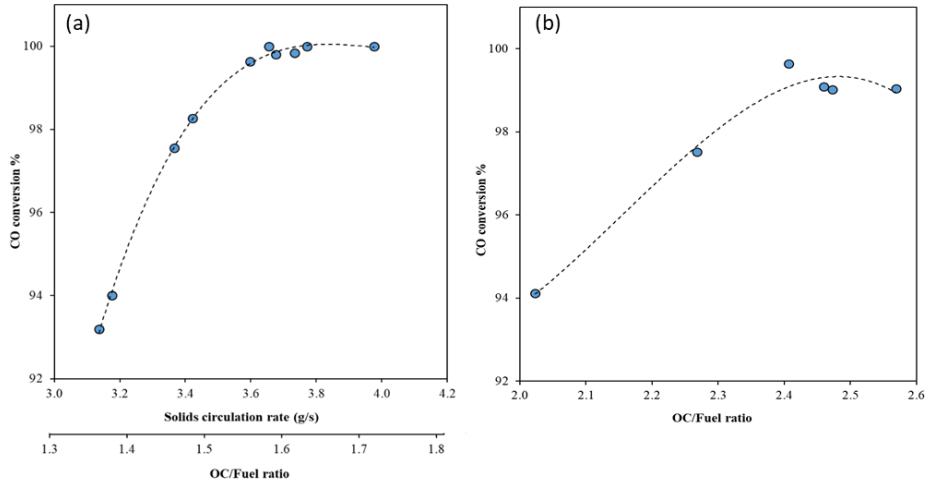

Fig. 69. a) CO conversion with different solids circulation rate and OC/fuel ratio, (solids inventory = 2.5 kg), b) CO conversion with different OC/fuel ratio, (solids inventory = 2.0 kg).

5.3.5 Correlation for the solids circulation rate

The experimental data of this study have revealed that the solids circulation rate (G_S) in the ICR reactor is affected mainly by four independent variables: solids inventory (m_s), pressure (P), air fluidization velocity in AR (U_{AR}) and fuel fluidization velocity in FR (U_{FR}). To better understand the ICR operation at different conditions, the obtained solids circulation rates from the different experiments have been correlated with the four independent variables using the following empirical correlation:

$$G_s = a\, m_s + b\, P + c\, U_{AR} + d\, U_{FR} + e \tag{5-10}$$

The correlation was evaluated using the non-linear regression method of Wolfram Mathematica. This proposed linear correlation is the simplest model possible from four independent variables. More complex correlations using additional model exponents to account for any non-linear influence of the four independent variables on the solids circulation rate were also evaluated, but this resulted in negligible improvement over the linear relationships shown in Eq.(5-10). The accuracy of the obtained correlation is judged by the correlation coefficient R^2, and the significance levels of the interaction terms were diagnosed by the P-value (the probability value) obtained from the analysis of variance (ANOVA). The P-value is the probability that the observed effect is simply random. Hence, the smaller the P-value, the more significant the observed effect. The values of the model parameters in Eq.(5-10) along with their corresponding 95% confidence limits (CLs) and P-Values are shown in Table 18. As can be seen in Fig. 70, the predicted solids circulation rate by the correlation fits the experimental data well. The correlation coefficient R^2 has a very high value of 0.9997, indicating that almost no further improvement can be gained from more complex correlations.

Among the four independent variables, U_{AR} shows the lowest P-value (Table 18), which means that the AR fluidization velocity is the most significant variable affecting the solids circulation rate. Based on the P-values, the four parameters of Eq. (5-10) affect the solids circulation rate with the following significance order: $U_{AR} > m_s > P > U_{FR}$. This result is expected given that the air fluidization velocity and the solids inventory are the main driving forces for lifting solids to the top port for circulation from the AR to the FR.

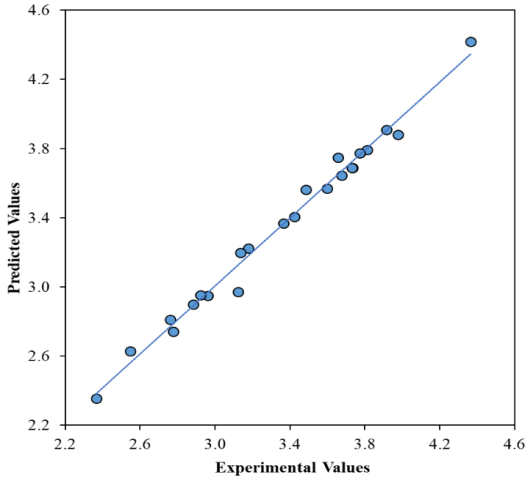

Fig. 70. Reconciliation plot between predicted and experimental solids circulation rate.

Table 18. Estimated parameters (at 95% confidence limit) and P-value for the correlation of solids circulation rate (Eq. (5-10))

	a	**b**	**c**	**d**	**e**
Estimated value	1.19 ± 0.14	0.14 ± 0.04	3.17 ± 0.29	-4.02 ± 1.83	-1.32 ± 0.34
P-Value	3.5E-13	3.2E-7	9.9E-15	0.0002	1.8E-6

Applying the developed correlation (Eq. (5-10)), a sensitivity analysis was carried out to gain further insight into the effects of the various independent variables on the solids circulation rate. It should be noted that the correlation was applied with some extrapolation, which could involve some uncertainty. The various independent variables were changed by ±50% from a reference values (m_s = 2.5 kg, P = 5 bar, U_{AR} = 0.53 m/s, U_{FR} = 0.13 m/s), while the solids circulation rate was evaluated using the developed correlation. Fig. 71 shows that increasing the solids inventory, pressure and U_{AR} resulted in an increase on the solids circulation rate, whereas increasing U_{FR} slightly decreased the circulation rate. A possible explanation for the small effect of U_{FR} is that the denser fuel reactor bed created by lower fluidization velocities leads to a more consistent presence of solids at the top of the bottom port, slightly increasing the circulation rate. Interestingly, Fig. 71 shows that the effect of solids inventory is considerably larger than that of air reactor velocity, even though the P-value of U_{AR} was lower than that of m_s (Table 18). Since only two different solids inventories were evaluated in the experiments, this effect involves more uncertainty than the others.

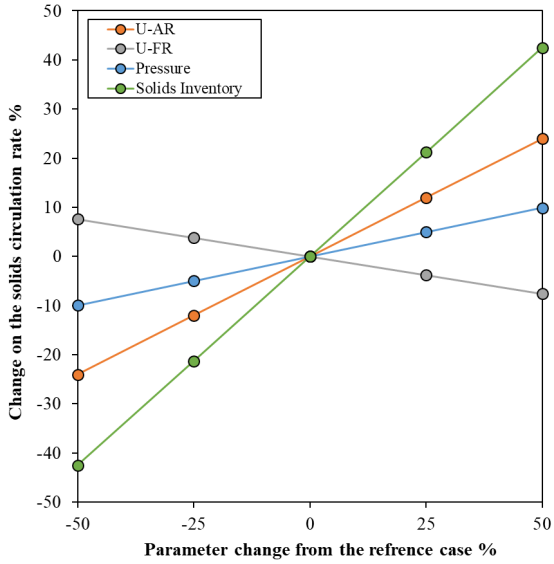

Fig. 71. Sensitivity analysis for the effects of the various independent variables on the solids circulation rate.

For practical application of ICR for PCLC, it will be beneficial to increase the gas mass flowrate in both FR and AR proportionally to the pressure, which would lead to a smaller reactor size for a given fuel input. However, as it has been observed from the current study, the solids circulation rate does not increase proportionally to the pressure in ICR, which will eventually lead to insufficient oxygen carrier circulation for converting the incoming fuel. Tuning the other process variables such as the solids inventory and the U_{AR} would be necessary if the mass flow rate to the FR is to be increased proportionally to the pressure.

An example of the adjustment to the process variables that should be applied at pressurized operation is illustrated by the following example. To achieve complete fuel conversion in ICR for 4 kW of thermal power of CO as fuel; the required solids circulation rate is around 4.0 g/s. This value is approximated based on the experimental case-22, in which the fuel conversion was 91% at a solids circulation rate of 3.7 g/s and a thermal power of CO feed of 4 kW (Table 16). Using the developed correlation (Eq.(5-10)), Fig. 72 shows the required air fluidization velocity U_{AR} at various pressures and at constant thermal power of CO input (4 kW) and constant solids circulation rate (4.0 g/s). It can be observed that the required U_{AR} decreases with increasing pressure (at which the volumetric flowrate of the fuel (V_{FR}) is maintained constant), which can be expressed by the following correlation:

$$U_{AR} = 1.1\, P^{-0.43} \tag{5-11}$$

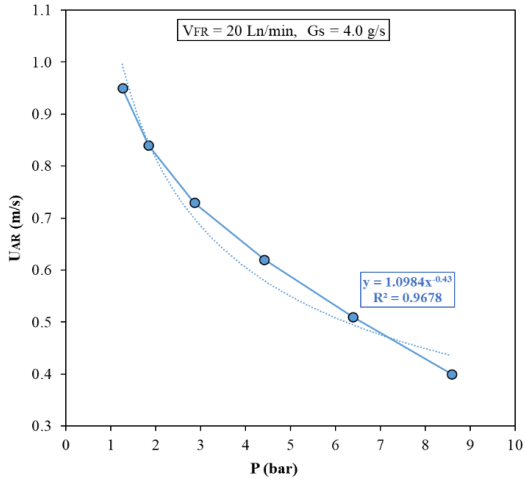

Fig. 72. Predicted U_{AR} as function of pressure at a constant solids circulation rate and thermal power of the fuel.

This result indicates that, to achieve a good operation at constant fuel power at higher pressures, the operation of ICR is possible at lower air fluidization velocity. A similar relationship between pressure and fluidization velocity was revealed by the work of Horio et. al [237] on PCFB; they found that, with similar solids circulation rate, the fluidization velocity scales with pressure as $U \propto P^{-0.3}$. It is noted, however, that another important constraint in CLC reactors is imposed by the ratio of air to fuel flowrate. In this example, even though the air fluidization velocity is reduced with pressure, the air mass flow rate increases by a factor of 3 from 1 to 7 bar if the reactor geometry is kept constant. This large increase in air flowrate relative to fuel flowrate will extract more heat and cool the reactor far below the desired operating temperature. Therefore, successful CLC operation will require changes to the cross-sectional area of the AR to also keep the fuel to air mass flow ratio constant.

The use of the fluidization regime diagram of Grace [242,243] provides additional insight for the effect of pressure on the flow regimes in ICR. Fig. 73 displays the fluidization regime at various pressures for the same conditions shown in Fig. 72. It can be seen that, in the AR, increasing the pressure shifts the behaviour slightly toward a more dilute phase. Although U_{AR} is reduced with increasing the pressure, the air density is strongly increased, increasing the gas-particle drag and shifting the flow regime toward the turbulent fluidization regime (U_c). This result is line with the work of Grace et al.

[244] and Horio et al. [237], in which they found that with increasing the pressure, a lower superficial gas velocities and higher gas mass flowrates is required for the transitions from bubbling to turbulent and fast fluidization regime.

The opposite trend occurs in the FR, since the fuel mass flowrate was held constant; increasing pressure strongly reduces the fluidization velocity, shifting the operating condition towards the minimum fluidization velocity (U_{mf}). Naturally, there will be constraints on how low the fluidization velocity in the FR can become before the bed defluidizes or no longer expands sufficiently to reach the top of the bottom port. In addition, optimal reactor design will always strive to maximize the gas fluidization velocity to reduce reactor size.

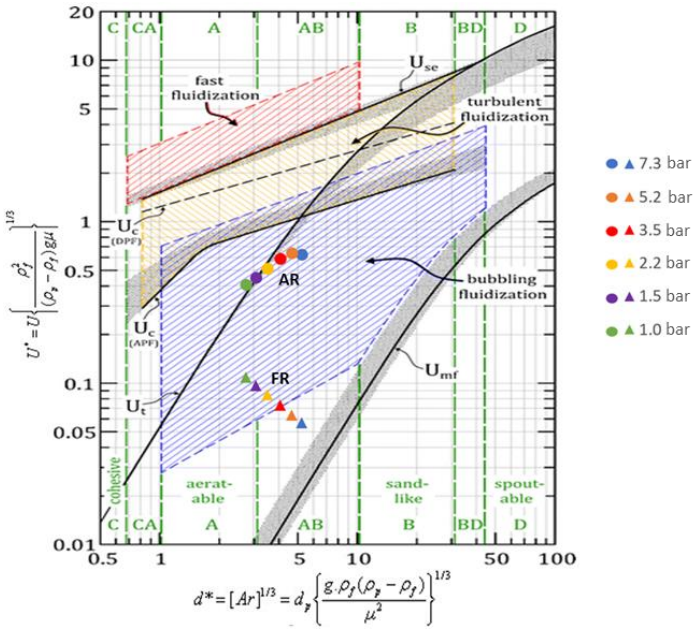

Fig. 73. Fluidization regime of AR (circle) and FR (triangle) under different pressure, the operating condition taken from Fig. 72.

Finally, an interesting practical application of the scaling of reactor behaviour with pressure can be mentioned: flexible operation of a CLC combined cycle power plant to balance variable wind and solar power. Such future CLC power plants will most likely be operated with added firing with natural gas or hydrogen after the CLC reactors to increase the turbine inlet temperature to the level of state-of-the-art gas turbines for achieving competitive efficiencies [229]. Part-load operation of the gas turbine reduces the turbine inlet temperature (requiring less added firing), as well as the pressure and air flow

rate. For example, ramping down a modern HA-class turbine from 100% to 40% load reduces the mass flow rate by 44% and the pressure by 40% [245], keeping the fluidization velocity almost constant. According to the present study (e.g. Fig. 66), a constant fluidization velocity at lower pressure will cause a moderate reduction in solids circulation rate. Such a moderate reduction should not be problematic because the fuel flowrate will be decreased almost proportionately to the air flowrate in part-load operation to keep the reactor outlet temperature constant. Although there are significant uncertainties in using this lab-scale correlation for projecting the performance of a commercial system, this discussion suggests that a future natural gas fired CLC power plant using ICR technology should be able to operate flexibly to balance variable wind and solar power.

5.3.6 Autothermal PCLC operation

Achieving autothermal operation is the primary design criterion of the CLC system. As the overall reaction in CLC systems is highly exothermic, the generated heat should be controlled. The choice of the heat removal will depend on the power generation strategy. For steam cycle applications, which will generally operate at atmospheric pressure, a direct heat extraction from the fluidized bed will result in a higher power plant efficiency and smaller reactor by using an equivalence ratio slightly higher than unity. For pressurized gas turbine applications, the PCLC system will be integrated with the gas combined cycle power plant, therefore, the use of high equivalence ratio will be favoured because the air serves as the primary heat removal mechanism. The higher required air flowrate is justified by the higher power plant efficiency resulting from the downstream combined power cycle.

In the current study, an autothermal CLC operation was achieved at 3 bar (case-8) with the use of an equivalence ratio of 3.4. Fig. 74 shows the temperature profile during autothermal CLC operation of this case. It can be seen that the temperature measurements was stable at various locations inside the reactor without the use of the external heater. The highly exothermic oxidation reaction in the AR resulted in a higher temperature compared to that in the FR. Increasing the equivalence ratio at higher pressure (4 to 6 bar) removed more heat from the reactor vessel which was compensated by adjusting the power of the electrical heater surrounding the reactor to maintain a constant temperature during CLC operation. The large heat losses from this lab-scale reactor is the main limitation to achieve autothermal operation in the current ICR system. The heat losses would be negligible in an industrial scale ICR; therefore, achieving autothermal operation would be feasible at a higher equivalence ratio, facilitating higher AR fluidization velocities.

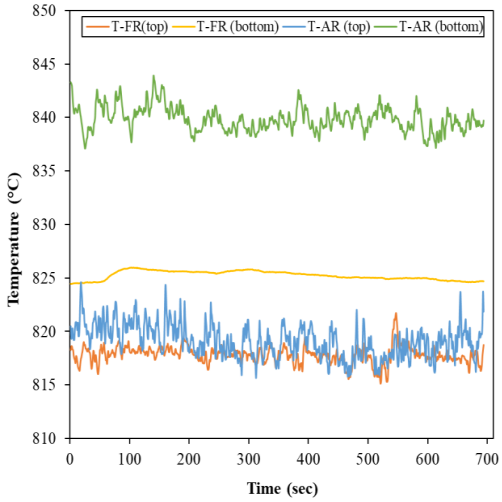

Fig. 74. Temperature profile in FR and AR during an autothermal PCLC test, P = 3 bar, AR flowrate = 120 Nl/min, FR flowrate = 20 Nl/min, solids inventory = 2.5 kg (case-8).

5.4 Summary and conclusions

This study reports the experimental demonstration of an internally circulating reactor (ICR) for pressurized operation of chemical looping-based technologies for minimizing the energy penalty involved in capturing CO_2 from hydrocarbon conversion. Pressurized experiments were completed for chemical looping combustion using CO as fuel and a NiO based oxygen carrier. Stable operation was achieved at pressures up to 6 bar, showing high fuel conversion and sufficiently high CO_2 purity and capture efficiency for all tested operating conditions (92-97%).

In addition to the operating pressure, the effect of other process variables (and their interaction) at elevated pressure, such as fluidization velocities in the air and fuel chambers, as well as the solids inventory, was evaluated. The CO_2 purity and capture efficiency were found to be negatively affected by the solids inventory, independently of the other process variables. The most sensitive performance indicator was the solids circulation rate that was found to increase (by order of influence) with the fluidization velocity in the AR, the solids inventory and the operating pressure, but almost insensitive to the fluidization velocity in the FR. A correlation for solids circulation rate was fitted to the different collected experimental data. The most important insight that could be revealed by the correlation is that, at constant fuel chamber section area, if the fuel mass feed rate is to be increased proportionally

to the operating pressure, larger solids inventory and higher fluidization velocity in the AR are required to establish sufficient solids circulation rate for high fuel conversion.

In the light of the reliable pressurized reactor operation, excellent fuel conversion, and good CO_2 separation performance demonstrated in this study, further scale-up of the ICR concept to 0.1-1 MW_{th} pilot plant size for application to pressurized chemical looping can be recommended.

List of symbols

AR	Air reactor
CLC	Chemical looping combustion
FR	Fuel reactor
ICR	Internally circulating reactor
OC	Oxygen carrier
$F_{i_{CO}}$	CO molar flowrate at FR inlet (mol/min)
$F_{o_{CO}}$	CO molar flowrate at FR outlet (mol/min)
$F_{AR,o_{CO_2}}$	CO_2 flowrate at AR outlet (Nl/min)
$F_{FR,i_{CO}}$	CO flowrate at FR inlet (Nl/min)
$F_{FR,o_{CO_2}}$	CO_2 flowrate at FR outlet (Nl/min)
$F_{FR,o_{tot}}$	Total FR outlet flowrate (Nl/min)
$F_{FR,i_{N_2}}$	N_2 flowrate at FR inlet (Nl/min)
$F_{O_{2,AR,in}}$	Inlet molar flowrate of oxygen to the AR
m_{OC}	Actual mass of the OC in its partially oxidized state (g)
$m_{OC_{ox}}$	Mass of the fully oxidized OC (g)
m_{O_2}	Mass of O_2 consumed during the re-oxidation test (g)
$\dot{m}_s$	Solids circulation rate (g/s)
M_{O_2}	Molecular weight of oxygen
$\dot{n}_{CO}$	Molar flowrate of CO (mol/s)
R_o	Oxygen transport capacity of the OC
$X_{s,FR}$	Solids conversion in FR
$X_{s,AR}$	Solids conversion in AR
x_{O_2}	Oxygen conversion at outlet of AR
ΔX_s	Solids conversion difference between AR and FR
γ_{CO}	Conversion of CO, %

Chapter 6 Pressurized chemical looping reforming

This chapter is based on the following paper:

Pressurized chemical looping methane reforming to syngas for efficient methanol production: experimental and process simulation study

Mogahid Osman, Abdelghafour Zaabout, Schalk Cloete, Shahriar Amini

(Under review, submitted to Advances in Applied Energy, 2021).

Abstract

This study investigates the potential of applying pressurized chemical looping reforming (CLR) technology for syngas to methanol production process combining of experimental demonstration of methane reforming to syngas and simulation for integration in methanol production. The experimental study was conducted using the internally circulating reactor (ICR) that was specially designed to enable pressurized CLR operation where several experimental cases were completed using a NiO-based oxygen carrier. Up to 4 kW of methane feed was reformed to syngas, achieving high conversion efficiencies and high syngas recovery and purity at pressurized conditions up to 4 bar. Co-feeding H_2O or CO_2 was found to affect mainly the H_2/CO ratio. The simulation study evaluated the potential of integrating the CLR process for large scale methanol production through comprehensive thermodynamic analysis using Aspen plus. The results revealed that CLR-based methanol plant is a highly attractive pathway achieving higher methanol production efficiency outperforming the conventional autothermal reforming (ATR) -based plant by ~5% efficiency. The main benefits of the CLR-based system is the avoidance of the air separation unit required for ATR plants, and the extra power generation through the gas turbine utilizing the hot exhaust gas of the air reactor. A detailed sensitivity study was also conducted to study the effects of the CLR operating pressure, and the reduced syngas purity caused by possible gas leakage in the ICR, on the overall methanol plant performance.

Mogahid Osman planned the experiments with cooperation with other authors. Mogahid conducted the experimental tests with guidance from Abdelghafour Zaabout. Mogahid develop the process model using Aspen plus with inputs from Schalk Cloete. All co-authors contributed on analyzing the results and writing the paper.

Chapter 7 Conclusion and Future work

Conclusion

Carbon Capture, Utilization and Storage (CCUS) considered playing a major role in most mitigation scenarios to meet the ambitions of Paris agreement in limiting future temperature increases to 2°C. Chemical looping process viewed as a promising technology that allows for cleaner energy generation and chemical production from fossil fuel utilization with inherent CO_2 capture and with high overall plant efficiency. Pressurized operation of the chemical looping system is a prerequisite for maximizing energy efficiency in most proposed configurations, introducing significant complexities related to system design, operation and scale-up. Therefore, the current PhD thesis aimed to demonstrate the technical attractiveness of the internally circulating reactor (ICR) concept based on the circulating fluidized bed reactor (CFB) configuration, but with innovative solution that facilitate pressurized operation of the chemical looping processes. The ICR integrates the two reactors, cyclones, loop seals and solids transport lines of the conventional CFB into a single unit that simplifies design and pressurized operation.

The current PhD thesis has successfully commissioned and demonstrated the pressurized lab-scale ICR reactor. The lab-scale ICR reactor employed to demonstrate two different chemical looping technologies under pressurized condition: chemical looping combustion (CLC), and chemical looping reforming (CLR). CLC is one of the most promising technologies for power generation with inherent CO_2 capture, where the best performance expected when integrated into a combined cycle, with the CLC reactor operated at high pressure. CLR has the capability of achieving higher overall plant energy efficiencies with lower carbon capture energy penalties for hydrogen and syngas production compared to conventional reforming technologies.

Comprehensive experimental campaigns conducted using the ICR unit. The aim of these campaigns was to examine the technical feasibility of the ICR concept for chemical looping process applications, as well as to obtain an extensive understanding of the effect of the various operating parameters on the overall reactor performance.

The first experimental campaign conducted in order to obtain an initial insight about the ICR concept. The experiments conducted at atmospheric pressure, using a NiO-based oxygen carrier. The initial non-reactive test showed that stable and continuous solids circulation rate

could achieved with minimal gas leakage. Subsequently, a fully reactive CLC and CLR tests conducted using methane as fuel. For CLC, methane feed adjusted to achieve full combustion of the fuel to CO_2 and H_2O. For CLR, syngas production achieved by altering the CH_4/O_2 ratio through controlling methane feed to the fuel reactor (FR), and oxygen feed to the air reactor (AR). A range of experiments showed that ICR behaved largely as expected showing almost no syngas production when the CH_4/O_2 ratio was close to 0.5 (stoichiometric ratio for combustion), but steadily increasing syngas production when the CH_4/O_2 ratio was increased.

The second experimental campaign designed to expand the knowledge of ICR operation by mapping out an operating window for the CLC process that maximizes the overall reactor performance. The campaign also conducted at atmospheric pressure, but with a wider range of other operating conditions; to develop a better understanding of the behavior of the concept. The experimental test conducted for CLC mode using CO as fuel and a MnO-based oxygen carrier. A wide range of operating conditions explored, including various solids inventories, and fluidization velocity in AR and FR. The main results of this campaign can be summarized as follows: 1) The air flowrate to the AR and the solids inventory are the main driving forces for the solids circulation in ICR, increasing both parameters led to an increase in the solids circulation rate. 2) CO_2 capture efficiency and purity were sensitive to the solids inventory but insensitive to other operating parameters, CO_2 capture efficiency and purity decreased with increasing the solids inventory. 3) The solids elutriation found to increase with increasing both the AR flowrate and solids inventory. 4) The reactor proved relatively simple to control over a range of operating conditions and showed predictable solids circulation and fuel conversion behavior. 5) An autothermal experimental run also completed to demonstrate this ease of operation.

The third experimental campaign aimed to demonstrate the ability of ICR to achieve pressurized CLC operation as well as to understand the role played by the pressure, the solids inventory and the fluidization velocity in AR and FR on various ICR performance measures. The experiments conducted using CO as fuel and with a NiO-based oxygen carrier. The results of this campaign showed a stable CLC operation with high fuel conversion for about 40 hours of steady state operation at pressures up to 6 bar, achieving reasonable CO_2 purity and capture efficiency (up to 97%). The solids circulation rate found to increase with increasing the operating pressure at a constant fluidization velocity with no effect on CO_2 capture and purity. The CO_2 purity and capture efficiency found to be most sensitive to the solids inventory, whereas the solids circulation rate was most sensitive to the air reactor fluidization velocity

and the solids inventory. Autothermal CLC operation also achieved at pressurized condition illustrating the full potential of the concept. Furthermore, a correlation for solids circulation rate derived from the collected experimental data, thus providing a robust tool for designing an ICR system for pressurized operation. This correlation can assist in further scale-up and designing an ICR pilot plant in the order of 0.1 to 1 MW at pressures relevant to real industrial conditions.

The fourth experimental campaign applied ICR for high-pressure chemical looping methane reforming to syngas (CLR) process. The tests conducted using a NiO-based oxygen carrier and methane thermal input of 4 kW. The results of the campaign revealed the capability of ICR to achieve a stable syngas production with high conversion efficiencies at pressurized conditions up to 4 bar. The composition of the syngas produced at the various operating pressure found to be close to the equilibrium compositions. An H_2/CO ratio of around 2.0 to 2.8 obtained, which is desirable for Fischer-Tropsch process and methanol synthesis.

Further insight of applying CLR process to a large-scale methanol production plant explored through a process modeling approach using Aspen Plus. The CLR based process compared with the state-of-the-art technology for methanol production from natural gas through autothermal reforming (ATR). The simulation results revealed that a CLR-based methanol plant achieve an equivalent methanol efficiency up to ~79% compared to ~74% for the conventional ATR-based process. A sensitivity analysis also conducted for the effects of CLR operating pressure, and gas leakage between AR and FR expected when using the ICR system. It found that increasing the pressure resulted in an increase on the overall efficiency up to a point where further increase have a negligible effect. As for the gas leakage in ICR, it was revealed that a decrease of the syngas purity and recovery from 100% to 95% resulted in a decrease on the overall plant efficiency by ~4%. This finding indicate that the gas leakage on ICR has a large impact on the overall plant performance, therefore, a careful considerations should be taken when designing a large scale ICR unit to ensure a minimum gas leakage between the two reactor sections.

In summary, this PhD thesis achieved its primary objective of building and demonstrating a unique lab-scale pressurized ICR unit. Extensive operational experience was gained over a wide range of operational parameters that significantly improved understanding of the concept. The results of the experimental demonstration clearly indicate the viability of the ICR concept for high-pressure chemical looping applications, and hence future scale-up is recommend.

Moreover, The ICR experimental outcome offers a substantial addition to the state of art when it comes to pressurized circulating fluidized-bed reactors, especially for chemical looping processes.

Future work

As with any experimental research, this PhD work answered some questions and raised many others. Following are some recommendations for future work that could be extend to add further value.

Future study that can be achieve using the existing ICR unit without extensive modifications:

- Conduct further operational experiences using different oxygen carrier materials, and possibly for different chemical looping applications.
- Study the effects of the top-port size on the ICR performances, specifically on the gas leakage between the two sections. The current unit designed with flexible modifications of the top-port size. However, it required complete dismantle of the reactor body from the shell and require welding works.
- Further ICR operations at higher pressure up to 10 bar. The unit already designed for operation up to 10 bar. Nevertheless, due to some technical limitations the maximum achievable pressure was 6 bar. Below are some modifications that needed to enable higher pressure operations:
    - The gas distributor should be modify to allow the injection of larger gas flowrate with much lower pressure drop. Due to the use of a small perforated holes on the current gas distributor; for stable operation at 6 bar, the air compressor was adjusted to 15 bar to allow delivering the high air flowrate to the AR required for this case.
    - The back-pressure regulator used to control the pressure inside the ICR unit and the shell needs to be changed, as it has a maximum design limit of 7 bar.
    - Additional heat supply is require to compensate the heat loss when using high air florwate during pressurized operations. The electrical heating element reached its maximum power when operating at 6 bar during this PhD thesis. One suitable option is to preheat the air feed to a higher temperature (>300°C) before feeding to the ICR. While autothermal operation is the prime goal for chemical looping

processes, a further modification on the dimension of the air reactor is required to achieve this goal at high pressure.

- Utilize the existing ICR unit to investigate new oxygen carrier materials. The current ICR allows for using 1 to 4 kg of oxygen carrier materials, which could be an advantageous level before proceeding to a large oxygen carrier production for a pilot plant scale. The studies could be conduct at atmospheric or pressurized conditions with the aim of extracting information about the oxygen carrier reactivity, products selectivity, solids attrition rate, and prolong operation stability.

Future study that can be achieve using the existing ICR unit with further modifications:

The current ICR designed to enable the flexibility of running a wide range of operating conditions needed in this research phase of the concept. Further refinement of the design of the different components of the reactor could be implemented as the general process behavior is well understood. Following are some recommendations for future work that required further design modifications of the ICR:

- Modify the existing ICR unit to enable local pressure measurements inside the reactor bed in different locations, to map out the hydrodynamic characteristics of the system during chemical looping operations.
    - There are four pressure measurement locations already exist in the current ICR, but it was not functional due to technical challenges with clogging of the lines with fines. Application of a purging gas to prevent the clogging has reduced the accuracy of the collected pressure data. A lot of effort was invested in the attempts to achieve reliable pressure measurements, but could not solve these challenges.
    - Further modifications could be by installing an incline measurement lines with fixed inert gas purging flowrate, this method could prevent solids clogging.
- Study the effects of purging or extracting gas in the bottom-port connecting the two reactor sections of the ICR.
    - The study could be achieve by installing a line with adjustable valve for either injecting or extracting gaseous in the bottom-port.
    - It is expected that the gas leakage to be reduced by purging or extracting gaseous in the bottom-port. For instance, when extracting small flowrate of gaseous from the bottom-port valve, it create a pressure relief for the air bypassing through the

port, hence, all the bypassed air will vent through the opened valve instead of leaking to the fuel section. It also derive the solids to circulate smoothly from the fuel section to the air section.

- Comprehensive fundamental study of the hydrodynamic characteristics of the ICR, by installing a non-invasive measurement props for in-situ analysis of the bed during operation.
    - The use of advanced prop technique is highly desirable for fluidized-bed process as it allow the measurements of several key properties inside the bed without interfere with the flow at high temperature and pressure operation.
    - The props could be used to quantify some or all of the following hydrodynamic properties: bubble size, solid hold up, solids circulation rate, solids agglomeration, and particle size and distribution.
    - The props could provide a qualitative or quantitative information based on the techniques and the advancement of the technology.
    - Such a study would add a substantial knowledge to the literature in the context of pressurized circulating fluidized-bed reactor.

Future study for scale-up of the ICR concept to a pilot scale in the range of 0.1 to 1 MW_{th}

Following the successful demonstration of the lab-scale ICR unit, a future study that aims to scale-up the ICR concept is highly recommended. At an initial stage, the scale-up study could combine a computational fluid dynamic model (CFD) and an experimental cold flow model (CFM) to develop the pilot-scale ICR unit. The coupling of CFD and CFM would reduce the overall risk of the scale-up. The experimental cold flow model (CFM) should be as a scaled copy of the pilot-scale ICR unit using scaling relationships. The CFM would provide a comprehensive understanding of the fluid hydrodynamic of the ICR system. Various measurement techniques could be used such as particle image velocimetry, gamma ray densitometry, fiber optical probes, and pressure probes. These techniques will extract key information with respect to the fluid dynamics and unit performance such as bed density profiles, solids holdup, bubble size, pressure loop profiles, solids circulation rate, solids entrainment rate, and solids residence time distribution.

The experimental data from the CFM will be used to validate the CFD simulations. Using the validated CFD, a detailed hydrodynamics of ICR in 3-D field can be revealed, which will

provide adequate data for the scale-up process. Hence, a reliable CFD model combined with CFM experimental study is an efficient way to facilitate the scale-up, design, and operation of the pilot-scale ICR unit. This strategy will establish the design fundamentals, the operating guidelines and the process control methodologies; that is require for the successful demonstration of the hot pilot-plant.

References

[1] "National Oceanic and Atmospheric Administration | U.S. Department of Commerce," can be found under https://www.noaa.gov/

[2] K. Von Schuckmann, L. Cheng, M. D. Palmer, J. Hansen, C. Tassone, V. Aich, S. Adusumilli, H. Beltrami, T. Boyer, F. José Cuesta-Valero, et al., *Earth Syst. Sci. Data* **2020**, *12*, 2013–2041.

[3] *IEA (International Energy Agency). World Energy Outlook, Paris; 2018***.**

[4] V. Masson-Delmotte, P. Zhai, H.-O. Pörtner, D. Roberts, J. Skea, P. R. Shukla, A. Pirani, W. Moufouma-Okia, C. Péan, R. Pidcock, et al., *An IPCC Special Report on the Impacts of Global Warming of 1.5°C above Pre-Industrial Levels and Related Global Greenhouse Gas Emission Pathways, in the Context of Strengthening the Global Response to the Threat of Climate Change, Sustainable Development,* **2018**.

[5] "Rystad Energy" https://www.rystadenergy.com/**.**

[6] M. Bui, C. S. Adjiman, A. Bardow, E. J. Anthony, A. Boston, S. Brown, P. S. Fennell, S. Fuss, A. Galindo, L. A. Hackett, et al., *Energy Environ. Sci.* **2018**, *11*, 1062–1176.

[7] E. S. Rubin, J. E. Davison, H. J. Herzog, *Int. J. Greenh. Gas Control* **2015**, *40*, 378–400.

[8] L. C. Tomé, I. M. Marrucho, *Chem. Soc. Rev.* **2016**, *45*, 2785–2824.

[9] M. Ishida, D. Zheng, T. Akehata, *Energy* **1987**, *12*, 147–154.

[10] M. Rydén, A. Lyngfelt, *Int. J. Hydrogen Energy* **2006**, *31*, 1271–1283.

[11] M. Ryden, A. Lyngfelt, T. Mattisson, *Fuel* **2006**, *85*, 1631–1641.

[12] L. F. De Diego, M. Ortiz, F. García-Labiano, J. Adánez, A. Abad, P. Gayán, *J. Power Sources* **2009**, *192*, 27–34.

[13] Y.-O. Chong, D. J. Nicklin, P. J. Tait, *Powder Technol.* **1986**, *47*, 151–156.

[14] Y. He, V. Rudolph, in *Chem. Enoineering Sci.*, **1995**, pp. 3443–3453.

[15] M. Fang, C. Yu, Z. Shi, Q. Wang, Z. Luo, K. Cen, *Chem. Eng. J.* **2003**, *94*, 171–178.

[16] B. Kronberger, E. Johansson, G. Löffler, T. Mattisson, A. Lyngfelt, H. Hofbauer, *Chem. Eng. Technol.* **2004**, *27*, 1318–1326.

[17] M. Rydén, M. Johansson, A. Lyngfelt, T. Mattisson, *Energy Environ. Sci.* **2009**, *2*, 970.

[18] E. Johansson, T. Mattisson, A. Lyngfelt, H. Thunman, *Fuel* **3AD**, *85*, 1428–1438.

[19] J. Herguido, J. A. Peña, E. Carazo, *Int. J. Hydrogen Energy* **2014**, *39*, 14050–14060.

[20] A. Zaabout, S. Cloete, S. Amini, *Chem. Eng. Technol.* **2016**, *39*, 1413–1424.

[21] S. Cloete, A. Zaabout, S. Amini, *Energy Procedia* **2017**, *114*, 446–457.

[22] T. Pröll, J. Bolhàr-Nordenkampf, P. Kolbitsch, H. Hofbauer, *Fuel* **2010**, *89*, 1249–1256.

[23] M. Ortiz, L. F. de Diego, A. Abad, F. García-Labiano, P. Gayá, J. Adá Nez, P. Gayán, J. Adánez, *Int. J. Hydrogen Energy* **2010**, *35*, 151–160.

[24] M. Rydén, M. Arjmand, *Int. J. Hydrogen Energy* **2012**, *37*, 4843–4854.

[25] L. F. Wang, S. Z. Wang, M. Luo, *Adv. Mater. Res.* **2014**, *953–954*, 966–969.

[26] P. Chiesa, G. Lozza, A. Malandrino, M. Romano, V. Piccolo, *Int. J. Hydrogen Energy* **2008**, *33*, 2233–2245.

[27] S. Cloete, A. Giuffrida, M. Romano, P. Chiesa, M. Pishahang, Y. Larring, *Fuel* **2018**, *220*, 725–743.

[28] B. Moghtaderi, *Energy & Fuels* **2010**, *24*, 190–198.

[29] J. Adánez, A. Abad, *Proc. Combust. Inst.* **2019**, *37*, 4303–4317.

[30] T. Mattisson, M. Keller, C. Linderholm, P. Moldenhauer, M. Rydén, H. Leion, A. Lyngfelt, *Fuel Process. Technol.* **2018**, *172*, 1–12.

[31] A. Lyngfelt, A. Brink, Ø. Langørgen, T. Mattisson, M. Rydén, C. Linderholm, *Int. J. Greenh. Gas Control* **2019**, *88*, 38–56.

[32] X. Zhu, Q. Imtiaz, F. Donat, C. R. Mü, F. Li, **2020**, DOI 10.1039/c9ee03793d.

[33] H. M. Kvamsdal, K. Jordal, O. Bolland, *Energy* **2007**, *32*, 10–24.

[34] J. Wolf, M. Anheden, J. Yan, *Fuel* **2005**, *84*, 993–1006.

[35] V. Subramani, P. Sharma, L. Zhang, K. Liu, in *Hydrog. Syngas Prod. Purif. Technol.*, John Wiley & Sons, Inc., Hoboken, NJ, USA, **2009**, pp. 14–126.

[36] F. García-Labiano, J. Adánez, L. F. de Diego, P. Gayán, A. Abad, *Energy & Fuels* **2006**, *20*, 26–33.

[37] A. Abad, F. García-Labiano, L. F. de Diego, P. Gayán, J. Adánez, *Energy & Fuels* **2007**, *21*, 1843–1853.

[38] R. Siriwardane, J. Poston, K. Chaudhari, A. Zinn, T. Simonyi, C. Robinson, *Energy & Fuels* **2007**, *21*, 1582–1591.

[39] H. Gu, L. Shen, J. Xiao, S. Zhang, T. Song, D. Chen, *Ind. Eng. Chem. Res.* **2013**, *52*, 1795–1805.

[40] S. Zhang, R. Xiao, W. Zheng, *Appl. Energy* **2014**, *130*, 181–189.

[41] S. Luo, L. Zeng, D. Xu, M. Kathe, E. Chung, N. Deshpande, L. Qin, A. Majumder, T.-L. Hsieh, A. Tong, et al., *Energy Environ. Sci.* **2014**, *7*, 4104–4117.

[42] H. P. Hamers, F. Gallucci, G. Williams, P. D. Cobden, M. van Sint Annaland, *Energy & Fuels* **2015**, *29*, 2656–2663.

[43] N. Deshpande, A. Majumder, L. Qin, L.-S. Fan, *Energy & Fuels* **2015**, *29*, 1469–1478.

[44] X. Lu, R. A. Rahman, D. Y. Lu, F. N. Ridha, M. A. Duchesne, Y. Tan, R. W. Hughes, *Appl. Energy* **2016**, *184*, 132–139.

[45] M. A. San Pio, F. Gallucci, I. Roghair, M. van Sint Annaland, *Int. J. Hydrogen Energy* **2017**, *42*, 12111–12121.

[46] Y. Tan, F. N. Ridha, D. Y. Lu, R. W. Hughes, *Energy & Fuels* **2017**, *31*, 14201–14210.

[47] Y. Tan, F. N. Ridha, M. A. Duchesne, D. Y. Lu, R. W. Hughes, *Energy & Fuels* **2017**, *31*, 7598−7605.

[48] L. Chen, L. Kong, J. Bao, M. Combs, H. S. Nikolic, Z. Fan, K. Liu, *Appl. Energy* **2017**, *195*, 1012–1022.

[49] S. Rana, Z. Sun, P. Mehrani, R. Hughes, A. Macchi, *Appl. Energy* **2019**, *238*, 747–759.

[50] L. Díez-Martín, G. Grasa, R. Murillo, M. Martini, F. Gallucci, M. van Sint Annaland, *Fuel* **2018**, *219*, 76–87.

[51] F. García-Labiano, J. Adánez, A. Abad, L. F. de Diego, P. Gayán, *Energy & Fuels* **2004**, *18*, 761–769.

[52] S. S. Chauk, R. Agnihotri, R. A. Jadhav, S. K. Misro, L.-S. Fan, *AIChE J.* **2000**, *46*, 1157–1167.

[53] R. Agnihotri, S. S. Chauk, S. K. Misro, L.-S. Fan, *Ind. Eng. Chem. Res.* **1999**, *38*, 3802–3811.

[54] K. Qiu, O. Lindqvist, *Chem. Eng. Sci.* **2000**, *55*, 3091–3100.

[55] K. Qiu, E. J. Anthony, L. Jia, *FUEL* **2001**, *80*, 549–558.

[56] F. Garcã A-Labiano, A. Abad, L. F. De Diego, P. Gayã, J. Adã Anez, *Calcination of Calcium-Based Sorbents at Pressure in a Broad Range of CO2 Concentrations*, **2002**.

[57] P. Basinas, Y. Wu, P. Grammelis, E. J. Anthony, J. R. Grace, C. Jim Lim, *Fuel* **2014**, *122*, 236–246.

[58] D. H. Ahn, B. M. Gibbs, K. H. Ko, J. J. Kim, *Fuel* **2001**, *80*, 1651–1658.

[59] W. C. Hecker, P. M. Madsen, M. R. Sherman, J. W. Allen, R. J. Sawaya, T. H. Fletcher, *Energy & Fuels* **2003**, *17*, 427–432.

[60] W. E. S. E. N. L. R. Byron Bird, *Transport Phenomena, 2nd Edition*, **2007**.

[61] J. W. Butler, C. Jim Lim, J. R. Grace, *Fuel* **2014**, *127*, 78–87.

[62] K. S. Oberoi, J. Abbasian, **2004**, DOI 10.1021/ie030282m.

[63] M. A. Kibria, P. Sripada, S. Bhattacharya, *Proc. Combust. Inst.* **2019**, *37*, 3023–3031.

[64] X. Guo, G. Chang, X. Tan, X. Hu, Q. Guo, **2020**, DOI 10.1021/acs.energyfuels.0c00500.

[65] Z. Zhang, J. G. Yao, M. E. Boot-Handford, P. S. Fennell, *Fuel Process. Technol.* **2018**, *171*, 205–214.

[66] R. C. Everson, H. W. J. P. Neomagus, R. Kaitano, *Fuel* **2011**, *90*, 2347–2352.

[67] J. Adanez, A. Abad, F. Garcia-Labiano, P. Gayan, L. F. de Diego, *Prog. Energy Combust. Sci.* **2012**, *38*, 215–282.

[68] J. Li, J. A. M. Kuipers, *Powder Technol.* **2002**, *127*, 173–184.

[69] I. Sidorenko, M. J. Rhodes, *Powder Technol.* **2004**, *141*, 137–154.

[70] M. Banaei, R. Dellaert, N. G. Deen, M. van Sint Annaland, J. A. M. Kuipers, *AIChE J.* **2018**, *64*, 3303–3311.

[71] M. A. Cuenca, E. J. Anthony, *Pressurized Fluidized Bed Combustion*, Springer Netherlands, Dordrecht, **1995**.

[72] P. E. G. Gogolek, J. R. Grace, *Prog. Energy Combust. Sci.* **1995**, *21*, 419–451.

[73] J. Shabanian, J. Chaouki, *Chem. Eng. J.* **2017**, *313*, 580–590.

[74] M. Alvarez Cuenca, E. J. Anthony, *Pressurized Fluidized Bed Combustion*, Springer Netherlands, Dordrecht, **1995**.

[75] S. Wang, G. Wang, F. Jiang, M. Luo, H. Li, *Energy Environ. Sci.* **2010**, *3*, 1353–1360.

[76] R. Xiao, L. Chen, C. Saha, S. Zhang, S. Bhattacharya, *Int. J. Greenh. Gas Control* **2012**, *10*, 363–373.

[77] R. W. Breault, *Handbook of Chemical Looping Technology*, WILEY-VCH Verlag, **2018**.

[78] H.-J. Ryu, D. Lee, S.-H. Jo, S.-Y. Lee, J.-I. Baek, in *14th Int. Conf. Greenh. Gas Control Technol. GHGT-14*, **2018**.

[79] R. H. Emma Moreside, Robert Symonds, Dennis Lu, in *Fluid. XVI, AIChE*, **2019**.

[80] A. Zaabout, S. Cloete, S. Amini, *Int. J. Greenh. Gas Control* **2017**, *63*, 175–183.

[81] A. Zaabout, S. Cloete, J. R. Tolchard, S. Amini, *Chem. Eng. Res. Des.* **2018**, *137*, 20–32.

[82] A. Zaabout, S. Cloete, S. T. Johansen, M. Van, S. Annaland, F. Gallucci, S. Amini, *Ind. Eng. Chem. Res* **2013**, *52*, 14241−14250.

[83] S. A. Wassie, Membrane-Assisted Chemical Switching Reforming for Pure Hydrogen Production with Integrated CO2 Capture, **2018**.

[84] S. Cloete, A. Zaabout, M. C. Romano, P. Chiesa, G. Lozza, F. Gallucci, M. van Sint Annaland, S. Amini, *Appl. Energy* **2017**, *185*, 1459–1470.

[85] A. Ugwu, A. Zaabout, J. R. Tolchard, P. I. Dahl, S. Amini, *Int. J. Hydrogen Energy* **2020**, *45*, 1267–1282.

[86] A. Zaabout, P. I. Dahl, A. Ugwu, J. R. Tolchard, S. Cloete, S. Amini, *Int. J. Greenh. Gas Control* **2019**, *81*, 170–180.

[87] "GaSTech - Demonstration of Gas Switching Technology for Accelerated Scale-up of Pressurized Chemical Looping Applications," can be found under https://www.sintef.no/projectweb/gastech/**.**

[88] S. A. Wassie, J. A. Medrano, A. Zaabout, S. Cloete, J. Melendez, D. A. P. Tanaka, S. Amini, M. van Sint Annaland, F. Gallucci, *Int. J. Hydrogen Energy* **2018**, *43*, 6177–6190.

[89] S. A. Wassie, S. Cloete, V. Spallina, F. Gallucci, S. Amini, M. van Sint Annaland, *Int. J. Greenh. Gas Control* **2018**, *72*, 163–174.

[90] M. Osman, A. Zaabout, S. Cloete, S. Amini, *Chem. Eng. J.* **2019**, *377*, 120076.

[91] M. Osman, A. Zaabout, S. Cloete, S. Amini, *Fuel Process. Technol.* **2020**, *197*, 106183.

[92] M. Osman, A. Zaabout, S. Cloete, S. Amini, *Chem. Eng. J.* **2020**, *401*, 125974.

[93] E. Kimball, H. P. Hamers, P. Cobden, F. Gallucci, M. van S. Annaland, *Energy Procedia* **2013**, *37*, 575–579.

[94] S. Bock, R. Zacharias, V. Hacker, *Sustain. Energy Fuels* **2020**, *4*, 1417–1426.

[95] S. Noorman, M. van Sint Annaland, Kuipers, *Ind. Eng. Chem. Res.* **2007**, *46*, 4212–4220.

[96] S. Cloete, F. Gallucci, M. van Sint Annaland, S. Amini, *Energy Technol.* **2016**, *4*, 1286–1298.

[97] V. Spallina, F. Gallucci, M. C. Romano, M. Van, S. Annaland, *Chem. Eng. J.* **2016**, *294*, 478–494.

[98] H. Jin, M. Ishida, *Ind. Eng. Chem. Res* **2002**, *41*, 4004–4007.

[99] F. Gallucci, H. P. Hamers, M. van Zanten, M. van Sint Annaland, *Chem. Eng. J.* **2015**, *274*, 156–168.

[100] H. P. Hamers, F. Gallucci, G. Williams, M. van Sint Annaland, *Fuel* **2015**, *159*, 828–836.

[101] S. Nestl, G. Voitic, M. Lammer, B. Marius, J. Wagner, V. Hacker, *J. Power Sources* **2015**, *280*, 57–65.

[102] G. Voitic, S. Nestl, M. Lammer, J. Wagner, V. Hacker, *Appl. Energy* **2015**, *157*, 399–407.

[103] G. Voitic, S. Nestl, K. Malli, J. Wagner, B. Bitschnau, F.-A. Mautner, V. Hacker, *RSC Adv.* **2016**, *6*, 53533–53541.

[104] S. Nestl, G. Voitic, R. Zacharias, S. Bock, V. Hacker, *Energy Technol.* **2018**, *6*, 563–569.

[105] R. Zacharias, S. Visentin, S. Bock, V. Hacker, *Int. J. Hydrogen Energy* **2019**, *44*, 7943–7957.

[106] R. Xiao, Q. Song, M. Song, Z. Lu, S. Zhang, L. Shen, *Combust. Flame* **2009**, *157*, 1140–1153.

[107] R. Xiao, Q. Song, S. Zhang, W. Zheng, Y. Yang, *Energy Fuels* **2009**, *24*, 1449–1463.

[108] S. Zhang, C. Saha, Y. Yang, S. Bhattacharya, R. Xiao, **2011**, *25*, 4357–4366.

[109] Z. Gu, K. Li, H. Wang, S. Qing, X. Zhu, Y. Wei, X. Cheng, H. Yu, Y. Cao, *Appl. Energy* **2016**, *163*, 19–31.

[110] H. Zhang, X. Liu, H. Hong, H. Jin, *Appl. Energy* **2018**, *213*, 285–292.

[111] H. Zhang, H. Hong, Q. Jiang, Y. Deng, H. Jin, Q. Kang, *Appl. Energy* **2018**, *211*, 259–268.

[112] D. Sridhar, A. Tong, H. Kim, L. Zeng, F. Li, L.-S. Fan, *Energy & Fuels* **2012**, *26*, 2292–2302.

[113] P. Gupta, L. G. Velazquez-Vargas, L.-S. Fan, *Energy & Fuels* **2007**, *21*, 2900–2908.

[114] F. Li, L. Zeng, L. G. Velazquez-Vargas, Z. Yoscovits, L.-S. Fan, *AIChE J.* **2010**, *56*, 2186–2199.

[115] A. Tong, D. Sridhar, Z. Sun, H. R. Kim, L. Zeng, F. Wang, D. Wang, M. V. Kathe, S. Luo, Y. Sun, et al., *Fuel* **2013**, *103*, 495–505.

[116] T.-L. Hsieh, D. Xu, Y. Zhang, S. Nadgouda, D. Wang, C. Chung, Y. Pottimurphy, M. Guo, Y.-Y. Chen, M. Xu, et al., *Appl. Energy* **2018**, *230*, 1660–1672.

[117] I. M. Dahl, E. Bakken, Y. Larring, A. I. Spjelkavik, S. F. Håkonsen, R. Blom, *Energy Procedia* **2009**, *1*, 1513–1519.

[118] Z. Zhao, T. Chen, A. F. Ghoniem, *Energy Fuels* **2013**, *27*, 327−343.

[119] S. F. Håkonsen, R. Blom, *Environ. Sci. Technol.* **2011**, *45*, 9619–9626.

[120] S. F. Håkonsen, C. A. Grande, R. Blom, *Appl. Energy* **2014**, *113*, 1952–1957.

[121] Z. Zhao, T. Chen, A. F. Ghoniem, *Energy Fuels* **2013**, *27*, 344−359.

[122] Z. Zhao, C. O. Iloeje, T. Chen, A. F. Ghoniem, *Fuel* **2014**, *121*, 327–343.

[123] Z. Zhao, A. F. Ghoniem, *Fuel* **2014**, *121*, 344–360.

[124] C. Iloeje, Z. Zhao, A. F. Ghoniem, *Int. J. Greenh. Gas Control* **2015**, *41*, 302–315.

[125] C. O. Iloeje, Z. Zhao, A. F. Ghoniem, *Appl. Energy* **2017**, *190*, 725–739.

[126] C. O. Iloeje, Z. Zhao, A. F. Ghoniem, *Appl. Energy* **2018**, *231*, 1179–1190.

[127] O. V. Ogidiama, M. Abu Zahra, T. Shamim, *J. Energy Resour. Technol.* **2018**, *140*, 112004.

[128] L. Zhu, Y. He, L. Li, P. Wu, *Energy* **2018**, *144*, 915–927.

[129] R. Porrazzo, G. White, R. Ocone, *Faraday Discuss.* **2016**, *192*, 437–457.

[130] O. V. Ogidiama, M. R. M. Abu-Zahra, T. Shamim, *Appl. Energy* **2018**, *228*, 724–735.

[131] G. Diglio, P. Bareschino, E. Mancusi, F. Pepe, *Ind. Eng. Chem. Res.* **2018**, *57*, 11299–11311.

[132] C. O. Iloeje, Z. Zhao, A. F. Ghoniem, *Appl. Energy* **2018**, *231*, 1179–1190.

[133] M. N. Khan, P. Chiesa, S. Cloete, S. Amini, *Energy Convers. Manag. X* **2020**, 100044.

[134] L. Mancuso, S. Cloete, P. Chiesa, S. Amini, *Int. J. Greenh. Gas Control* **2017**, *64*, 223–233.

[135] S. Cloete, A. Tobiesen, J. Morud, M. Romano, P. Chiesa, A. Giuffrida, Y. Larring, *Int. J. Greenh. Gas Control* **2018**, *78*, 354–363.

[136] A. Farooqui, A. Bose, D. Ferrero, J. Llorca, M. Santarelli, *J. CO2 Util.* **2018**, *27*, 500–517.

[137] S. M. Nazir, J. F. Morgado, O. Bolland, R. Quinta-Ferreira, S. Amini, *Int. J. Greenh. Gas Control* **2018**, *78*, 7–20.

[138] S. M. Nazir, S. Cloete, O. Bolland, S. Amini, *Int. J. Hydrogen Energy* **2018**, *43*, 8754–8769.

[139] S. M. Nazir, J. H. Cloete, S. Cloete, S. Amini, *Int. J. Hydrogen Energy* **2020**, DOI 10.1016/j.ijhydene.2020.01.234.

[140] S. A. Wassie, S. Cloete, V. Spallina, F. Gallucci, S. Amini, M. van Sint Annaland, *Int. J. Greenh. Gas Control* **2018**, *72*, 163–174.

[141] V. Spallina, D. Pandolfo, A. Battistella, M. C. Romano, M. Van, S. Annaland, F. Gallucci, *Energy Convers. Manag.* **2016**, *120*, 257–273.

[142] V. Spallina, A. Shams, A. Battistella, F. Gallucci, M. V. S. Annaland, in *Energy Procedia*, Elsevier Ltd, **2017**, pp. 419–428.

[143] S. Cloete, M. N. Khan, S. Amini, *Int. J. Hydrogen Energy* **2019**, *44*, 3492–3510.

[144] M. N. Khan, T. Shamim, *Int. J. Hydrogen Energy* **2016**, *41*, 22677–22688.

[145] M. N. Khan, T. Shamim, *Int. J. Hydrogen Energy* **2019**, *44*, 11525–11534.

[146] D. A. Chisalita, C. C. Cormos, *Energy* **2019**, *181*, 331–344.

[147] D. Xiang, Y. Zhou, *Appl. Energy* **2018**, *229*, 1024–1034.

[148] F. Zerobin, S. Penthor, O. Bertsch, T. Pröll, *Powder Technol.* **2017**, *316*, 569–577.

[149] C. Arnaiz del Pozo, S. Cloete, J. H. Cloete, Á. Jiménez Álvaro, S. Amini, *Int. J. Greenh. Gas Control* **2019**, *83*, 265–281.

[150] C. Pozo, J. Cloete, S. Cloete, Á. Álvaro, S. Amini, *Int. J. Energy Res.* **2020**.

[151] A. Zaabout, S. Cloete, S. T. Johansen, M. van Sint Annaland, F. Gallucci, S. Amini, *Ind. Eng. Chem. Res.* **2013**, *52*, 14241–14250.

[152] S. Szima, S. M. Nazir, S. Cloete, S. Amini, S. Fogarasi, A.-M. Cormos, C.-C. Cormos, *Renew. Sustain. Energy Rev.* **2019**, *110*, 207–219.

[153] S. Cloete, L. Hirth, *Energy* **2020**, *192*, 116671.

[154] C. Arnaiz del Pozo, S. Cloete, P. Chiesa, Á. Jiménez Álvaro, S. Amini, *Energy Convers. Manag. X* **2020**, *7*, 100050.

[155] S. M. Nazir, J. H. Cloete, S. Cloete, S. Amini, *Energy* **2019**, *185*, 372–385.

[156] S. Cloete, M. N. Khan, S. M. Nazir, S. Amini, *Chem. Eng. J.* **2021**, *404*, 126550.

[157] R. J. Lee Pereira, P. A. Argyris, V. Spallina, *Appl. Energy* **2020**, *280*, 115874.

[158] V. Spallina, G. Motamedi, F. Gallucci, M. van Sint Annaland, *Int. J. Greenh. Gas Control* **2019**, *88*, 71–84.

[159] J. C. Abanades, B. Arias, A. Lyngfelt, T. Mattisson, D. E. Wiley, H. Li, M. T. Ho, E. Mangano, S. Brandani, *Int. J. Greenh. Gas Control* **2015**, *40*, 126–166.

[160] D. P. Harrison, *Ind. Eng. Chem. Res.* **2008**, *47*, 6486–6501.

[161] E. J. Ben Anthony, *Greenh. Gases Sci. Technol.* **2011**, *1*, 36–47.

[162] J. W. Butler, J. R. Grace, in *Calcium Chem. Looping Technol. Power Gener. Carbon Dioxide Capture*, Woodhead Publishing, **2015**, pp. 377–408.

[163] Q. Wang, N. Rong, H. Fan, Y. Meng, M. Fang, L. Cheng, K. Cen, *Int. J. Hydrogen Energy* **2014**, *39*, 5781–5792.

[164] J. G. Yao, M. E. Boot-Handford, Z. Zhang, G. C. Maitland, P. S. Fennell, *Ind. Eng. Chem. Res.* **2020**, *59*, 8571–8580.

[165] A. Obradović, J. Levec, *Ind. Eng. Chem. Res.* **2017**, *56*, 13301–13309.

[166] Y. Fan, J. G. Yao, Z. Zhang, M. Sceats, Y. Zhuo, L. Li, G. C. Maitland, P. S. Fennell, *Fuel Process. Technol.* **2018**, *169*, 24–41.

[167] X. Zhou, X. Yang, J. Li, J. Zhao, C. Li, M. Du, Z. Yu, Y. Fang, *Energy Convers. Manag.* **2019**, *198*, 111899.

[168] I. Martínez, M. Martini, L. Riva, F. Gallucci, M. Van Sint Annaland, M. C. Romano, *Int. J. Greenh. Gas Control* **2019**, *81*, 216–239.

[169] J. R. Fernández, J. M. Alarcón, J. C. Abanades, *Catal. Today* **2019**, *333*, 176–181.

[170] L. Díez-Martín, J. M. López, I. Martínez, G. Grasa, R. Murillo, J. R. Fernández, *Int. J. Greenh. Gas Control* **2019**, *83*, 43–50.

[171] V. Manovic, E. J. Anthony, *Environ. Sci. Technol.* **2011**, *45*, 10750–10756.

[172] J. R. Fernández, J. C. Abanades, *Curr. Opin. Chem. Eng.* **2017**, *17*, 1–8.

[173] Y. Hu, H. Cui, Z. Cheng, Z. Zhou, *Chem. Eng. J.* **2019**, *377*, 119823.

[174] M. A. Soria, C. Rocha, S. Tosti, A. Mendes, L. M. Madeira, *Chem. Eng. J.* **2019**, *356*,

727–736.

[175] J. R. Rostrup-Nielsen, *Catal. Today* **2002**, *71*, 243–247.

[176] P. Nikolaidis, A. Poullikkas, *Renew. Sustain. Energy Rev.* **2017**, *67*, 597–611.

[177] I. Dincer, C. Acar, *Int. J. Hydrogen Energy* **2015**, *40*, 11094–11111.

[178] J. D. Holladay, J. Hu, D. L. King, Y. Wang, *Catal. Today* **2009**, *139*, 244–260.

[179] Y. Khojasteh Salkuyeh, B. A. Saville, H. L. MacLean, *Int. J. Hydrogen Energy* **2017**, *42*, 18894–18909.

[180] M. Rydén, A. Lyngfelt, T. Mattisson, *Energy and Fuels* **2008**, *22*, 2585–2597.

[181] P. Moldenhauer, M. Rydén, T. Mattisson, A. Lyngfelt, *Int. J. Greenh. Gas Control* **2012**, *9*, 1–9.

[182] F. García-Labiano, E. García-Díez, L. F. De Diego, A. Serrano, A. Abad, P. Gayán, J. Adánez, J. A. C. Ruíz, *Fuel Process. Technol.* **2015**, *137*, 24–30.

[183] B. Dou, Y. Song, C. Wang, H. Chen, M. Yang, Y. Xu, **2014**, DOI 10.1016/j.apenergy.2014.05.061.

[184] H. Ge, W. Guo, L. Shen, T. Song, J. Xiao, *Chem. Eng. J.* **2016**, *286*, 174–183.

[185] H. Ge, W. Guo, L. Shen, T. Song, J. Xiao, **2016**, DOI 10.1016/j.cej.2015.11.008.

[186] M. Luo, Y. Yi, S. Wang, Z. Wang, M. Du, J. Pan, Q. Wang, *Renew. Sustain. Energy Rev.* **2018**, *81*, 3186–3214.

[187] W. Wang, Y. Cao, *Int. J. Energy Res.* **2013**, *37*, 25–34.

[188] S. M. Nazir, O. Bolland, S. Amini, *Energy Procedia* **2017**, *114*, 2146–2155.

[189] T. Song, T. Shen, L. Shen, J. Xiao, H. Gu, S. Zhang, *Fuel* **2013**, *104*, 244–252.

[190] S. Noorman, M. V. S. Annaland, H. Kuipers, *Ind. Eng. Chem. Res* **2007**, *46*, 4212–4220.

[191] S. A. Wassie, F. Gallucci, A. Zaabout, S. Cloete, S. Amini, M. Van, S. Annaland, *Int. J. Hydrogen Energy* **2017**, *42*, 14367–14379.

[192] S. Cloete, F. Gallucci, M. van Sint Annaland, S. Amini, *Energy Technol.* **2016**, *4*, 1286–1298.

[193] A. Tong, L. Zeng, M. V. Kathe, D. Sridhar, L.-S. Fan, *Energy & Fuels* **2013**, *27*, 4119–4128.

[194] A. Abad, T. Mattisson, A. Lyngfelt, M. Ryden, *Fuel* **2006**, *85*, 1174–1185.

[195] T. Mattisson, F. García-Labiano, B. Kronberger, A. Lyngfelt, J. Adánez, H. Hofbauer, *Int. J. Greenh. Gas Control* **2007**, *1*, 158–169.

[196] E. Johansson, T. Mattisson, A. Lyngfelt, H. Thunman, *Chem. Eng. Res. Des.* **2006**, *84*, 819–827.

[197] E. Jerndal, T. Mattisson, I. Thijs, F. Snijkers, A. Lyngfelt, *Energy Procedia* **2009**, *1*, 479–486.

[198] J. Bolhàr-Nordenkampf, T. Pröll, P. Kolbitsch, H. Hofbauer, *Energy Procedia* **2009**, *1*, 19–25.

[199] T. Mattisson, J. Adanez, T. Proell, R. Kuusik, C. Beal, J. Assinkf, F. Snijkers, A. Lyngfelt, *Energy Procedia* **2009**, *1*, 1557–1564.

[200] C. Linderholm, Thesis for the Degree of Doctor of Philosophy, CO2 Capture Using Chemical-Looping Combustion-Operational Experience with Gaseous and Solid Fuels, **2011**.

[201] A. Y. Khodakov, W. Chu, P. Fongarland, *Chem. Rev.* **2007**, *107*, 1692–1744.

[202] Q. Zafar, T. Mattisson, R. Gevert, B. Gevert, *Ind. Eng. Chem. Res* **2005**, *44*, 3485–3496.

[203] D. Kang, M. Lee, H. S. Lim, J. W. Lee, *Fuel* **2018**, *215*, 787–798.

[204] D. Kang, H. S. Lim, M. Lee, J. W. Lee, J. W. Lee, *Appl. Energy* **2018**, *211*, 174–186.

[205] M. Ortiz, L. F. de Diego, A. Abad, F. García-Labiano, P. Gayán, J. Adánez, *Energy & Fuels* **2012**, *26*, 791–800.

[206] T. Mattisson, M. Johansson, A. Lyngfelt, *Fuel* **2006**, *85*, 736–747.

[207] Outotec HSC Chemistry Software 9.2, Equilibrium Compositions Module. https://www.outotec.com/products/digital-solutions/hsc-chemistry**.**

[208] M. Johansson, T. Mattisson, A. Lyngfelt, A. Abad, **2007**, DOI 10.1016/j.fuel.2007.08.010.

[209] J.-I. Baek, J.-W. Kim, J. B. Lee, T. H. Eom, J. Ryu, C. K. Ryu, J. Yi, *Oil Gas Sci. Technol. – Rev. d'IFP Energies Nouv.* **2011**, *66*, 223–234.

[210] L. F. de Diego, M. Ortiz, F. García-Labiano, J. Adánez, A. Abad, P. Gayán, *Energy Procedia* **2009**, *1*, 3–10.

[211] J. Li, H. Zhang, Z. Gao, J. Fu, W. Ao, J. Dai, *Energy & Fuels* **2017**, *31*, 3475–3524.

[212] A. Lyngfelt, B. Leckner, T. Mattisson, *Chem. Eng. Sci.* **2001**, *56*, 3101–3113.

[213] M. M. Hossain, H. I. De Lasa, *Chem. Eng. Sci.* **2008**, *63*, 4433–4451.

[214] P. Ohlemüller, M. Reitz, J. Ströhle, B. Epple, *Proc. Combust. Inst.* **2019**, *37*, 4353–4360.

[215] P. Hallberg, M. Hanning, M. Rydén, T. Mattisson, A. Lyngfelt, *Int. J. Greenh. Gas Control* **2016**, *53*, 222–229.

[216] E. Bakken, T. Norby, S. Stølen, *Solid State Ionics* **2005**, *176*, 217–223.

[217] H. Leion, Y. Larring, E. Bakken, R. Bredesen, T. Mattisson, A. Lyngfelt, **2009**, DOI 10.1021/ef900444d.

[218] M. Arjmand, H. Leion, T. Mattisson, A. Lyngfelt, *Appl. Energy* **2014**, *113*, 1883–1894.

[219] A. Thon, M. Kramp, E.-U. Hartge, S. Heinrich, J. Werther, *Appl. Energy* **2014**, *118*, 309–317.

[220] M. Rydén, A. Lyngfelt, T. Mattisson, *Int. J. Greenh. Gas Control* **2010**, *5*, 356–366.

[221] A. Abad, J. Adánez, F. García-Labiano, L. F. de Diego, P. Gayán, J. Celaya, *Chem. Eng. Sci.* **2007**, *62*, 533–549.

[222] M. Arjmand, M. Keller, H. Leion, T. Mattisson, A. Lyngfelt, *Energy & Fuels* **2012**, *26*, 6528–6539.

[223] Ajmal Latif, A Study of the Design of Fluidized Bed Reactors for Biomass Gasification, **1999**.

[224] S. Shrestha, B. S. Ali, B. M. Jan, M. D. B. Hamid, K. El Sheikh, *Powder Technol.* **2015**, *286*, 246–256.

[225] J. H. Goo, M. W. Seo, D. Kyoo Park, S. D. Kim, S. H. Lee, J. G. Lee, B. H. Song, *J. Chem. Eng. Japan* **2008**, *41*, 686–690.

[226] B. Kronberger, A. Lyngfelt, G. Löffler, H. Hofbauer, *Ind. Eng. Chem. Res.* **2005**, *44*, 546–556.

[227] F. F. Snieders, A. C. Hoffmann, D. Cheesman, J. G. Yates, M. Stein, J. P. K. Seville, *Powder Technol.* **1999**, *101*, 229–239.

[228] V. Spallina, M. C. Romano, P. Chiesa, F. Gallucci, M. Van, S. Annaland, G. Lozza, *Int. J. Greenh. Gas Control* **2014**, *27*, 28–41.

[229] M. N. Khan, S. Cloete, S. Amini, *Energy Technol.* **2019**, *7*, 1900567.

[230] C. Arnaiz del Pozo, S. Cloete, J. H. Cloete, Á. Jiménez Álvaro, S. Amini, *Int. J. Greenh. Gas Control* **2019**, *83*, 265–281.

[231] T. Mattisson, E. Jerndal, C. Linderholm, A. Lyngfelt, *Chem. Eng. Sci.* **2011**, *66*, 4636–4644.

[232] C. Linderholm, A. Abad, T. Mattisson, A. Lyngfelt, *Int. J. Greenh. Gas Control* **2008**, *2*, 520–530.

[233] I. Sidorenko, M. J. Rhodes, *Int. J. Chem. React. Eng.* **2003**, *1*.

[234] P. E. G. Gogolek, J. R. Grace, *Fundamental Hydrodynamics Related to Pressurized Fluidized Bed Combustion*, **1995**.

[235] A. W. Weimer, G. J. Quarderer, *AIChE J.* **1985**, *31*, 1019–1028.

[236] D. F. King, D. Harrison, *Trans. Inst. Chem. Eng.* **1982**, *60*, 26–30.

[237] M. Tsukada, D. Nakanishi, M. Horio, *Int. J. Multiph. Flow* **1993**, *19*, 27–34.

[238] A. Mahapatro, P. Mahanta, K. Jana, *Energy* **2019**, *189*, 116234.

[239] Y. Zhang, F. Lei, Y. Xiao, *Powder Technol.* **2018**, *327*, 17–28.

[240] J. G. Yates, *Chem. Eng. Sci.* **1996**, *51*, 167–205.

[241] J. H. Cloete, M. N. Khan, S. Cloete, S. Amini, *Processes* **2019**, *7*, 723.

[242] J. R. Grace, *Can. J. Chem. Eng.* **1986**, *64*, 353–363.

[243] K. S. Lim, J. X. Zhu, J. R. Grace, *Int. J. Multiph. Flow* **1995**, *2*, 141–193.

[244] H. T. Bi, J. R. Grace, *Can. J. Chem. Eng.* **1996**, *74*, 1025–1027.

[245] S. C. Gülen, *Gas Turbines for Electric Power Generation*, Cambridge University Press, **2019**.

[246] F. Kong, A. Tong, M. V. Kathe, L. S. Fan, D. Tomasko, *Chem. Eng. Process. - Process Intensif.* **2019**, *143*, 107566.

[247] M. Osman, A. Zaabout, S. Cloete, S. Amini, *Chem. Eng. J.* **2020**, *401*, 125974.

[248] M. Osman, A. Zaabout, S. Cloete, S. Amini, *Fuel Process. Technol.* **2020**, *197*, 106183.

[249] M. Osman, A. Zaabout, S. Cloete, S. Amini, *Chem. Eng. J.* **2020**, *401*, 125974.

[250] W. Summers, *Baseline Analysis of Crude Methanol Production from Coal and Natural Gas*, **2014**.